STUDIES OF INERTIAL DEPOSITION OF PARTICLES ONTO HEAT EXCHANGER ELEMENTS

Thesis by

Susan Elizabeth Fuhs

In Partial Fulfillment of the Requirements

for the degree of

Doctor of Philosophy

California Institute of Technology

Pasadena, California

1988

(Submitted October 1, 1987)

© 1988

Susan Elizabeth Fuhs

All Rights Reserved

ACKNOWLEDGMENTS

I would like to thank Professor Glen Cass for his most patient assistance. Much appreciation goes to Elton Daly, Joe Fontana, Rich Eastvedt, Gregory Haussman, Joe Yang, and Ichiro Sugioka for their help in constructing experimental equipment and to Art Esnayra, Harold Sanders, and Todd Ross for their beautiful art work. I would also like to acknowledge the practical guidance of Dr. Webb Marner.

Most of all I appreciate the constant support of my husband, David Huff, who was there when things got tough (and did a little typing, too). Thanks to you all.

ABSTRACT

Although the magnitude of the fouling problem in heat transfer equipment is well recognized, few investigations have been conducted into the mechanisms that lead to such fouling. The work reported in this thesis has been designed to examine gas-side fouling mechanisms that involve the inertial impaction of small particles onto tubular heat exchanger surfaces.

An aerosol processes wind tunnel has been constructed which facilitates quantitative studies of particle interactions with heat exchanger surfaces. Three sets of experiments were performed. First, single heat exchanger tubes were exposed to a cross-flow of particle laden air. Stainless steel tubes coated with a thin layer of grease to ensure that particle collisions resulted in capture were used to verify a numerical model for the inertial transport of ammonium fluorescein particles to the tube surface. Particle bounce has been quantified for the case of clean tubes and solid particles. Experimental results compared favorably with the results of a numerical simulation based on the concept of a critical incident particle velocity normal to the surface needed to induce the particle to bounce with enough energy to escape collecton by the tube.

Second, the transient deposition of particles onto single heat exchanger tubes in cross-flow was studied. It was found that a steady-state condition could be reached for cases in which particle bounce occurred. Finally, the deposition patterns for the aerosol particles as they passed through a tube bank were studied. The quantities of aerosol deposited on various tubes depended on tube surface condition, tube position within the tube bank, and the overall geometry of the bank.

Conditions have been identified in which the aerosol deposits that lead to gas-side heat exchanger fouling can be kept to very low levels by deliberately selecting high fluid velocities that induce solid particles to bounce upon impact with the heat exchanger surfaces. Transient fouling experiments have identified conditions under which high fluid velocities can be used to achieve very low, steady-state particle accumulations on tubes in a cross-flow of solid particles. Using these findings, heat exchangers can be designed that will resist gas-side fouling.

Table of Contents

Table of Contents

Table of Contents

Table of Figures

Table of Tables

1 INTRODUCTION

1.1 BACKGROUND

Heat exchangers are a vital part of many industrial processes. They may be found in circumstances as varied as cement plants, glass furnaces, chemical processing plants, and metallurgical industries (1-9). Whatever the application, heat exchangers are designed to transfer energy efficiently from one process stream or reservoir to another.

A typical heat exchanger enables heat transfer from a hot fluid through a barrier wall to another, colder, fluid stream. While observing this basic premise, many different heat exchanger geometries may be seen. Examples may be as simple as a bank of tubes placed in a boiler exhaust gas stream to promote waste heat recovery or as complex as a compact finned tube heat exchanger used in aircraft applications.

Fouling occurs as a result of the accumulation of deposits on the heat transfer surfaces of a heat exchanger. These deposits may build up as a result of one or more mechanisms: particulate deposition, scaling, chemical reaction, corrosion, biofouling, and changes of phase (freezing or condensation) (10, 11). All of these deposits provide barriers to heat transfer, and they may also cause other disadvantages, including higher pumping costs due to restricted flow areas, increased cleaning costs, increased time out of service, and the additional capital investment necessary to build larger heat exchangers to provide adequate heat transfer even under fouled conditions (12, 13).

1.2 PROBLEM

Fouling of heat exchangers has been acknowledged as a major problem since at least the 1950's (14). The design of heat exchangers can be difficult if the processes and geometries are complex. The typical heat exchanger design procedure makes use of an extensive body of empirical data on the heat transfer resistance because of fouling, especially for cooling water systems. The expected fouling resistance will be estimated, and then additional heat transfer area is included in the design to allow for the eventual accumulation of fouling deposits. This purely empirical approach may lead to problems of overdesign, including heat exchangers that foul rapidly when clean because of the higher than desired temperature differences present in the overdesigned heat exchanger while it is still clean (14).

Few attempts have been made to explain the mechanics of many of the fouling processes. An understanding of the physical processes involved would aid in the treatment of fouling during the heat exchanger design process. This work examines the mechanisms of particle deposition onto the gas-side external surface of compact heat exchanger tube banks in cross-flow. This type of fouling is commonly seen in combustion systems such as coal or oil fired boilers, gas turbines, and diesel engines.

1.3 TEST CASES

This thesis presents an experimental investigation of the accumulation of deposited particulate matter on the surfaces of compact heat exchanger elements. The model heat

exchanger elements were built to typical compact heat exchanger dimensions as given by Kays and London (15). The flow regime was chosen so that inertial impaction would be the dominant process governing particle collection on surfaces. Three problems were examined: the collection of particles on single tubes in cross-flow, the build-up of particulate deposits on single tubes over time, and the deposition of particles within tube banks in cross-flow.

1.3.1 PARTICLE COLLECTION ON SINGLE TUBES

Data were gathered on the interaction of particulate matter with single tubes in cross-flow. Two cases were studied: stainless steel tubes coated with a very thin grease layer to ensure that particles that strike the tube surface would stick, and clean tubes used to examine the degree of particle bounce that occurs when solid particles strike a solid tubular surface. In the first case the focus was on describing the particle transport to the surface. Comparisons were drawn between experimental results and numerical simulations of the particle transport processes. In the second case, emphasis was placed on testing methods for predicting the probability that a particle striking a clean heat exchanger surface would bounce rather than stick. The concept of a critical incident velocity above which particle bounce would occur was found to be useful in describing the results. In all tests the fraction of the tube surface that was covered with particles was kept low to minimize possible particle-particle interaction.

1.3.2 TRANSIENT DEPOSITION ON SINGLE TUBES

Empirical models of the heat exchanger fouling process often assume that a steady-state fouling resistance (constant deposit thickness) is reached because of competition between

particle attachment and deposit removal. Some models also suggest the presence of an induction period during which a clean heat exchanger will operate for some period of time without noticeable fouling, followed by a period of rapid deposit accumulation (16). Data were gathered on the transient build-up of particle deposits on initially clean tubes. The purpose was to illuminate the role of particle bounce in maintaining clean tubular surfaces over time. Greased tubes were found to show no appreciable removal of particles from the collected deposits, and thus a steady state between particle deposition and removal was not achieved over the time periods tested. Ungreased tubes arrived very quickly at a near steady state between particle attachment and removal.

1.3.3 TUBE BANK DEPOSITS

Two different geometries of tube banks, staggered and in-line tube banks, were tested to examine the deposition of particles on tubes within the banks as well as the overall collection efficiencies for the entire tube banks. As might be expected, the number of particles collected by a particular tube in a tube bank depended both on the position of the tube within the bank and on the overall geometry of the bank itself. In general, tubes in the staggered arrangement collected more particles than tubes in the in-line geometry. Overall collection efficiency was higher for the staggered arrangement as well. As in the single tube experiments, the tube banks with greased tubes collected far more particles than those with clean tubes. However, qualitative deposition patterns observed in the greased tube banks were also seen in the ungreased tube banks.

1.4 OBJECTIVES

Objectives were:

1. to collect data on the interactions of a specific particle-surface pair and to provide a basis for examination of other particle surface pairs.

2. to document conditions and behavior of particle bounce.

3. to examine the transient build up of deposits.

4. to examine the deposits of particles throughout a tube bank in a cross-flow of an aerosol.

1.5 BIBLIOGRAPHY

1. Marner, W.J., An assessment of gas-side fouling in cement plants, Report No. 82-83, Jet Propulsion Laboratory, California Institute of Technology, Pasadena, CA (1982).

2. Berry, E.E., Kraszewski, L. and Luckman, C.G., An evaluation of electrical co-generation for waste heat recovery in the cement industry, Energy, Mines and Resources Canada (1981).

3. Bhatty, M.S.Y., Cement kiln system buildup, Proceedings of the 16th International Cement Seminar, Chicago, IL, 110-115 (1981).

4. Kulkarni, A.K., Yang, W.J. and Webb, R.L., Fouling and corrosion in glass furnace regenerators, Presented at the International Conference on Fouling of Heat Exchanger Surfaces, White Haven, PA (1982).

5. Webb, R.L. and Kulkarni, A., Heat exchanger needs for recovering waste heat in the glass making industry, Final Report, DOE Contract DE-FG07-811D12225, The Pennsylvania State University, University Park, PA (1982).

6. Reeve, D.W., Tran, H.N. and Barham, D., Superheater fireside deposits and corrosion in kraft recovery boilers, TAPPI, The Journal of the Technical Association of the Pulp and Paper Industry, 64, 5, 109-113 (1981).

7. Reeve, D.W., Tran, H.N. and Barham, D., The effluent-free bleached kraft pulp mill - Part XI, Pulp and Paper Canada, 82, 9, T315-T320 (1981).

8. Tran, H.N., Reeve, D.W. and Barham, D., Formation of kraft recovery boiler superheater fireside deposits, Presented at the International Conference on Recovery of Chemicals, Vancouver, B.C. (1981).

9. D'Angelo, S., Report of the proceedings of the Energy Research and Development Administration workshop on high temperature waste heat recovery and utilization, Report No. TID-28400, Washington Scientific Marketing, Inc., Washington, D.C. (1977).

10. Epstein, N., Fouling in heat exchangers, Proceedings of the Sixth International Heat Transfer Conference, 6, 235-253, Washington, D.C. (1979).

11. Epstein, N., Fouling: Technical aspects (afterword to fouling in heat transfer exchangers), Fouling of Heat Transfer Equipment, Hemisphere, Washington, D.C. (1981), pp. 31-53.

12. Thackery, P.A., The cost of fouling in heat exchanger plant, Effluent and Water Treatment Journal, 20, 112-115 (1980).

13. Leach, S.H., and Factor, S.A., Monitoring fouling in refinery and petrochemical plant heat exchanger equipment, ASME Heat Transfer Division Publication, Vol. 17, presented at the ASME/AIChE Heat Transfer Conf, Milwaukee, WI (1981).

14. Taborek, J., Aoki,T., Ritter, R.B., Palen, J.W. and Knudsen, J.G., Fouling: The major unresolved problem in heat transfer, Chemical Engineering Progress, 68, 2, 59-67 (1972).

15. Kays, W.M., and London, A.L., Compact Heat Exchangers, McGraw-Hill, New York, 1964.

16. Gupta, J.P., Fouling of heat exchanger surfaces, Chemical Age India, 29, 1, 33-40 (1978).

2 LITERATURE REVIEW/THEORETICAL DEVELOPMENT

2.1 ORGANIZATION OF THIS CHAPTER

First, the types of heat exchanger fouling that have been observed are discussed, with references to previous technical reviews of this subject. Attention is focused on the role of fouling considerations in heat exchanger design, with emphasis on the effect of fouling deposits on heat transfer.

Next, modeling procedures that have been used to describe the physical processes of particle deposition and removal are examined. Models based on theoretical considerations are compared to models based on laboratory experiments and models based on data from in-service units.

The next section of this chapter presents a more detailed examination of the fundamental physical processes governing particle deposition on surfaces. Mechanisms of transport from the working fluid to heat transfer surfaces are reviewed, followed by a discussion of the questions of particle adhesion and particle bounce. Particle re-entrainment is briefly considered.

Finally, a brief summary is provided and the implications of this literature survey for research into the gas-side fouling process are examined. The experiments chosen are discussed.

2.2 PREVIOUS REVIEWS OF FOULING BEHAVIOR

The state of the technical literature on heat exchanger fouling has been reviewed by a number of authors in recent years (1-12). Processes that lead to the fouling of heat transfer surfaces are commonly classified into six categories (3-4):

Scaling - the precipitation of inverse solubility salts onto a superheated transfer surface.

Particulate Fouling - the accumulation of particles onto a heat transfer surface. This includes gravitational settling of relatively large particles, as well as deposition by other mechanisms such as convective diffusion, thermophoresis, diffusiophoresis, inertial impaction, electrical migration, and vapor diffusion.

Chemical Reaction Fouling - deposits formed by chemical reactions at the heat transfer surface, with the surface itself not included as a reactant. Polymerization, cracking, and coking of hydrocarbons are prime examples.

Corrosion Fouling - the heat transfer surface itself reacts to produce corrosion products that foul the surface and may foster the attachment of other potential fouling materials.

Biofouling - micro- or macrobiological organisms attach themselves to the heat transfer surface and may generate slimes that also remain attached.

Freezing Fouling - the solidification of a pure liquid or constituents of a liquid solution onto a subcooled surface.

The emphasis of this work is on particulate fouling of gas-side heat transfer surfaces.

2.3 ROLE OF FOULING CONSIDERATIONS IN THE DESIGN PROCESS

The basic equation of conductive heat transfer is Fourier's Law, which in one dimension is

$$\frac{dQ}{dt} = -kA\frac{dT}{dx}. \tag{2.1}$$

Here Q is the amount of heat transferred, t is time, k is the thermal conductivity of the material through which conduction is occurring, dT/dx is the temperature gradient in the direction of heat flow (taken here as the x coordinate direction), and A is the cross-sectional area of the material normal to the direction of the temperature gradient. Equation (2.1) in effect defines the thermal conductivity of the material, k.

Convective heat transfer occurs because of the joint action of bulk fluid motions, conduction, and energy storage, usually as a fluid flows adjacent to a heated or cooled solid surface. Two types of convection are generally distinguished: free and forced. Free convection occurs when the motion of the fluid is a result of changes in the fluid density because of the heating that is taking place. An example is the heat transfer that occurs when a heated plate is placed in a quiescent pool of liquid. Forced convection, on the other hand, takes place when the motion of the fluid is driven by some other means that does not depend on the heat transfer. A good example is that of the heat transferred to a

cool fluid moving through a hot pipe under an externally imposed pressure gradient. Forced convection is by far the more important of the two processes within most conventional heat exchangers, although within some low velocity flows, combined free and forced convection can occur.

The governing equation for forced convection is

$$\frac{dQ}{dt} = hA\Delta T, \tag{2.2}$$

where h is the heat transfer coefficient of film coefficient, ΔT is the temperature difference across the solid/fluid interface, and Q, t, and A are as in Equation 2.1.

Most of the important heat exchanger applications involve convective heat transfer. Thus, the determination of the heat transfer (or film) coefficient, h, in Equation 2.2 becomes of major importance. Analytical values for h for a given situation can generally be determined only for simple geometries and flow situations, but many correlations exist to aid in obtaining approximate values for use in design (13-15).

The transfer of heat from the hot working fluid to the cold working fluid involves heat transfer film coefficients, h, on both the hot and cold sides of the exchanger, plus a resistance to heat transfer due to conduction through the metal wall that separates the two fluids. Over time, the heat transfer surfaces may accumulate fouling deposits that further retard heat transfer. Although fouling is, in fact, a transient process, to simplify analysis it is assumed that the fouling deposits have reached a quasi-steady state. It is often convenient to picture such systems using an electrical analog, assuming a one-dimensional steady-state system with constant heat transfer coefficients and thermal

conductivities. The fluid film adjacent to the hot-side wall of the heat exchanger provides resistance to heat transfer, followed in series by the hot side fouling layer, the wall of the heat exchanger, the cold side fouling layer and the cold-side fluid film. See Figure 2.1. At steady state, the heat flow through each layer of the planar system shown in Figure 2.1 must be the same:

$$\begin{aligned} q &= h_1 A (T_1 - T_2) \\ &= \frac{k_{f1} A}{\Delta x_{23}} (T_2 - T_3) \\ &= \frac{k_w A}{\Delta x_{34}} (T_3 - T_4) \\ &= \frac{k_{f2} A}{\Delta x_{45}} (T_4 - T_5) \\ &= h_2 A (T_5 - T_6). \end{aligned} \tag{2.3}$$

Here q is the heat transfer rate, dQ/dt; h_1 and h_2 are the convective heat transfer coefficients on the hot and cold sides, respectively; k_w is the thermal conductivity of the wall material; k_{f1} and k_{f2} are the thermal conductivities of the fouling deposits on the hot and cold sides, respectively; the Δx_{ij} are the thicknesses of the fouling deposits and wall, and the T_i are temperatures at the points indicated in Figure 2.1. Rearranging terms:

$$q = \frac{T_1 - T_6}{\frac{1}{h_1 A} + \frac{\Delta x_{23}}{k_{f1} A} + \frac{\Delta x_{34}}{k_w A} + \frac{\Delta x_{45}}{k_{f2} A} + \frac{1}{h_2 A}}. \tag{2.4}$$

The above equations take the form:

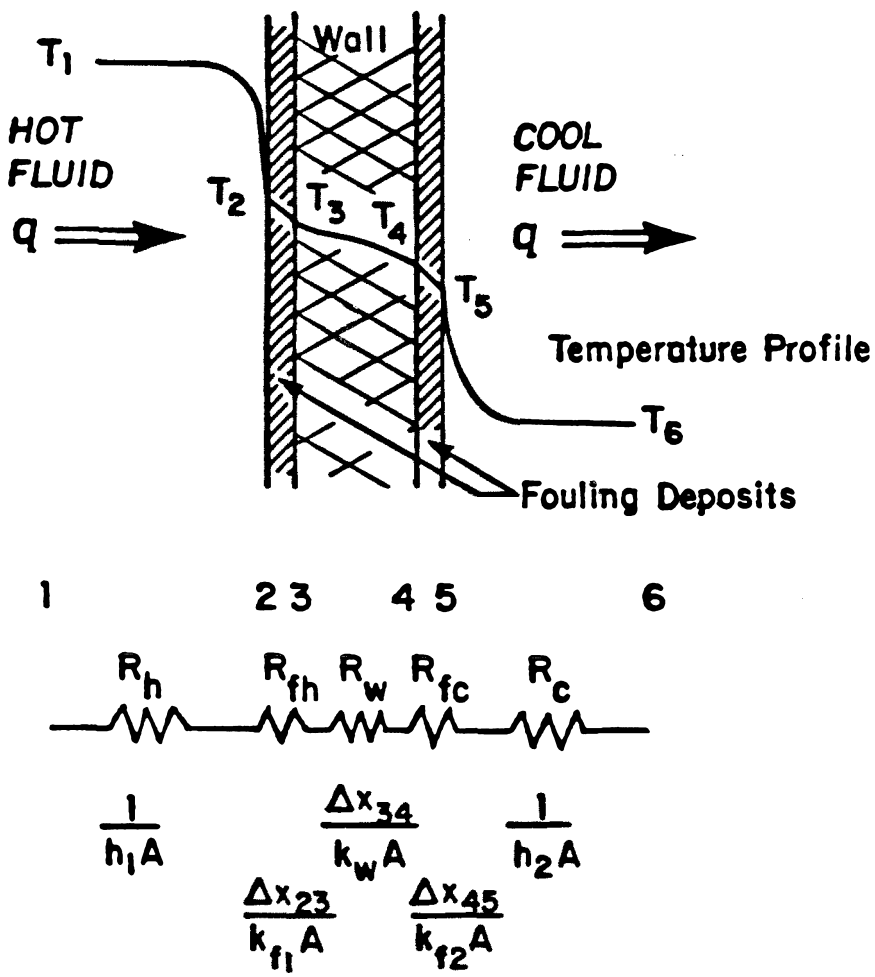

Figure 2.1. Electrical resistance analog for convective heat transfer through a plate covered with fouling deposits.

$$q = \mathrm{U}A(T_1 - T_6), \tag{2.5}$$

where U is the overall heat transfer coefficient:

$$\mathrm{U} = \frac{1}{\frac{1}{h_1} + \frac{\Delta x_{23}}{k_{f1}} + \frac{\Delta x_{34}}{k_w} + \frac{\Delta x_{45}}{k_{f2}} + \frac{1}{h_2}}. \tag{2.6}$$

The thermal properties of fouling deposits are seldom known in detail, so fouling resistances are seldom calculated from thermal conductivity and deposit thickness. Instead, the practice has been to determine fouling resistances directly by comparison of the performance of clean vs. dirty heat exchangers:

$$R_1 = \frac{1}{h_{f1}} = \frac{1}{\mathrm{U}_{f1}} - \frac{1}{\mathrm{U}_*}, \tag{2.7}$$

where $1/h_{f1}$ is a unit fouling resistance on side 1, U_* is the overall heat transfer coefficient of the clean heat exchanger, and U_{f1} is the overall heat transfer coefficient of the exchanger after fouling has occurred on side 1. For the planar geometry shown in Figure 2.1:

$$\mathrm{U} = \frac{1}{\frac{1}{h_1} + R_1 + \frac{\Delta x_{34}}{k_w} + R_2 + \frac{1}{h_2}}. \tag{2.8}$$

Generalizing:

$$q = U_d A_r (T_h - T_c), \tag{2.9}$$

and

$$U_d = \frac{1}{\frac{A_r}{A_i}\left(\frac{1}{h_i} + R_i\right) + \frac{A_r \Delta x_w}{k_w A_{mw}} + \frac{A_r}{A_o}\left(\frac{1}{h_o} + R_o\right)}, \tag{2.10}$$

where A_r is a reference area chosen for evaluation of the design overall heat transfer coefficient, U_d; Δx_w is the barrier wall thickness, A_{mw} is the mean barrier wall area, and the remaining variables A, h and R are wall areas, heat transfer coefficients, and fouling resistances on the inside, i, and outside, o, of the device, respectively. A convenient choice for A_r remains either the inside or outside surface area of the device.

From Equation 2.10, it is quickly seen that as heat exchanger fouling resistances R_o and R_i increase because of deposit accumulation, the overall design heat transfer coefficient, U_d, drops. In order to compensate for this decrease in U_d at any given temperature difference, $(T_h - T_c)$, Equation 2.9 shows that the response is to force an increase in the heat transfer surface area designed into the heat exchanger. Depending on expected service conditions and the type of heat exchanger chosen, fouling factors can account for a 10% to 500% increase in the heat transfer resistance expected in practice above that of a "clean" heat exchanger. The result is that about 30% to 40% of the heat transfer surface of an average heat exchanger design is included to accommodate fouling (16).

2.4 FOULING MODELS

2.4.1 OVERVIEW

The design of heat exchangers requires knowledge of the fouling resistance expected. See Equation 2.8. Due to the complexity of even the simplest real life situation, analytical predictions of deposit build-up and fouling resistance are beyond current capability. As a result, estimations of the fouling resistance are based on theoretical analysis, laboratory experiments, or data from similar in-service units.

Once an estimate of the fouling resistance is obtained from a model, typical practice is to "over-surface" the heat exchanger, that is, to provide additional heat transfer surface beyond that needed for clean operation. Figure 2.2 provides an example of such design advice.

For optimum heat exchanger operation it is important not to under- or overestimate the fouling resistance. Underestimation leads to inadequate heat transfer when the exchanger is fouled. Overestimation leads to less obvious but equally important problems. First is the increased capital cost of an overlarge heat exchanger. Second is the concern that lower-than-desired gas temperatures and velocities may be encountered at start-up of an overlarge exchanger. In many cases these conditions will promote the accumulation of heavier deposits than would be obtained operating at design conditions (9).

Consideration must also be given to the relationship of the flow velocity and the fouling rate. Flow velocities in a heat exchanger are often selected by comparing the energy

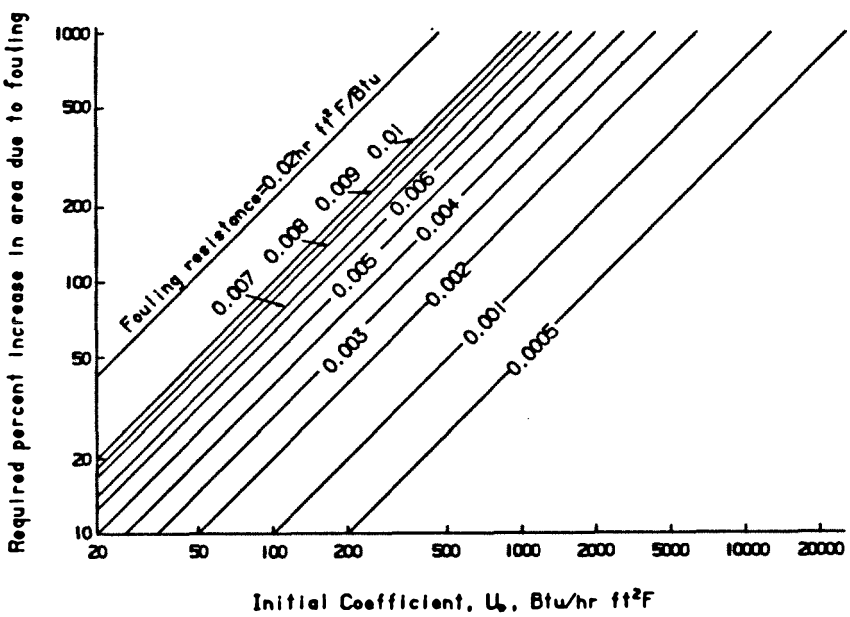

Figure 2.2. Heat exchanger oversurfacing required as a function of fouling resistance encountered and the initial "clean" exchanger coefficient. Adapted from Gupta (17).

saved because of enhanced heat transfer for a given velocity to the energy expended (pumping costs) to achieve such a velocity. Observations indicate, however, that asymptotic fouling rates decrease with increasing flow velocities (3,17-19), leading to the possibility that higher flow velocities may be optimal when the effects of fouling are taken into account.

2.4.2 THEORETICALLY BASED MODELS FOR FOULING BEHAVIOR

Most theoretically based fouling models make use of the observation that industrial heat exchangers frequently foul asymptotically. That is, at first a fouling rate is observed that leads to deposit build-up. Over time, however, the fouling rate often decreases as a steady state is reached and deposit thickness remains constant (3,4,9,10,17,20,21). This suggests that fouling deposit thickness is controlled by a competition between simultaneous deposition and removal.

Kern and Seaton (20) first proposed a model based on this balance, writing a simple material balance:

$$\frac{dR_f}{dt} = \phi_d - \phi_r, \tag{2.11}$$

where dR_f is the net rate of fouling resistance accumulation, ϕ_d is the rate of heat transfer resistance increase because of deposit build-up and ϕ_r is the heat transfer resistance removal rate. Using the Kern-Seaton model, several types of behavior can be

demonstrated (Figures 2.3 and 2.4). If there is no removal term, or if there is a constant net deposition rate, the fouling curve will show a linear increase. The more common case of asymptotic fouling occurs when the deposition and removal terms become equal. Both are shown in Figure 2.3. Figure 2.4 shows similar Kern-Seaton curves beginning after some time of relatively clean operation, an induction period. Such induction periods may often be seen when new, clean heat exchangers are first put into service. The length of the induction period, when present, is usually short compared to the in-service time for the exchanger.

The Kern-Seaton model is normally used by making assumptions, frequently based on empirical data, concerning the deposition and removal terms. One common assumption is that for given operating conditions, the deposition rate will be constant and the removal rate will be proportional to the deposit thickness (4). This leads to an analytic solution for the fouling resistance as a function of time:

$$\begin{aligned} R_f &= R_f^*(1-e^{-Bt}) \\ &= R_f^*\left(1-e^{-t/t_c}\right), \end{aligned} \tag{2.12}$$

where R_f^* is the asymptotic fouling resistance, $t_c=1/B$ is the characteristic time, and B is the constant of proportionality between deposit fouling resistance and resistance removal rate; $\phi_r=BR$.

More sophisticated assumptions are available in the literature; often these are for the more widely studied case of cooling water fouling (6).

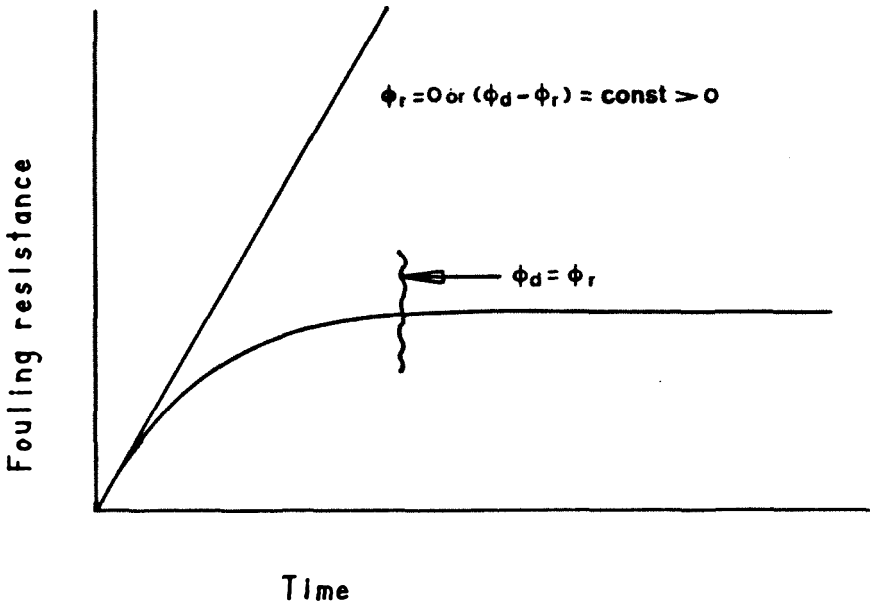

Figure 2.3. Build-up of fouling resistance predicted by the Kern-Seaton fouling model with no induction period. Adapted from Gupta (17).

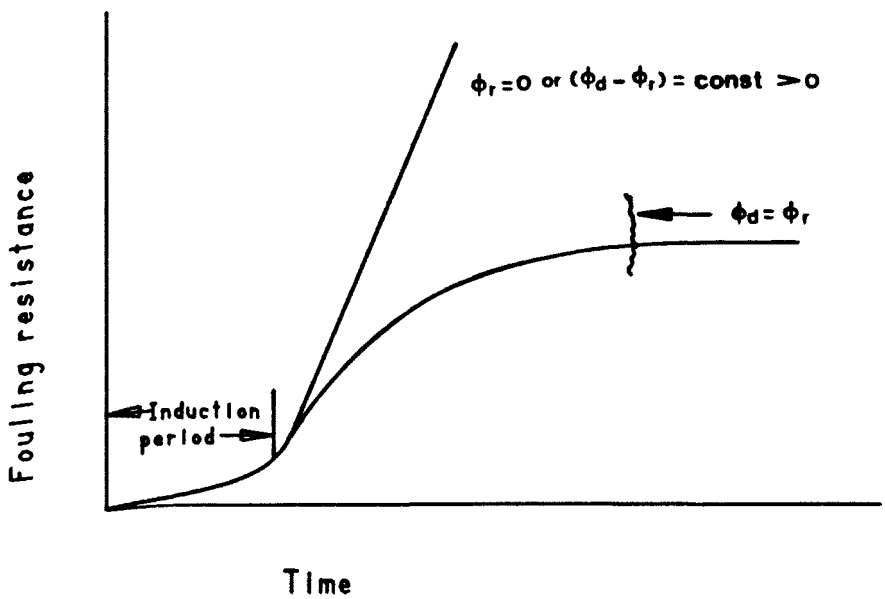

Figure 2.4. Buildup of fouling resistance predicted by the Kern-Seaton fouling model with an induction period that represents the time period before the fouling described by equation 2.11 begins. Adapted from Gupta (17).

2.4.3 MODELS BASED ON LABORATORY EXPERIMENTS

In many heat exchanger applications theoretical models do not provide effective estimates for fouling rates and resistances. "Real life" situations have large numbers of variables that are difficult to quantify; as a result, laboratory experimentation is often necessary to provide a basis for accurate fouling predictions.

Laboratory models of fouling processes are especially numerous for combustion systems using coal as a primary fuel. Coal is a common fuel that varies widely in composition; the ash-related fouling problems encountered when burning coal depend on the composition of the coal. Experimental work on coal ash fouling has been performed by a number of researchers (22-25).

In general, experimental work is used to obtain estimates of the fouling problems that will occur in full-scale systems without the expense of constructing full scale test units. One example is the analysis performed by Wenglarz (26), where data from particulate fouling of bench scale turbines were used to extrapolate to utility turbines. Another example of experimental work that can be used to model fouling in full scale units is the study of major fouling trends with respect to a fixed number of variables. Cohn (27) showed that deposition onto heat exchanger components from combustion products of residual fuel oil is a strong function of gas and metal temperature. In a similar study, the deposition rate for K_2SO_4 as a function of metal temperature was studied by Rosner and Atkins (28).

2.4.4 MODELS BASED ON DATA FROM IN-SERVICE UNITS

In some cases even laboratory-based programs are unable to recreate the fouling conditions of the in-service heat exchangers. This is most often due to the inability to accurately characterize the process streams, especially in cases of severe fouling such as process streams containing sooty diesel exhaust, coal ash fouling or solid waste combustion products. In these cases, on-site studies, often combined with some laboratory modeling, have been found to provide useful information for the design and operation of heat exchangers.

Examples are most numerous in the areas of large diesel engine waste heat recovery systems, such as those used in generation of electric power (29-34). Although it has been found that fouling and corrosion characteristics of diesel exhaust may be estimated from a knowledge of the fuel characteristics and the engine operating parameters, the necessity for testing actual heat exchanger elements in the sooty exhaust streams is not eliminated. Although generalization about fouling characteristics is difficult beyond the specific fuel and engine conditions tested, information about methods for deliberate deposit removal is more easily transferred from one installation to another. Techniques developed include steam lancing, chemically enhanced scale and soot removal, and high temperature baking. Henslee and Bogue (29) have carried out a general study of fouling in diesel exhaust streams. They concluded that the effect of diesel exhaust fouling on the necessary oversizing of a heat exchanger was found to be roughly independent of the quality of the fuel consumed with an asymptotic value for the fouling resistance, which

was reached more quickly with lower grade fuel. The oversizing required to accommodate fouling was found to increase heat exchanger surface area by a factor of 2.2 unless extensive steps were taken to remove deposits during on-line operation.

Chojnowski and Chew (35) found that on-site studies were necessary in their work with coal ash fouling of industrial rotary air heaters. Cleaning protocols were proving inadequate and pressure drops across the air heaters were often two or three times design values. Significant load reductions were required. On-site studies enabled development of a new configuration for the heater elements. The design has shown better fouling characteristics, lower pressure drops, and easier cleaning procedures.

Another example of a process gas stream that is difficult to recreate is found in the combustion of solid waste. Krause, Vaughan, and Boyd (36) studied the fouling and corrosion resistance of different materials exposed to such gas streams at large municipal incinerators. Nowak (37) studied the effects of corrosion on an entire electrical generating system with a view towards optimizing flow velocities and combustion conditions to reduce fouling deposits.

2.5 PARTICULATE FOULING OF HEAT EXCHANGERS

Particulate fouling in its simplest form can be broken down into three steps: (1) the physical mechanisms of particle transport to the heat transfer surface; (2) the attachment of these particles to the surface; and (3) the re-entrainment of previously deposited particles or groups of particles into the bulk fluid flow. Each of these steps will be discussed in the following sections.

2.5.1 MECHANISMS OF TRANSPORT TO THE SURFACE

Of the three steps mentioned above, the problem of particle transport to surfaces is the most well understood, with both experimental and theoretical work available in the literature. In a general situation, the mechanisms of particle transport may include inertial impaction, convective diffusion, sedimentation, thermophoresis, diffusiophoresis, electrophoresis, and vapor diffusion/condensation. Although any or all of these processes may be present in an industrial heat exchanger, this work is focused on inertial impaction.

As a particle in a moving fluid approaches an obstacle in the flow, its behavior will be influenced both by the nature of the flow field and by the inertial properties of the particle. A useful parameter to characterize this particle-obstacle interaction is the Stokes number, which can be thought of as a ratio of the inertial forces on the particle to the viscous forces it experiences. Thus, for large values of the Stokes number, inertial forces will predominate and impaction will occur, while for small values viscous forces will enable the particle to follow the fluid streamlines and move past the obstruction.

Consider a particle suspended in an air stream. As the airstream is diverted around an obstruction, the fluid streamlines bend around the object. But if the particle has sufficient inertia, it will be unable to follow the fluid streamlines exactly and instead will move relative to the fluid. The motion of the particle can be described by a force balance (38):

$$m\frac{d\underline{u}}{dt} = -f(\underline{u} - \underline{u}_f), \tag{2.13}$$

where m is the mass of the particle, $\underline{u}_f$ is the velocity of the fluid, $\underline{u}$ is the velocity of the particle, t is time, and f is the drag on the particle. For the simplest case, where the motion of the particle and the fluid do not differ greatly, the drag may be expressed by the Stokes law drag:

$$f = 3\pi\mu d_p. \tag{2.14}$$

Here μ is the dynamic viscosity of the fluid and d_p is the diameter of the particle. If one substitutes the Stokes form of the drag in Equation 2.13, assumes a spherical particle, and non-dimensionalizes with respect to U_∞, the freestream fluid velocity, and L, a characteristic length of the obstruction encountered by the particle (e.g., the radius of the heat exchanger tube), the resulting expression is

$$\mathrm{St}\frac{d\underline{u}'}{d\theta} = -(\underline{u}' - \underline{u}_f'), \tag{2.15}$$

where St is the Stokes number, $\theta = U_\infty t/L$ is the non-dimensional time, and $\underline{u}'$ and $\underline{u}_f'$ are the respective velocities non-dimensionalized with U_∞. The Stokes number is defined as

$$\mathrm{St} = \frac{\rho_p U_\infty d_p^2}{18\mu L} \tag{2.16}$$

The density of the particle is ρ_p, and the density of the fluid is ρ.

In most real cases, however, especially if the Stokes number is large, the relative speeds of the particle and fluid differ enough for the Stokes law drag to be an inadequate description of the situation. In this situation the most common solution is to parameterize the drag on the particle, f, in terms of a drag coefficient, C_D:

$$f = \frac{C_D(\mathrm{Re}_{p-local}) \cdot \mathrm{Re}_{p-local}}{24}(3\pi\mu d_p) \tag{2.17}$$

It should be noticed that here C_D and f are functions of the local particle Reynolds number:

$$\mathrm{Re}_{p-local} = \frac{d_p |\underline{u} - \underline{u}_f|}{\nu}, \tag{2.18}$$

where ν is the kinematic viscosity of the fluid. Since the particle Reynolds number, Re_p, is given by

$$\mathrm{Re}_p = \frac{d_p U_\infty}{\nu}, \tag{2.19}$$

it can be seen by combining (2.18) and (2.19) that

$$\mathrm{Re}_{p-local} = \mathrm{Re}_p |\underline{u}' - \underline{u}_f'|. \tag{2.20}$$

A typical correlation for C_D, applicable for Re <1000 is

$$C_D(\mathrm{Re}) = \frac{24}{\mathrm{Re}}(1 + 0.158\,\mathrm{Re}^{2/3}). \tag{2.21}$$

If one substitutes Equation 2.17 into Equation 2.13 and non-dimensionalizes again, the resulting expression is

$$\frac{d\underline{u}'}{d\theta} = -\frac{C_D(\mathrm{Re}_{p-local}) \cdot \mathrm{Re}_{p-local}}{24} \cdot \frac{1}{\mathrm{St}}(\underline{u}' - \underline{u}_f'). \tag{2.22}$$

This reduces correctly to Equation 2.15 for $\mathrm{Re}_{p\text{-}local} \ll 1$. However, for cases where the relative motion between the particle and the fluid is large and the Stokes law drag does not apply,

$$\frac{d\underline{u}'}{d\theta} = -\frac{C_D(\mathrm{Re}_p|\,\underline{u}' - \underline{u}_f'\,|) \cdot \mathrm{Re}_p}{24} \cdot \frac{1}{\mathrm{St}}|\,\underline{u}' - \underline{u}_f'\,|(\underline{u}' - \underline{u}_f'), \tag{2.23}$$

and it can be seen that particle impaction is determined by the Stokes number, the particle Reynolds number, and the nature of the flow field, $\underline{u}_f'$, above.

Brun et al. (39) have calculated theoretical capture efficiencies for impaction of particles in an inviscid flow field around a cylinder. Capture efficiency, η_R, is the fraction of the particles in the upstream cross-sectional area of the obstacle, which, in fact, impact on the collector. These calculations result in a family of curves, Figure 2.5, which present

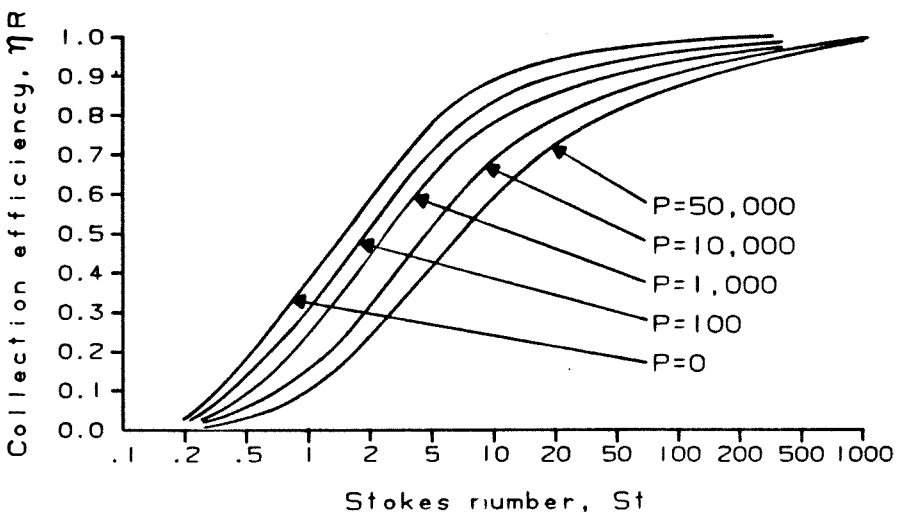

Figure 2.5. Collection efficiency for cylinders in an inviscid flow with point particles. The parameter, P, is defined as Re_p^2/St. The Stokes number is based on cylinder radius as the characteristic dimension of the collector. Adapted from Brun et al. (39).

collection efficiency as a function of the Stokes number and the parameter $P=Re_p^2/St$. In these calculations it has been assumed that all particles that come in contact with the cylinder are captured.

It would be convenient to be able to reduce the dependence of η_R from two dimensionless parameters, Re_p and St, to a single dimensionless group. By acknowledging that the conventional definition of the Stokes number underestimates particle drag at high Re_p, Rosner et al. (40) have developed a generalized or effective Stokes number, St_{eff}, expressed by

$$St_{eff} = \frac{4}{3}\left(\frac{\rho_p}{\rho}\right)\left(\frac{d_p}{L}\right)\int_0^{Re_p} \frac{d\,Re'}{C_D(Re')\cdot Re'}. \tag{2.24}$$

If one designates the function $\Psi(Re_p)$ as:

$$\Psi(Re_p) = \frac{24}{Re_p}\int_0^{Re_p} \frac{d\,Re'}{C_D(Re')\cdot Re'}, \tag{2.25}$$

then

$$St_{eff} = \Psi(Re_p)\,St, \tag{2.26}$$

and one can see that $\Psi(Re_p)$ represents the modification of the Stokes number to allow for non-Stokesian drag. Figure 2.6 shows $\Psi(Re_p)$ as a function of Re_p. It can be seen that for $Re_p << 1$, $\Psi(Re_p)$ approaches unity as required.

Rosner et al. have used the effective Stokes number to replot a modified collection efficiency graph from Brun's numerical simulations. It can be seen, Figure 2.7, that the family of curves in Figure 2.5 has been collapsed onto a single collection efficiency curve. Rosner et al. suggest an empirical fit to the curve in Figure 2.7 of the form:

$$\eta(St_{eff}) = [1 + 1.25\left(St_{eff} - \frac{1}{8}\right)^{-1} - (1.4 \times 10^{-2})\left(St_{eff} - \frac{1}{8}\right)^{-2} + (5.08 \times 10^{-5})\left(St_{eff} - \frac{1}{8}\right)^{-3}]^{-1}. \quad (2.27)$$

As before, all particles that were predicted to impact on the cylinder were assumed to stick.

2.5.2 PARTICLE ATTACHMENT

The phenomena that govern particle attachment to surfaces during particle impaction have not been explored as thoroughly as the transport problems discussed previously; no applications of such an analysis have yet been made to the problem of gas-side particulate fouling of heat exchangers. Usually the question is "answered" as in Section 2.5.1, by assuming "perfect sticking", i.e., that all particle-surface collisions result in particle capture. Although this assumption is very convenient (it leads to a zero concentration

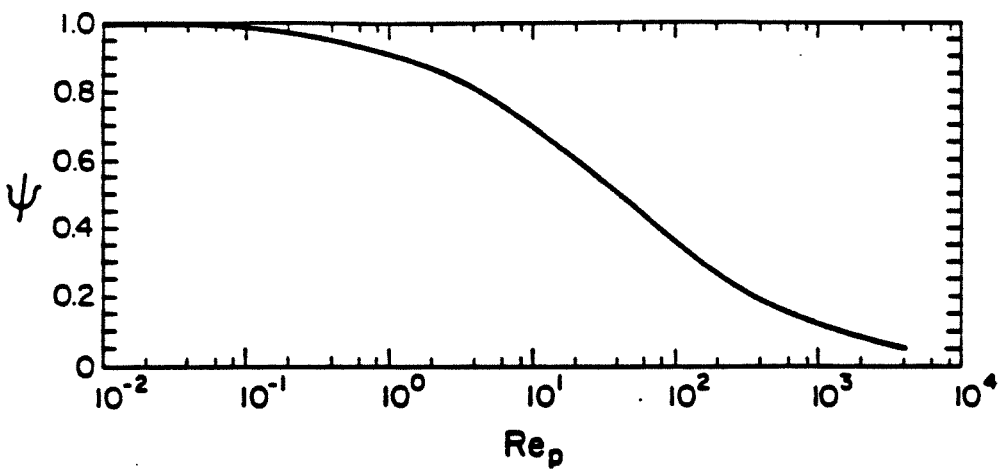

Figure 2.6. Modification factor for the Stokes number due to increases in particle drag. The effective Stokes number, St_{eff}, is given by $\Psi(Re_p)*St$. Adapted from Rosner et al. (40).

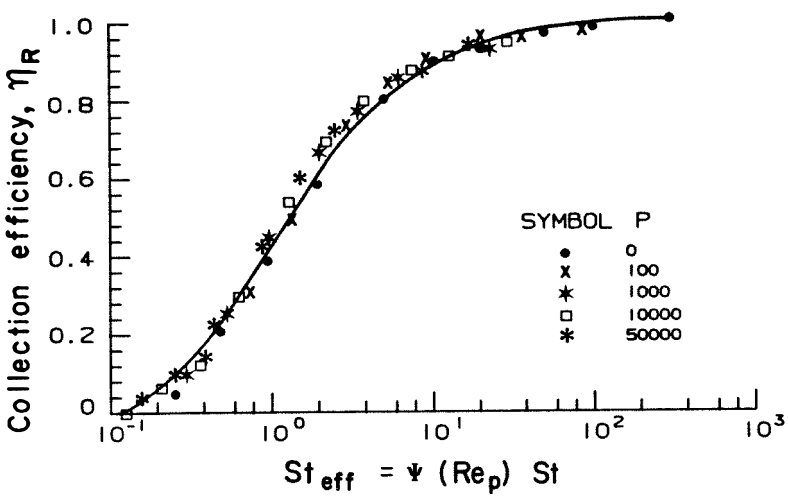

Figure 2.7. Correlation of capture efficiency behavior of a cylinder. Points plotted are theoretical predictions based on numerical integration of particle trajectories computed by Brun et al. (39). The Stokes number is based on cylinder radius as the characteristic dimension of the collector. Adapted from Rosner et al. (40).

boundary condition), that assumption has been shown to be inadequate to describe the many ranges of impact velocities, impact angles, and particle and surface properties, where particle bounce occurs (1,41-44). This section presents information on cases of particle bounce from the literature, followed by a discussion of the forces involved in particle attachment. The concept of a limiting incident velocity for particle capture is presented, together with a brief discussion of sticking probability functions.

2.5.2.1 EXAMPLES OF PARTICLE BOUNCE

Particle bounce is seen in many applications. Beal (41) has presented experimental data showing bounce in turbulent flows of hydrosols within pipes and channels. In this work, Beal employs the concept of a sticking probability for collisions, which varies between zero and one. Perfect sticking is represented by a probability of one; reductions in that probability indicate particle bounce.

D'Ottavio and Goren (42) examined impaction-dominated particle collection in packed beds. In this regime collection efficiency can be shown to be a function of the effective Stokes number. For experiments using liquid aerosol particles (which to a first approximation do not bounce), theoretical predictions can be used to model the experimental data well. For solid aerosol particles, however, collection efficiencies well below predicted values are found, indicating particle bounce.

Cascade impactors provide more evidence of particle bounce. These devices use inertial deposition to collect size separated aerosol samples. An air stream passes through a series of successively smaller jets. Each stream is impinged on a flat plate. Aerosol

particles are collected by inertial impaction with the largest particles removed in the lower velocity collisions that occur in the first few jets in the impactor. Successively smaller particles are removed in subsequent higher velocity stages. Cheng and Yeh (43) studied impaction on clean and greased impactor plates. For the greased plates, collection efficiencies increase with Stokes number to a maximum of 100% collection. For the clean plates the collection efficiency increases with Stokes number, reaches a maximum, and then decreases as the Stokes number increases even further. The decrease may be attributed to particle bounce, with the indication that the higher the incident velocity of the particle as it hits the collector, the greater the probability of bounce.

2.5.2.2 THE FORCES INVOLVED IN PARTICLE ATTACHMENT

One basic approach to the particle adhesion problem is to look at the particle-surface interaction from an energy viewpoint (45-49). Several different types of forces are involved. Adhesion is aided by van der Waals, electric double layer, capillary, and electrostatic forces, while repulsion is assisted by deformation of the particle (50). Chemical bonding between the particle and substrate may also occur (51). These interactive forces create a potential energy "well" with maximum depth E_i, which the incident particle will see as it approaches the surface, and another well with depth E_r (which may vary from E_i), which the reflected particle will see. In addition to the particle-surface forces discussed above, aerodynamic forces (drag and lift) exerted on the particle by the passing fluid can have a substantial effect on the retention of the particle by the surface (52,53).

By summing the energy terms that prevail in the particle/surface system (and neglecting aerodynamic effects-an approximation strictly valid only in a vacuum), one can calculate

a limiting velocity for particle capture, V_{ni}^{*}. This is the maximum normal incident velocity a particle can have (outside the potential well) and still stick (45). Each contributor to the particle/surface interaction will be discussed, followed by a discussion of the limiting velocity for particle capture. An estimate of the relative magnitudes of the interactive forces as a function of particle size is provided by Leong et al. (50).

2.5.2.2.1 VAN DER WAALS FORCES

The van der Waals force is an attractive force due to electrical field interactions between molecules. For the case of a spherical particle and a flat surface, the force is most easily obtained by using the textbook example of the van der Waals attraction between two spheres and letting the diameter of one sphere go to infinity. The result is (46,49):

$$F_{vdW} = -\frac{AR}{6z^2}, \tag{2.28}$$

where R and z are defined in Figure 2.8, and A is the Hamaker-van der Waals constant:

$$A = \pi^2 n_1 n_2 \lambda_{12}. \tag{2.29}$$

Here λ_{12} is the London-van der Waals constant between species 1 and 2, and n_1 and n_2 are the number densities of species 1 and 2, respectively. Expression (2.29) can be modified (46,49) to account for flattening of the particle and deformation of the substrate upon impact. The modified result is

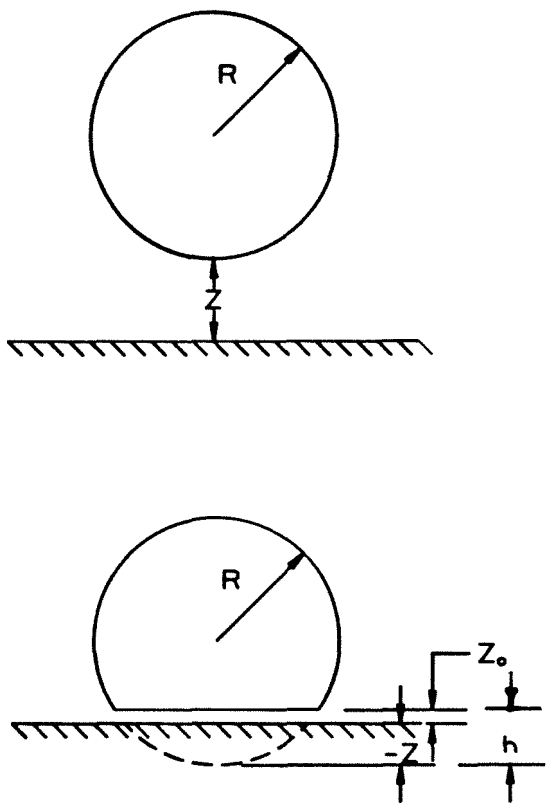

Figure 2.8. Coordinate convention for a particle of radius R approaching a surface located at distance Z from the particle's leading edge. The lower figure depicts the deformation of the particle during collision. Adapted from Dahneke (46).

$$F_{vdW} = \begin{cases} -\dfrac{AR}{6z_o}\left(1+\dfrac{2h}{z_o}\right) & , \quad h=(z_o-z)\geq 0; \\ -\dfrac{AR}{6z^2} & , \quad z \geq z_o. \end{cases} \tag{2.30}$$

Again, A is the Hamaker constant and the remaining parameters are defined in Figure 2.8.

2.5.2.2.2 ELECTRICAL DOUBLE LAYER

The electric double layer force is an attraction due to the contact potential difference between two interacting surfaces. When two materials with different electron work functions and local energy states (indications of how tightly the electrons are held) are brought together, electrons will be exchanged between the two. Initially, the different work functions result in different charge flows in each direction and a net charge transfer takes place. Eventually, the changed charge distribution results in equal charge flow in each direction and an equilibrium state is reached. Since, however, there has been a net transfer of charge, a contact potential difference, Φ, results. Φ ranges typically from 1 to 0.5 volts. For the case of a conductive particle and a grounded conductive surface, the attractive force is (49,54):

$$F_{edl} = -\frac{\pi \eta_a R \Phi^2}{z} \quad , \quad z \ll R, \tag{2.31}$$

where η_a is the permittivity of air, z and R are defined in Figure 2.8, and a constant potential difference, Φ, has been assumed. Krupp reviews the electric double layer force for several geometries (54).

2.5.2.2.3 CAPILLARY FORCES

Capillary forces result in an attraction when a thin film of some liquid is present between the particle and the substrate. This occurs most commonly when the relative humidity is high and condensation may occur on the particles or on the collection surface. It may also be used to model surfaces with sticky coatings such as melted deposits. This force can be expressed as (49,50):

$$F_{cap} = -4\pi\sigma_t R\cos\theta, \tag{2.32}$$

where σ_t is the surface tension of the liquid, R is defined in Figure 2.8, and θ is the contact angle of the particle and liquid.

2.5.2.2.4 ELECTROSTATIC FORCES

Electrostatic forces are attractive forces due to charges on the entire particle surface or substrate, usually arising from contact. For example, a conducting half-space seeing a particle carrying charge Q has an opposite charge induced on its surface and an attractive force results (49,54):

$$F_{es} = -\frac{Q^2}{\left\{16\pi\eta_a[\gamma+\frac{1}{2}\ln(\frac{2R}{z})]^2 RZ\right\}}, \tag{2.33}$$

where η_a is the permittivity of air, γ is Euler's constant and R and z are defined in Figure 2.8. For conducting materials, however, these induced excess charges and resulting attraction will be balanced by contact charge flow if the surfaces are brought in contact. Again Krupp (54) reviews electrostatic forces for various situations.

2.5.2.2.5 DEFORMATION

Deformation of the particle and substrate leads to a repulsive force given by (46)

$$F_{def} = \frac{4R^{1/2}}{3K} h^{3/2} \quad , \quad h \geq 0, \tag{2.34}$$

where $K=K_1+K_2$ is the sum of the bulk mechanical properties of the two materials. These are given for species i by (46)

$$K_i = \frac{(1-\nu_i)^2}{Y_i}, \tag{2.35}$$

where ν_i is Poisson's ratio and Y_i is Young's modulus for the species of interest.

2.5.2.2.6 CHEMICAL BONDING

Often the surfaces of the particle and substrate are chemically saturated, and formation of bonds across the interface is unusual (54). Under some conditions (high temperatures, readily polymerizable depositing material, etc.), however, bonding may play a role in the adhesion process (51). When this occurs, an additional term related to the bonding must be included in the consideration of forces.

2.5.2.2.7 OTHER FORCES

Other forces may be relevant, depending on the situation. Gravity provides a force acting toward the center of the earth given by

$$\begin{aligned} F_g &= -mg \\ &= -\frac{4}{3}\pi R^3 \rho_p g, \end{aligned} \tag{2.36}$$

where ρ_p is the density of the particle, R is defined in Figure 2.8, and g is the acceleration due to gravity. Depending on the orientation, gravity may act to aid or hinder adhesion or may have little effect. In any case, for particles less than about 20 μm in diameter, the force of adhesion due to gravity will be much less than the total force of adhesion for the system.

At extremely high temperatures, processes such as sintering, diffusive mixing, and alloy formation may occur (54-56). Sintering of two solid bodies causes an increase in their

adhesive area by means of recrystallization, diffusion, evaporation and recondensation, and creep. Elevated temperatures are generally required. Mutual diffusion of solids into one another and mutual dissolution leading to alloy formation also require high temperatures and special materials (54).

2.5.2.2.8 COEFFICIENT OF RESTITUTION

The coefficient of restitution, e, is defined as the ratio of normal particle velocity at the moment of rebound to that at the moment of contact. The coefficient of restitution is determined by energy losses during the particle-substrate collision. Such energy is dissipated in four principal ways:

(i) plastic deformation

(ii) "internal friction," resulting in the generation of heat when a material is subjected to a stress cycle

(iii) radiation of compressive, shear, and Rayleigh surface waves (i.e., acoustic waves) into the surface material

(iv) flexural work if the collection surface is a thin (flexible) body

Of these (ii) and (iii) usually have little effect on the value of (1-e), which is important to the particle capture limit calculation of Equation 2.41 in the following section of this review. For particles striking surfaces much larger than themselves, (iv) may be neglected, and with small areas of contact and relatively low incoming velocities (the

range of interest) (i) may be neglected. Thus, e for a solid particle is estimated to be of the order 0.99. In situations where processes (i) and (iv) above cannot be neglected, values of e significantly different from unity may occur (45).

2.5.2.3 LIMITING VELOCITY FOR PARTICLE CAPTURE

All of the force terms acting on a particle as it approaches a surface may be summed to provide the total force on the particle as a function of the distance between the particle and the surface. If one assumes that there is no interaction between the particle and the surface at very large distances, the expression for the total force can be integrated to give the potential energy for the particle-surface system as function of the separation z:

$$E(z) = -\int_{\infty}^{z} \left(\sum_{\text{forces}} F(z) \right) dz. \tag{2.37}$$

It should be noted that attractive forces are negative and repulsive forces are positive. Figure 2.9 shows a typical profile resulting from such calculations. The profile takes the shape of a potential energy well, which has a depth E. In general, the potential well seen by an incident particle will have depth E_i, while the potential well seen by a particle that has rebounded will have depth E_r, which will be different from E_i. Dahneke (45) describes a particle moving toward a surface with incident normal velocity v_{ni}, and incident normal kinetic energy KE_{ni}. Tangential velocity components are assumed to be conserved and are neglected. As the particle approaches the surface, it falls into the particle-surface potential well. If, after collision, the particle does not have sufficient kinetic energy to escape the potential well, it has been captured.

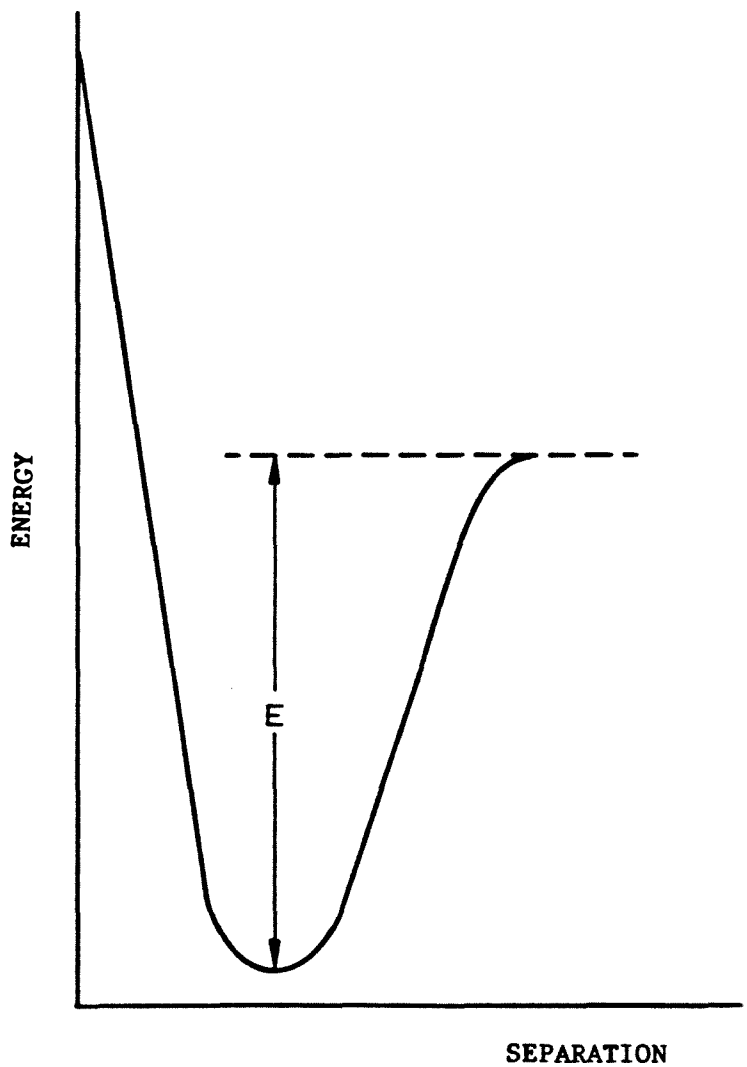

Figure 2.9. Typical interaction energy curve (potential well) for a solid particle-solid surface system. At infinite distance the interaction energy is 0. The curve is characterized by a depth, E.

At the moment of rebound, the kinetic energy, KE_{nr}, of the particle is

$$KE_{nr} = (KE_{ni} + E_i)e^2, \tag{2.38}$$

where e is the coefficient of restitution described in Section 2.5.2.2.8. Since capture occurs if $KE_{nr} \leq E_r$, a critical kinetic energy, KE_{nr}^*, may be defined to be that kinetic energy necessary for the particle just to climb out of the potential well:

$$KE_{nr}^* = E_r. \tag{2.39}$$

Combining 2.38 and 2.39 gives a critical incident kinetic energy, KE_{ni}^*, which the particle must have to avoid capture:

$$KE_{ni}^* = \frac{E_r - e^2 E_i}{e^2}. \tag{2.40}$$

Furthermore, substituting for KE_{ni}^* in terms of particle mass, m, and velocity, v_{ni}, gives a similar expression for the critical incident velocity v_{ni}^*:

$$v_{ni}^* = \left[\frac{2}{me^2}(E_r - e^2 E_i) \right]^{1/2}. \tag{2.41}$$

Thus, bounce (escape) will occur only for incident normal velocities greater than v_{ni}^*. If the further assumption is made that $E_i = E_r = E$, Equation 2.41 reduces to

$$v_{ni}^{*} = \left[\frac{2E}{m}\left(\frac{1-e^2}{e^2}\right)\right]^{1/2}. \qquad (2.42)$$

Both Equations 2.41 and 2.42 are themselves quite simple. It can be seen that for any given situation, there should be a value of the incident particle velocity above which the particle will bounce rather than stick; the difficulties arise in the determination of E_i, E_r, and e.

2.5.2.4 PARTICLE STICKING PROBABILITIES

The discussion of limiting velocity (Section 2.5.2.3) gives a deterministic prediction for particle rebound in an idealized situation. In real systems, some fraction of the particle-surface collisions result in actual particle capture. For a set of collisions between particles and a surface, one can define a sticking probability function, P_s, which will vary between zero and unity, depending on characteristics of the collisions. These characteristics include, but are not limited to, particle size, incident velocity and angle, particle and substrate material properties, collision geometry, contamination on particle or substrate surfaces, and temperature. Little is known about the detailed dependence of P_s on these factors, although general trends may be established from analysis and experimental data. Beal (41,57) has discussed a theoretical fouling model that introduces the sticking probability. See Section 2.5.2.1.

2.5.3 DEPOSIT REMOVAL

Deposit removal can be regarded in two ways: first, the aerodynamic considerations of re-entrainment that occur naturally in an undisturbed heat exchanger, and second, the

augmented removal schemes necessary to deliberately clean off large deposits that have accumulated within a heat exchanger during normal service. If the interactive forces between a particle and substrate are not large, the fluid or air stream passing over the particle deposit may lift it away from the surface. If, on the other hand, particle-surface attraction is strong, large and firmly attached deposits may occur. In these cases some sort of removal protocol is necessary; several are discussed.

2.5.3.1 PARTICLE RE-ENTRAINMENT

Hydro- or aerodynamic drag and lift forces acting on a particle may be sufficient to remove the particle from a surface. Less is known, however, about the problems of particle re-entrainment than about particle attachment. The situation can be examined from a macroscopic or a microscopic point of view.

Kern and Seaton (20) have demonstrated the dependence of particle removal on wall shear stress with a macroscopic analysis. They postulate that the rate of removal of deposited material is proportional to the wall shear stress and the thickness of the deposit layer:

$$\phi_r = K_1 \tau_w x. \tag{2.43}$$

Here ϕ_r is the rate of removal of heat transfer resistance due to deposit removal, τ_w is the wall shear stress, and x is the deposit thickness. The proportionality constant, K_1, may be thought of as related to the strength of the deposit. Taborek et al., (9,10) modified Equation 2.43 to give:

$$\phi_r = K_2 \frac{\tau_w}{\psi} x^m, \tag{2.44}$$

where ψ is a function of the deposit structure and m and K_2 are addition parameters that may be fit to experimental data. For the special case of cooling water fouling with few suspended solids they found that ψ is a function of fluid velocity only. Their analysis was not extended to the gas-side fouling problem. Suitor et al. (11) also demonstrated the connection between wall shear stress and deposit removal by examining experimental data to show that there is a critical value of the wall shear stress that must be exceeded before particle removal rates will equal particle deposition rates and asymptotic fouling will occur.

The microscopic approach was used by Corn and Silverman (58) and Corn and Stein (59) to examine the drag and lift of particles attached to filter collection surfaces. By assuming that the particles were small enough to be submerged in the laminar sublayer of the flow around the surfaces, they postulated that the drag force on a single particle could be described by

$$F = C\rho U^2 \frac{A}{2}, \tag{2.45}$$

and that the lift on a roughly spherical particle would be negligible compared to the drag force above. In Equation 2.45, C is the drag coefficient, A is the cross-sectional area of the particle, U is the fluid velocity, and ρ is the fluid density. Standard fluid mechanics texts give methods for calculating C (correlated with the particle Reynolds number, Re_p)

and U. Integration of F over the projected area of the particle is necessary, since U and C are not constant. Theory and experiment agree for high removal efficiencies (75% and above).

Corn and Stein also gathered data showing that particle removal by an airstream is time-dependent. They attributed this to the penetration of the laminar sublayer by turbulent eddies. This idea was further developed by Cleaver and Yates (52,53,60) to postulate the lifting forces due to these bursts. From these predictions, a particle removal criterion based on the wall shear stress, T_w, can be obtained. A particle will be detached from a surface by aerodynamic forces. if

$$T_w d^{4/3} \geq \beta, \tag{2.46}$$

where d is the particle diameter and β is a constant related to the particle-substrate adhesive forces. No further development of methods for predicting the value of β has been made.

2.5.3.2 AUGMENTED REMOVAL

Most augmented removal schemes tend to be mechanical in nature, although some success has also been achieved with sonic horns and chemical additives. Soot blowers are the most common way of dealing with gas-side fouling and have the added advantage of being operational while the equipment is on line. Two main types are available, the rotary soot blower and the long-retractable type (61-64). Rotary soot blowers are essentially multinozzled elements mounted permanently in the exchanger with a rotating

nozzle for each tube row. Unfortunately, since the nozzle element is permanently mounted in the exchanger, it may be subjected to some of the same fouling and corrosion problems as the exchanger elements. The long-retractable type soot blower consists of an extendable arm or lance with two nozzles at the end. The lance can be rotated and drawn back and forth to direct concentrated cleaning as needed. It may be protected by being retracted when not needed. Both types of blowers may use compressed air, steam, or a mixture of steam and water (65).

High energy sonic horns provide a non-intrusive method of cleaning heat exchangers. Low (20Hz) or high (250Hz) frequency horns are available, which loosen the particles so they may be carried away by the process stream (66,67). Other on-line cleaning procedures include cold water jets, sudden process stream temperature and velocity changes, flow reversals, and the use of elevated metal temperatures (68,69).

Severely fouled heat exchangers require off-line cleaning as well. Typically plain water or water with chemical cleaning agents is used to dissolve soluble compounds and (hopefully) dislodge other deposits (70-73). As a last resort, mechanical cleaning is employed. Methods include use of tube scrapers for plugged tubes and scrapers for shell side cleaning (75,75). Partial dismantling and chiseling by hand are also employed (76). Long periods of down time may be required for off-line cleaning of hardened deposits.

2.6 SUMMARY

Section 2.5.1 describes a detailed theoretical development for the mechanics of inertial deposition of aerosol particles. Most of this theory has been worked out in the context of

the aerosol mechanics literature, and little experimental confirmation is available. When data are available (43), they are for flow regimes and geometries of interest for inertial impactors, not for heat exchangers. The question of particle attachment and bounce is addressed in Section 2.5.2. Again, detailed microscopic theories are available in the literature with scarce experimental confirmation.

Section 2.4 discusses the largely empirical development of models for heat exchanger fouling in the heat transfer literature. In most cases limited theoretical development has been used to provide a basis for correlation of experimental data. Most of the work done has been in the area of cooling water fouling.

The experiments described in Chapters 4, 5, and 6 were chosen to provide a bridge between these two bodies of knowledge. The single tube deposition experiments in Chapter 4 were chosen to attempt to verify the model discussed in Section 2.5.2.3 and to attempt to quantify particle bounce for particles impacting on a cylinder in cross-flow (a common heat exchanger geometry). The transient experiments described in Chapter 5 were designed to examine the effect of particle bounce on the build-up of deposits. Interest was focused on the possibility that increased flow velocities would promote particle bounce and extend the length of time before clean tubes would begin to accumulate deposits. Chapter 6 describes a set of experiments studying particle deposition through tube banks. Of special interest was the possible applicability of filter models from the aerosol mechanics literature to the close-packed geometry of a compact heat exchanger.

2.7 BIBLIOGRAPHY

1. Beal, S.K., Particulate fouling of heat exchangers. Presented at the International Conference on Fouling of Heat Exchanger Surfaces, White Haven, PA (1982).

2. Bemrose, C.R. and Bott, T.R., Theory and practice in gas-side particulate fouling of heat exchangers. Presented at the International Conference on Fouling of Heat Exchanger Surfaces, White Haven, PA (1982).

3. Epstein, N., Fouling in heat exchangers, Proceedings of the Sixth International Heat Transfer Conference, 6, 235-253, Washington, D.C. (1979).

4. Epstein, N., Fouling: Technical aspects (afterword to fouling in heat transfer exchangers), Fouling of Heat Transfer Equipment, Hemisphere, Washington, D.C. (1981), pp. 31-53.

5. Gudmundsson, J.S., "Particulate Fouling," in Somerscales, E.F.C., and Knudsen, J.G. (Editors), Fouling of Heat Transfer Equipment, Hemisphere, Washington, D.C., (1981), pp. 357-387.

6. Knudsen, J.G., "Fouling of heat exchangers: are we solving the problem?" Donald Q. Kern Award Lecture before the 21st. National Heat Transfer Conference, Seattle, WA July 24-27 (1983).

7. Lister, D.H., "Corrosion Products in Power Generating Systems," in Somerscales, E.F.C., and Knudsen, J.G. (Editors), Fouling of Heat Transfer Equipment, Hemisphere, Washington, D.C., (1981), 135-200.

8. Stearns, C.A., Kohl, F.J. and Rosner, D.E., Combustion system processes leading to corrosive deposits, Report No. NASA TM-81752, NASA Lewis Research Center, Cleveland, OH (1981).

9. Taborek, J., Aoki,T., Ritter, R.B., Palen, J.W. and Knudsen, J.G., Fouling: The major unresolved problem in heat transfer, Chemical Engineering Progress, 68, 2, 59-67 (1972).

10. Taborek, J., Aoki, T., Ritter, R.B., Palen, J.W. and Knudsen, J.G., Predictive methods for fouling behavior, Chemical Engineering Progress, 68, 7, 69-78 (1972).

11. Suitor, J.W., Marner, W.J., and Ritter, R.B., The history and status of research in fouling of heat exchangers in cooling water service, The Canadian Journal of Chemical Engineering, 55, 374-380 (1977).

12. Cooper, A., Suitor, J.W., and Usher, J.D., Cooling water fouling in plate heat exchangers, Heat Transfer Engineering, 1, 3, 50-55 (1980).

13. Kays, W., Convective Heat and Mass Transfer, McGraw Hill, N.Y. (1966).

14. Holman, J.P., Heat Transfer, McGraw Hill, N.Y. (1981)

15. Krieth, F., Principles of Heat Transfer. 2d ed., International Textbook Co., London, England (1965).

16. Thackery, P.A., The cost of fouling in heat exchanger plant, Effluent and Water Treatment Journal, 20, 112-115 (1980).

17. Gupta, J.P., Fouling of heat exchanger surfaces, Chemical Age India, 29, 1, 33-40 (1978).

18. Kuznetsov, V.A., Selecting gas velocities and optimum profiles for the convective surfaces in steam boilers taking fouling into account, Thermal Engineering, 16, 8, 68-72 (1969).

19. Rogalski, R.D., Fouling effects of turbine exhaust gases on heat exchanger tubes for heat recovery systems, SAE Transactions, 88, 3, 2223-2239 (1979).

20. Kern, D.Q., and Seaton, R.E., "A Theoretical Analysis of Thermal Surface Fouling," British Chemical Engineering, 4, 258-262 (1959).

21. Crittenden, B.D. and Kolaczkowski, S.T., Energy savings through the accurate prediction of heat transfer fouling resistances, Energy for Industry, A Collection of Science and Engineering Papers Concerned with Utility Energy with Maximum Efficiency in Industry, Pergamon Press, New York (1979).

22. Lin, C.J. and Winegartner, E.C., Coal ash fouling test in a laboratory furnace, ASME Paper No. 81-JPGC-Fu-8. Presented at the Joint ASME/IEEE Power Generation Conference, St. Louis, MO (1981).

23. Wynnyckyj, J.R. and Rhodes, E., Mechanisms of furnace fouling, Heat Exchangers: Theory and Practice, Hemisphere, Washington, D.C., (1983), pp. 817-831.

24. Tufte, P.H. and Beckering, W., A proposed mechanism for ash fouling burning northern Great Plains lignite, ASME Journal of Engineering for Power, 97, 407-412 (1975).

25. Wibberly, L.J. and Wall, T.F., Alkali-ash reactions and deposit formation in pulverized-coal-fired boilers: experimental aspects of sodium silicate formation and the formation of deposits, Fuel, 61, 93-99 (1982).

26. Wenglarz, R.A., Evaluations of particulate fouling in gas turbines and fuel cells. Presented at the International Conference on Fouling of Heat Exchanger Surfaces, White Haven, PA (1982).

27. Cohn, A., Effect of Gas and Metal Temperatures on Gas Turbine Deposition, ASME Paper 82-JPGC-GT-4 (1982).

28. Rosner, D.E. and Atkins, R.M., Experimental studies of salt/ash deposition rates from combustion products using optical techniques. Presented at the International Conference on Experimental Research into Fouling and Slagging Due to Impurities in Combustion Gases, Engineering Foundation, Henniker, New Hampshire (1981).

29. Henslee, S.P. and Bogue, J.L., Fouling of a Finned-Tube Heat Exchanger in the exhaust of a stationary diesel engine: final report, DOE contract No. DE-AC07-76ID01570, Idaho National Engineering Laboratory, Idaho Falls, ID (1983).

30. Engle, P.K., Thompson, R.E. and Silvestrini, R., Corrosion and fouling potential in diesel exhausts, ASME Journal of Engineering for Power, 101, 598-606 (1979).

31. DeAnda, E., Heat exchanger fouling and corrosion evaluation, Report No. 81-18003, AiResearch Manufacturing Company of California, Torrance, CA (1981).

32. Niggeman, R.E. and Greenlee, W.J., The design, performance and operating experience of the heat transfer equipment in the Sundstrand 600 KW organic rankine bottoming cycle, Advancement in Heat Exchangers, International Centre for Heat and Mass Transfer 1981 Summer Seminar, Dubrovnik, Yugoslavia (1981).

33. Greenlee, W.J. and Berger, R.E., Gas-side fouling experience in the waste heat boiler of a 600 KWe organic rankine bottoming cycle. Presented at the International Conference on Fouling of Heat Exchanger Surfaces, White Haven, PA (1982).

34. Berger, R.E., Fouling and acid corrosion of an organic rankine bottoming system vaporizer exposed to diesel engine exhaust, Easton, Maryland, Sundstrand Engineering Report No. AER 1835, Sundstrand Aviation Operations, Rockford, IL (1980).

35. Chojnowski, B. and Chew, P.E., Getting the best out of rotary air heaters, Central Electricity Generating Board Research, 7, 14-21 (1978).

36. Krause, H.H., Vaughan, D.A. and Boyd, W.K., Corrosion and deposits from combustion of solid waste, Part III: effects of sulfur on boiler tube metals, ASME Journal of Engineering for Power, 97, 448-452 (1975).

37. Nowak, F., Considerations in the construction of large refuse incinerators, Proceedings of the National Incinerator Conference, Cincinnati, OH, 86-92 (1970).

38. Friedlander, S.K., Smoke, Dust and Haze, John Wiley, New York (1977).

39. Brun, R.J., Lewis, W., Perkins, P.J., and Serafini, J.S., Impingement of cloud droplets on a cylinder and procedure for measuring liquid-water content and droplet sizes in supercold clouds by rotating multicylinder method, Report 1215, 141-183 (1955).

40. Rosner, D.E., Gokoglu, S. and Israel, R., Rational correlations of diffusional and inertial particulate deposition behavior in nonisothermal forced convection environments. Presented at the International Conference on Fouling of Heat Exchanger Surfaces, White Haven, PA (1982).

41. Beal, S.K., Correlations for the sticking probability and erosion of particles, Journal of Aerosol Science, 9, 455-461 (1978).

42. D'Ottavio, T., and Goren, S.L., Aerosol capture in granular beds in the impaction dominated regime, Aerosol Science and Technology, 2, 91-108 (1983).

43. Cheng, Y-S., and Yeh, H-C., Particle bounce in cascade impactors, Environmental Science and Technology, 13, 1392-1396 (1979).

44. Gillespie, T., On the adhesion of drops and particles on impact at solid surfaces, I., Journal of Colloid Science, 10, 266-280 (1955).

45. Dahneke, B., The capture of aerosol particles by surfaces, Journal of Colloid and Interface Science, 37, 342-353 (1971).

46. Dahneke, B., The influence of flattening on the adhesion of particles, Journal of Colloid and Interface Science, 40, 1-13 (1972).

47. Dahneke, B., Measurements of bouncing of small latex spheres, Journal of Colloid and Interface Science, 45, 584-590 (1973).

48. Esmen, N. A., Ziegler, P., and Whitfield, R., The adhesion of particles upon impaction, Journal of Aerosol Science, 9, 547-556 (1978).

49. Bowling, R. A., An analysis of particle adhesion on semiconductor surfaces, Journal of the Electrochemical Society: Solid State Science and Technology, 132, 2208-2214 (1985).

50. Leong, K. H., Stukel, J. J., and Hopke, P. K., Effects of surface properties of collectors on the removal of charged and uncharged particles from aerosol suspensions, Pub. No. 81-2, Advanced Environmental Control Technology Research Center, Urbana, Illinois (1981).

51. Bott, T. R., and Walker, R. A., Fouling in heat transfer equipment, The Chemical Engineer, 255, 391-395 (1971).

52. Cleaver, J.W. and Yates, B., Mechanism of detachment of colloidal particles from a flat substrate in a turbulent flow, Journal of Colloid and Interface Science, 44, 464-474 (1973).

53. Cleaver, J.W. and Yates, B., The effect of reentrainmnt on particle deposition, Chemical Engineering Science, 31, 147-151 (1976).

54. Krupp, H., Particle adhesion. Theory and experiment, Advances in Colloid and Interface Science, 1, 111-238 (1967).

55. Zimon, A. D., Adhesion of Dust and Powder, Plenum Press, New York (1969).

56. Gronhovd, G.H., Beckering, W. and Tufte, P.H., Study of facts affecting ash deposition from lignite and other coals, ASME Paper No. 69-WA/CD-1. Presented at ASME Winter Annual Meeting, Los Angeles, CA (1969).

57. Beal, S.K., Deposition of particles in turbulent flow on channel or pipe walls, Nuclear Science and Engineering, 40, 1-11 (1970).

58. Corn, M., and Silverman, L., Removal of solid particles from a solid surface by a turbulent air stream, American Industrial Hygiene Association Journal, 22, 337-347 (1961)

59. Corn, M. and Stein, F., Re-entrainment of particles from a plane surface, American Industrial Hygiene Association Journal, 26, 325-336 (1965).

60. Cleaver, J.W. and Yates, B., A sub-layer model for the deposition of particles from a turbulent flow, Chemical Engineering Science, 30, 983-992 (1975).

61. DiCarlo, J.T., Guidelines aid in application, operation of soot blowers, The Oil and Gas Journal, 77, 19, 88-96 (1979).

62. Flitner, D.P., A heavy fuel fired heat recovery steam generator for combined cycle applications, ASME Paper No. 75-Pwr-30. Presented at the ASME-IEEE Joint Power Generation Conference, Portland, OR (1975).

63. Ots, A.A. and Suurkuusk, J.N., Heat absorption and corrosive-erosive platen superheaters when employing steam lancing, Combustion, 48, 2, 33-37 (1976).

64. MacDuff, E.J., and Clark, N.D., Ljungstrom air preheater design and operation--Part II: Corrosion and fouling, Combustion, 47, 9, 24-30 (1976).

65. Shenker, J.D., White, A.R. and Ziels, B.D., Water tempered cleaning medium for sootblowers, ASME Journal of Engineering for Power, 103, 561-565 (1981).

66. Marner, W.J. and Webb, R.L., Workshop on an assessment of gas-side fouling in fossil fuel exhaust environments, Report No. 82-67, Jet Propulsion Laboratory, California Institute of Technology, Pasadena, CA (1982).

67. Berlant, M.J. and Schwartz, J.A., An application summary of high energy sonic cleaning applied to electrostatic precipitators. Presented at the Third Symposium on the Transfer and Utilization of Particulate Control Technology, Orlando, FL (1981).

68. Roberts, P.B. and Marron, H.D., Soot and the combined cycle boiler, ASME Paper No. 79-GT-67. Presented at the Gas Turbine Conference and Exhibit and Solar Energy Conference, San Diego, CA (1979).

69. Roberts, P.B. and Kubasco, A.J., Combined cycle steam generator gas side fouling evaluation, Report No. SR79-R-4557-20, Solar Turbines International, San Diego, CA (1979).

70. Roddy, C.P., Maintaining clean heat exchangers, Power, 119, 3, 56-58 (1975).

71. Loucks, C.M., and Groom, C.H., Chemical cleaning of heat-exchanger equipment, ASME Paper No. 48-A-113. Presented at the annual meeting, New York, N.Y., (1949).

72. Butler, R.C., McCurdy, W.N., and Linden, N.J., Fouling rates and cleaning methods in refinery heat exchangers, ASME Paper No. 48-A-117. Presented at the Annual Meeting, New York, N.Y. (1949).

73. Dougherty, P.F., and Brooks, C.H., Cleaning tubular heat exchangers, ASME Paper No. 48-A-116. Presented at the annual meeting, New York, N.Y. (1949).

74. John, A., The mechanical cleaning of fouled heat-exchanger tubes, ASME Paper No. 48-A-114. Presented at the annual meeting, New York, N.Y. (1949).

75. Weiland, J.H., McCay, R.C. and Barnes, J.E., Rates of fouling and cleaning of unfired heat-exchanger equipment, ASME Paper No. 48-A-112. Presented at the annual meeting, New York, N.Y. (1949).

76. Marner, W.J., An assessment of gas-side fouling in cement plants, Report No. 82-83, Jet Propulsion Laboratory, California Institute of Technology, Pasadena, CA (1982).

3 EXPERIMENTAL

3.1 EQUIPMENT

A wind tunnel has been constructed to expose model heat exchanger elements to a particle laden air stream under carefully controlled conditions. As seen in Figure 3.1, inlet air is passed through a High Efficiency Particulate Air (HEPA) filter to remove pre-existing particles from the supply (room) air. Particles with known properties are generated, introduced into the wind tunnel, and passed through a test section that holds the heat exchanger models. A second filter placed downstream from the test section is used to capture those particles that do not adhere to the heat exchanger models. By comparison of the number of particles deposited on the heat exchanger model to the number of particles that passed through the system to the after filter, it is possible to determine overall particle collection efficiency for a specific heat exchanger geometry at a given particle size and air flow rate. A variable speed motor connected to a centrifugal fan draws air through the system and permits system operation at a variety of fluid velocities and hence at a variety of values of the Stokes number. The fan exhausts to a fume hood.

3.1.1 PARTICLE GENERATION

Particles are generated using a Berglund-Liu Model 3050 vibrating orifice aerosol generator manufactured by Thermo-Systems, Inc. (1) with an accompanying Harvard Apparatus syringe pump. Using this system, a monodisperse aerosol can be produced. Solid ammonium fluorescein particles are produced, since they can be detected using spectrophotofluorimetric methods. See Section 3.2.5. The techniques used are quite sensitive and allow for the measurements of small quantities (nanograms) of particulate

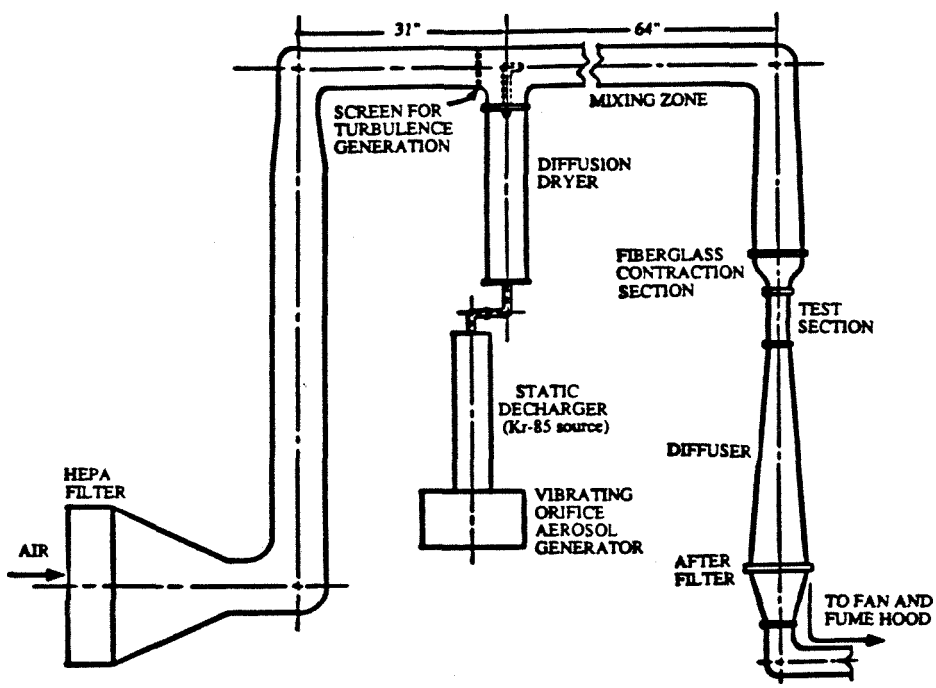

Figure 3.1. Aerosol processes wind tunnel and particle generation equipment.

matter deposited on the heat exchanger sections. Particles have been collected and examined with a scanning electron microscope to verify particle size and morphology. See Section 3.2.1. The particles used in this work ranged from approximately 4.5 to 5.5 micrometers in diameter.

To produce particles using a vibrating orifice aerosol generator (VOAG), the substance from which the particles will be made is dissolved in a volatile solvent. The solution is then passed through a small (typically 10-50 micron) orifice, producing a liquid jet. A piezoelectric crystal driven by a signal generator is attached to the orifice plate, causing it to vibrate at a controlled frequency. These vibrations break the liquid jet into uniform size droplets. See Figure 3.2. The diameter of the droplets is given by

$$d_d = \left(\frac{6Q}{\pi f}\right)^{1/3}, \tag{3.1}$$

where Q is the liquid flow rate and f is the vibration frequency. These droplets then dry, and since each droplet contains an equal amount of the solute, uniform size particles are formed with diameter d_p (1):

$$d_p = C^{1/3} d_d = \left(\frac{6Q\,C}{\pi f}\right)^{1/3}, \tag{3.2}$$

where C is the solution concentration.

The liquid feedstock used for particle generation in these experiments was composed of

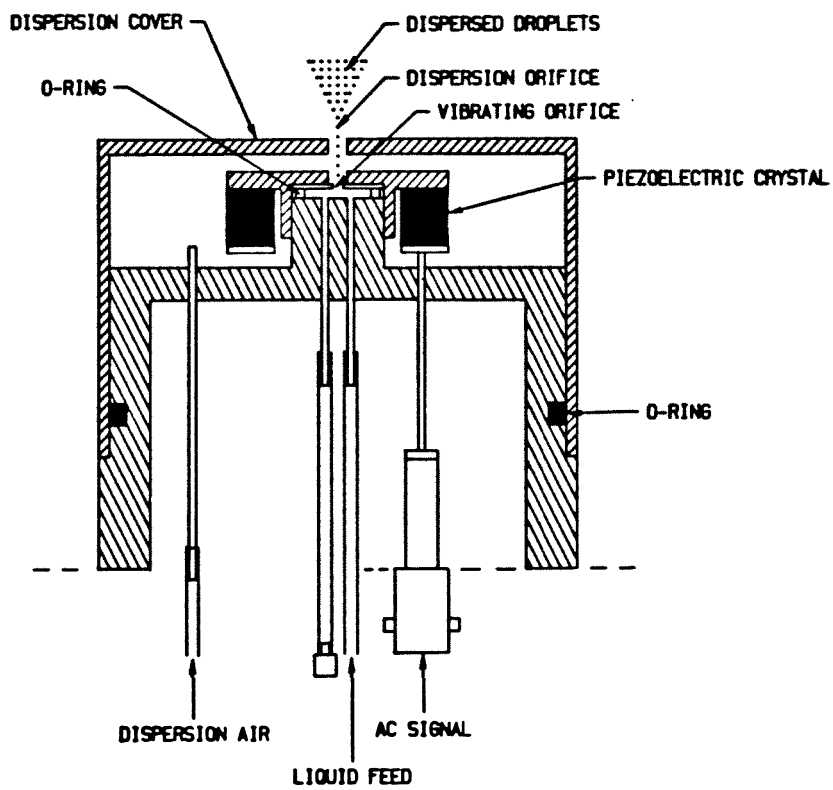

Figure 3.2. Berglund-Liu model 3050 vibrating orifice aerosol generator. Adapted from Thermo-Systems, Inc. (1).

1.58 grams of ammonium fluorescein (1.50 grams of fluorescein) dissolved in a mixture of 20% pure isopropanol and 80% dilute ammonium hydroxide solution (approximately 0.1 molar) to make 1 liter of solution. Fluorescein is readily available in two forms, a hydrophobic powder (MW=332.2) and a hydrophilic powder, which is actually sodium fluorescein (MW=376.28). The hydrophobic fluorescein was used since the hydrophilic sodium fluorescein produces droplets that dry very slowly under the conditions of these experiments. To dissolve the hydrophobic fluorescein powder, it is necessary to provide a basic solution, such as dilute ammonium hydroxide. When using ammonium hydroxide solution to dissolve fluorescein (formula: $C_{20}H_{12}O_5$) a replacement occurs with an ammonium ion (NH_4^+) replacing a single H from the fluorescein molecule. The particles formed in the subsequent drying process will be ammonium fluorescein ($C_{20}H_{15}O_5N$, MW=349.2, ρ=1.35g/cm^3). It is recommended (2) that the molarity of the ammonium hydroxide solution be at least twice that required by the stoichiometry of the dissolution.

To generate particles in the 4.5 to 5.5 micrometer range, a 20 micron orifice was used, with the signal generator frequency set between approximately 45 and 80 kHz. A 60 ml plastic disposable syringe was used with the syringe pump set to produce an approximate flow rate of 0.21 cm^3/min. These combinations of frequencies and flow yielded a single stable jet through the orifice. To produce dry, electrically neutral particles, it was also necessary to pass the droplets through a static decharger and a diffusion drying column. The static decharger (Thermo-Systems, Inc. model 3054) consists of a Kr-85 source that produces ionizing radiation. As particles pass through the decharger, they accumulate a balanced complement of positive and negative ions. The diffusion dryer consists of a 10.8 centimeter (4.25 inch) diameter plexiglass tube with a wire screen of 5.08 centimeter

(2 inch) diameter concentrically placed inside. Large 4-8 mesh silica gel fills the annulus between the plastic tube and the screen, and the particle-laden air stream passes axially through the passage formed by the screen. See Figure 3.3.

Since the syringe pump used is calibrated for use with glass syringes, its stated flow deliveries can be used only as a guide to eventual particle size when plastic syringes are used. Final determination of particle diameter is made using a scanning electron microscope. See Section 3.2.1.

3.1.2 WIND TUNNEL

After passing through the static decharger and diffusion dryer, the particles are introduced upstream from the test section. Particle injection occurs immediately downstream from a turbulence grid designed to promote mixing of the particles with the main air supply. At this point the flow is contained within a 20.32 centimeter (8 inch) horizontal cylindrical galvanized steel duct. After 8 duct diameters (64 inches or 152.56 cm), the flow makes a 90 degree turn and passes downward through a metal round-to-square transition followed by a fiberglass contraction. The fiberglass contraction accelerates the flow just before it enters the clear plexiglass test section. The test section is 17.78 cm (7 inches) in the direction of flow and has a square cross section, which is 4.76 centimeters (1.875 inches) on a side.

Stainless steel heat exchanger tubes are mounted in the test section. They are supported by fitting the ends of the tubes into matching holes drilled in removable plexiglass panels that snap into opposite sides of the test section. The stainless steel tubes have an outside

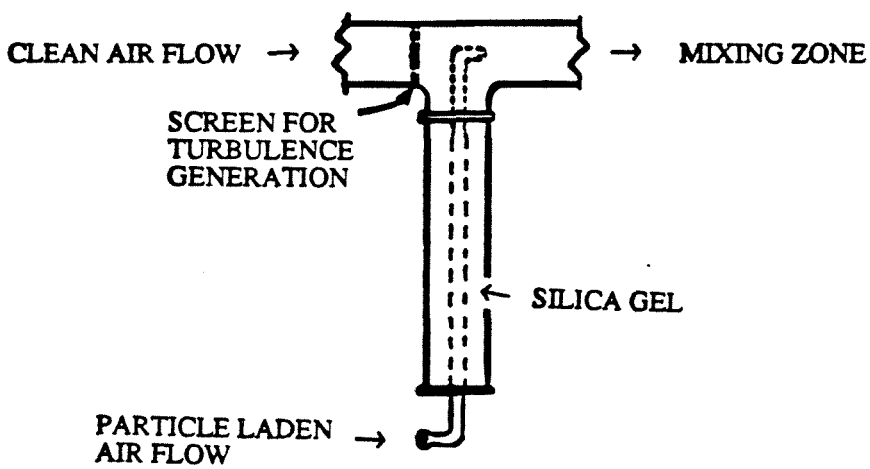

Figure 3.3. Diffusion dryer.

diameter of 0.25 inch (0.635 cm), chosen on the basis of an actual compact heat exchanger design (3). See Figure 3.4. Single tubes and staggered or in-line tube bundles can be inserted into the test section and then removed for analysis.

A pair of pressure taps located across the fiberglass contraction are connected to a manometer. See Figure 3.5. The manometer is calibrated against pitot tube readings in the test section. By this means the air velocity upstream of the heat exchanger models can be monitored during the experiments. The variable speed fan provides air velocities in the empty test section that range from a minimum velocity of 1489 ft/min (756 cm/sec) to a maximum of 9820 ft./min (4989 cm/sec). At these velocities, flow in the test section is turbulent, but the Mach number is much less than 1.

After passing the test section, the flow enters a diffuser, which expands to a standard 8 by 10 inch filter holder. A double thickness of fiberglass air conditioning filter material is placed in the filter holder to capture particles that do not deposit on the models in the test section. A single layer of filter material is 95% effective for collection of 5 micrometer diameter particles; a double layer was used to achieve more than 99% collection efficiency for these particles.

3.2 PROCEDURE

3.2.1 PARTICLE SAMPLING PROCEDURE

Before each set of experiments, a sample of the aerosol particles was collected for determination of particle diameter by scanning electron microscopy (SEM). To do this, a section of flexible tubing was run into the test section and then connected to a standard

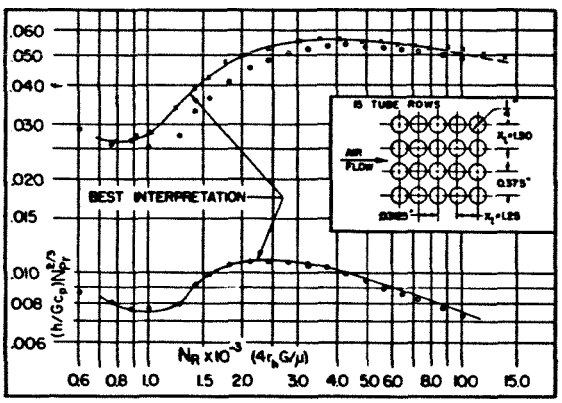

Tube outside diameter - 0.250 in.
Hydraulic diameter, $4r_h$ = 0.166 ft
Free-flow area/frontal area, σ = 0.338
Heat transfer area/total volume, α = 80.4 ft^2/ft^3

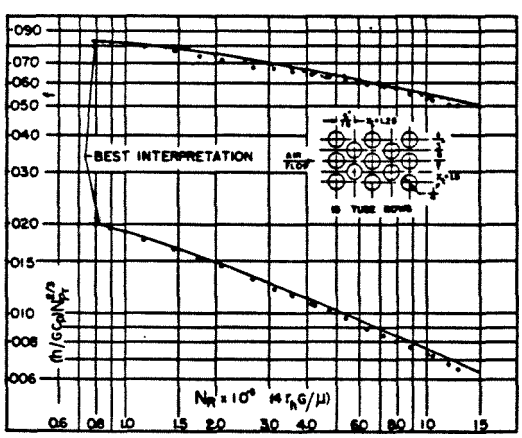

Tube outside diameter = 0.250 in.
Hydraulic diameter, $4r_h$ = 0.0166 ft
Free-flow area/frontal area, σ = 0.333
Heat transfer area/total volume, α = 80.3 ft^2/ft^3
Note: Minimum free-flow area is in spaces transverse to flow.

Figure 3.4. Heat transfer and flow friction data for two compact heat exchanger tube banks. Geometries correspond to those used in the test section of the aerosol processes wind tunnel. Adapted from Kays and London (3).

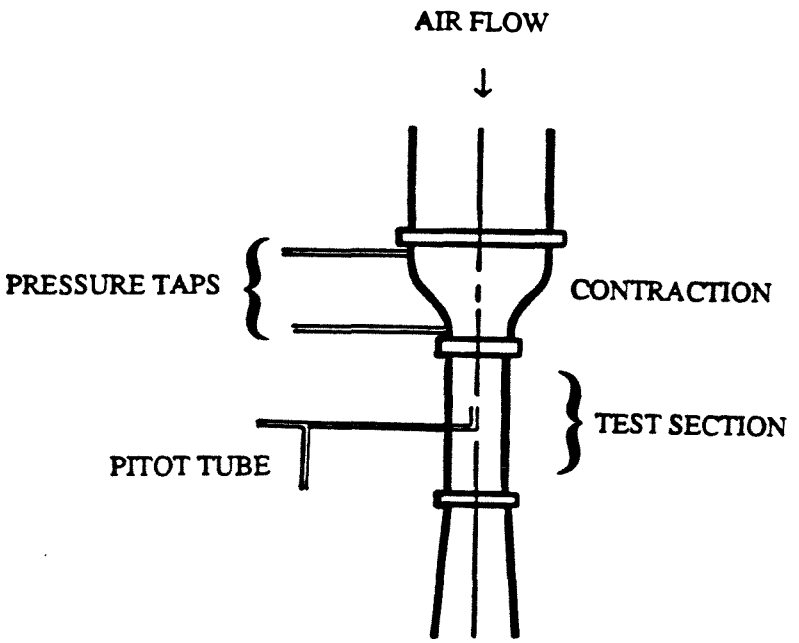

Figure 3.5. Pressure taps across contraction and pitot tube in test section. The pitot tube was used to calibrate the pressure taps and was removed during particle depostion experiments.

47 mm filter holder. A 47 mm diameter nucleopore filter with 0.4 micrometer pore size was used in the filter holder, and the flow was controlled by means of a critical orifice located downstream from the filter holder. The filter assembly was attached to a vacuum pump and the aerosol was sampled for approximately 30 minutes. Preparation of the samples for SEM examination involved cutting a small segment from the middle of the filter and attaching it to an SEM stub. Since it was necessary to provide a conductive path to the top of the filter which would be coated with a 10 angstrom coating of gold and palladium for use in the SEM, the filter segment was attached to the stub by "tacking" it at each corner with a colloidal silver suspension (Ted Pella, Inc.). After the previously mentioned coating was applied, the samples could be examined to verify that the particles were monodisperse and dry, and to determine an exact particle diameter.

3.2.2 TUBE PREPARATION

A standard cleaning procedure was followed to prepare the stainless steel heat exchanger tubes for use in the wind tunnel. Each tube was washed in toluene, then washed in dilute ammonium hydroxide, and then washed in distilled water. The tubes were allowed to dry in air at least overnight. For experiments with clean, ungreased tubes, the tubes were used as they were after the cleaning procedure. For runs with greased tubes, the tubes were dipped in a 2% solution of Vaseline in toluene and allowed to dry for at least four hours before use.

3.2.3 EXPERIMENTAL PROCEDURE

To initiate a series of experiments, the vibrating orifice aerosol generator (VOAG) was brought up according to recommended procedure (1). The sampling equipment described in Section 3.2.1 was placed in the test section. The variable speed motor and fan were

turned on to draw air through the wind tunnel, and the outlet of the VOAG was connected to the wind tunnel to allow particles to pass through the system. A particle sample was taken for SEM analysis. The particle generator outlet was then disconnected from the wind tunnel and the motor was turned off. The sampling equipment was removed. The desired tube or tubes were placed inside the test section and sealed, a fresh set of fiberglass filters was placed in the 8 by 10 inch filter holder, and the motor was turned on. After the desired air flow velocity was established, the VOAG outlet was reconnected to the wind tunnel and the experiment began. After the desired length of time the particle generator outlet was disconnected and the motor turned off (in that order). The filters and tubes were then removed and stored for later analysis and a new experiment was begun. The particle generator was kept running continuously throughout a set of experiments for consistency, and a vent line was provided to the fume hood for the particles produced when the VOAG outlet was not connected to the wind tunnel.

3.2.4 DEPOSIT EXTRACTION

In each experiment, ammonium fluorescein particles were collected on stainless steel tubes and fiberglass after filters. The mass of particles collected on the tubes and filters was found by a procedure involving extraction of the ammonium fluorescein in a known volume of dilute ammonium hydroxide solution, followed by determination of the concentration of the fluorescein solution using a spectrophotofluorimeter. Then for the monodisperse aerosols used, the number of particles collected was readily determined from the mass of the deposited material. Since two types of tubes were used, clean and greased, two different extraction procedures were necessary for removal of the deposits from the tubes. Details follow.

3.2.4.1 UNGREASED TUBES

For the clean tube experiments, each tube was agitated in 10 ml of 0.1 molar sodium hydroxide solution in a test tube. Agitation was on a small mechanical shaker table for approximately 30 minutes. The resulting solution was drawn off for spectrophotofluorimetric analysis.

3.2.4.2 GREASED TUBES

For the greased tubes, a slightly more complicated procedure was required. First, it was necessary to strip the grease and embedded fluorescein particles from the tubes with an organic solvent (toluene); then the fluorescein particles were dissolved in an aqueous phase (dilute ammonium hydroxide solution) for measurement. The first step involved two washes of the greased tube in enough toluene to cover the tube in a 125 ml Erlenmeyer flask. During each wash cycle the flask was agitated for approximately 30 minutes on a small shaker table, and then the extract was transferred to a ground glass stoppered 125 ml Erlenmeyer flask. The vaseline is soluble in the toluene; however, the fluorescein particles, although stripped from the tube along with the vaseline, do not dissolve. Preparation of a solution suitable for analysis was then accomplished by agitating the toluene washes with 25 ml of 0.1 molar sodium hydroxide solution. The ground glass stoppered flask was sealed by wrapping twice with teflon tape and then with parafilm. Agitation was for approximately 10 minutes on a larger, more vigorous shaker table. Although a sonicater may be used for the earlier washes, it is not recommended for the interphase transfer, because an emulsion is formed during sonication, which takes several days to separate. Since the fluorescein is readily soluble in the sodium hydroxide solution, but the aqueous and organic phases are immiscible, the ammonium fluorescein

was then found in the aqueous phase. After a settling period, the aqueous phase was drawn off and the fluorescein concentration determined spectrophotofluorimetrically as for the clean tubes.

3.2.4.3 FILTERS

In each case the number of particles on the after filters must also be determined. This is accomplished by extracting the filters in 400 ml of 0.1 molar sodium hydroxide solution. Once again, agitation was on a small mechanical shaker table for approximately 30 minutes. The resulting solution was drawn off and passed through a Gelman Sciences Acrodisc 0.45 micrometer filter to eliminate after filter fibers from the solution before spectrophotofluorimetric analysis.

3.2.5 SPECTROPHOTOFLUORIMETRIC ANALYSIS

Solution concentrations were determined using an Aminco-Beckman Spectrophotofluorimeter (SPFM). When a solution of ammonium fluorescein is excited at 325 nm, the strength of its subsequent emission at 510 nm is directly proportional to the solution concentration. By using several standards prepared with known concentrations of ammonium fluorescein for calibration, the concentrations of the test solutions may be determined. The SPFM is quite sensitive and can accurately detect fluorescein concentrations of nanograms per milliliter.

3.3 DATA REDUCTION AND ANALYSIS

From the solution concentrations (SPFM readings) and the known size of the monodisperse aerosol (see Section 3.2.1 above), the mass of the deposit and number of particles on each tube or filter may be determined, as well as the total number of aerosol particles

entering the test section:

$$M_{t \text{ or } f} = C \; S_{t \text{ or } f} \tag{3.3}$$

$$N_{t \text{ or } f} = \frac{M_{t \text{ or } f}}{(\rho \pi d_p^3/6)} \tag{3.4}$$

$$N_{tot} = \frac{M_f + M_t}{(\rho \pi d_p^3/6)} = \frac{M_f + \sum_{tubes} M_i}{(\rho \pi d_p^3/6)}, \tag{3.5}$$

where M is the mass of the ammonium fluorescein deposit, S is the volume of ammonium fluorescein solution, C is the concentration of the solution, ρ is the mass density of solid ammonium fluorescein, and N is the number of ammonium fluorescein particles. The subscripts f, t, and tot refer to filter, tubes, and total, respectively.

For many of these experiments, a relevant quantity is the collection efficiency. For any general collector, the collection efficiency is defined as the number of particles deposited on the collector divided by the number of particles in the upstream cross-sectional projected area of the collector. For a single tube in cross-flow, the collection efficiency is the ratio of the number of particles actually collected on the tube to the total number of particles present in the upstream projected cross-sectional area of the tube. Since the cross-sectional area of the test section is 7.5 times the cross-sectional projected area of a tube, the number of particles in the upstream cross-sectional area swept by the tube is found to be:

$$N_{cross-section} = \frac{N_{tot}}{7.5}, \tag{3.6}$$

and since the number of ammonium fluorescein particles deposited on the tube is known, the collection efficiency of the tube is easily determined:

$$\eta_R = \frac{N_t}{(N_{tot}/7.5)}. \tag{3.7}$$

In practice the linear relationship between fluorescence, solution concentration, mass of deposit, and number of monodisperse particles is used to simplify the data reduction (see Section 3.2.6):

$$\begin{aligned} \eta_R &= \frac{N_t}{(N_{tot}/7.5)} \\ &= \frac{7.5M_t}{M_{tot}} \\ &= \frac{7.5\,S_t C_t}{S_t C_t + S_f C_f} \\ &= \frac{7.5\,S_t KR_t}{S_t KR_t + S_f KR_f} \\ &= \frac{7.5\,S_t R_t}{S_t R_t + S_f R_f}, \end{aligned} \tag{3.8}$$

where R is the magnitude of the SPFM reading, and K is the constant of proportionality between the signal and the solution concentration (C=K*R) as determined by the calibration using standard fluorescein solutions. As used in equation 3.8, the products S_tC_t, S_tKR_t, and S_tR_t represent the sums over all tubes, i, of the products S_iC_i, S_iKR_i, and S_iR_i, respectively.

3.4 ESTIMATION OF ERRORS

Errors in gathering of data were of three types: errors in determination of particle size (diameter), errors in estimation of upstream air flow velocity, and errors in determination of solution volume and concentration. Each is discussed.

Particle diameter was determined by use of the scanning electron microscope using the procedure described in Section 3.2.1. The results produced were photographs of particles samples. Magnification was chosen so that particles could be large enough to measure, yet small enough that typically five to seven particles were included in the photograph. A 10 micron calibrated bar was included in each photograph. Particle diameters and the calibration scale were measured with a clear ruler with a scale marked in fiftieths of an inch. The image of a particle of approximately five microns was typically 10 to 15 units (fiftieths of an inch) depending on the magnification selected. The 10 micron bar was typically 20 to 30 units long. Measurements were made to the nearest 0.25 unit. Thus, errors in particle diameter determination could be as large as 2.8%.

Upstream flow velocities were determined by calibrating the manometer readings for a set of pressure taps in the contraction against the velocity readings from a pitot tube in the test section. See Figure 3.5. Since the air flow velocity is linearly proportional to the square root of the pressure drop, a linear regression was used to determine the relationship between the square of the air flow velocity and the pressure tap manometer readings. The square of the correlation coefficient, R^2, was determined to be 0.99. The manometer attached to the pressure taps could be read to an accuracy of approximately 7.0%. Thus, the maximum error in air flow velocity measurement is on the order of 5.0%.

Solution concentrations were determined using the Aminco-Beckman Spectrophotofluorimeter (SPFM). The SPFM was calibrated for each data set, using five standard concentration solutions ranging from 7.90×10^{-9} g/ml to 1.58×10^{-6} g/ml. Since the emission signal strength is a linear function of solution concentration, it is possible to use a linear regression to determine the relationship between the two. The square of the correlation coefficient, R^2, was always at least 0.99 for each set of data processed. Errors in reading the emission signal strength on the SPFM meter were approximately 1.0% and thus a worst-case error in determination of solution concentration is 1.4%. In addition, error in measuring extraction solution volume is approximately 0.1%.

These errors in measurements result in errors in the derived results, the Stokes numbers and the collection efficiencies. By examining how these quantities are calculated and by using the percent errors determined above, it is possible to estimate maximum possible errors in the Stokes number to be 6.4% and in the collection efficiencies to be 2.0%.

3.5 BIBLIOGRAPHY

1. Instruction Manual for Model 3050 Berglund-Liu Vibrating Orifice Monodisperse Aerosol Generator, Thermo-Systems, Inc., St. Paul, MN.

2 Vanderpool, R. W., and Rubow, K. L., Generation of large, solid, monodisperse calibration aerosols, TSI Quarterly, X, 1, 3-6 (1984).

3. Kays, W.M., and London, A.L., Compact Heat Exchangers, McGraw-Hill, New York, 1964.

4 SINGLE TUBE BOUNCE EXPERIMENTS

In this section, the problem of particle bounce off a single heat exchanger tube in cross-flow is examined both experimentally and theoretically. Using the aerosol processes wind tunnel described in Figure 3.10 and Section 3.1.2, experiments have been conducted to examine the interaction of particles in a gas stream with both greased and ungreased tubes. Using these results, experimental values for the collection efficiencies as a function of St_{eff} have been calculated. See Section 2.5.1. A computer program has been developed which plots particle trajectories in flow approaching a single tube. Using this program, greased tube collection efficiencies are modeled well. If a critical incident particle velocity normal to the tube surface at the point of tube-particle collision is assumed as a criterion for particle bounce, ungreased tube behavior is also modeled.

4.1 EXPERIMENTAL RESULTS

4.1.1 GREASED TUBES

Two sets of experimental data have been generated. The first set of experiments used greased tubes and was intended to mimic the situation in which all particles that hit the tube will stick. Data were generated for a range of St_{eff} from 0.25 to 0.98. Particles were produced with diameters between 4.35 and 5.47 microns, and flow velocity was varied over a range from 756 to 4989 cm/sec (1489 to 9820 ft/min) to achieve the different effective Stokes numbers. In each experiment, a 0.635 cm (0.25 inch) diameter stainless steel tube was exposed to particle-laden air for a period of 5 minutes. This run time was chosen to give a very light (0.3 %) coverage of deposited particles over the front face of the tube so that incoming particle interaction would be with the tube rather than with

other particles already captured by the tube. Collection efficiencies ranged from 0.05 to 0.41. Experimental conditions and collection efficiency calculation results are given in Table 4.1. Experimental data are plotted in Figure 4.1. It can be seen that the data show a gradual increase in the particle collection efficiency of the tube with increasing effective Stokes number. This is to be expected for the "perfect sticking" case since increasing St_{eff} indicates an increasing dominance of inertial over viscous forces on the particle and thus a reduced ability of particles to follow the fluid streamlines around the tube (see Section 2.5.1). As the effective Stokes number increases, more particles hit the tube and since the tube is greased to mimic "perfect sticking" more particles stick. Refer to Chapter 3 for more details on experimental procedure.

4.1.2 UNGREASED TUBES

The second set of data was collected with clean tubes and was intended to quantify the phenomenon of particle bounce off cylinders. Data were generated for a range of St_{eff} from 0.19 to 1.09. Particles were produced with diameters between 4.73 and 5.29 microns, and flow velocity was varied over a range from 1489 to 9820 ft/min (756 to 4989 cm/sec) to achieve the different effective Stokes numbers. As for the greased tubes, each experiment lasted five minutes. In this case, only a fraction of the particles that strike the clean tube surface actually stick, and much lower collection efficiencies are observed, ranging from 0.01 to 0.12. Experimental conditions and collection efficiency calculation results are given in Table 4.2. Experimental data are also plotted in Figure 4.1. From a comparison of the two sets of data, it can be seen that for small effective Stokes numbers (e.g., less than 0.3), the greased and ungreased tube cases yield similar collection efficiencies. This implies that the particles that strike the tube are sticking and

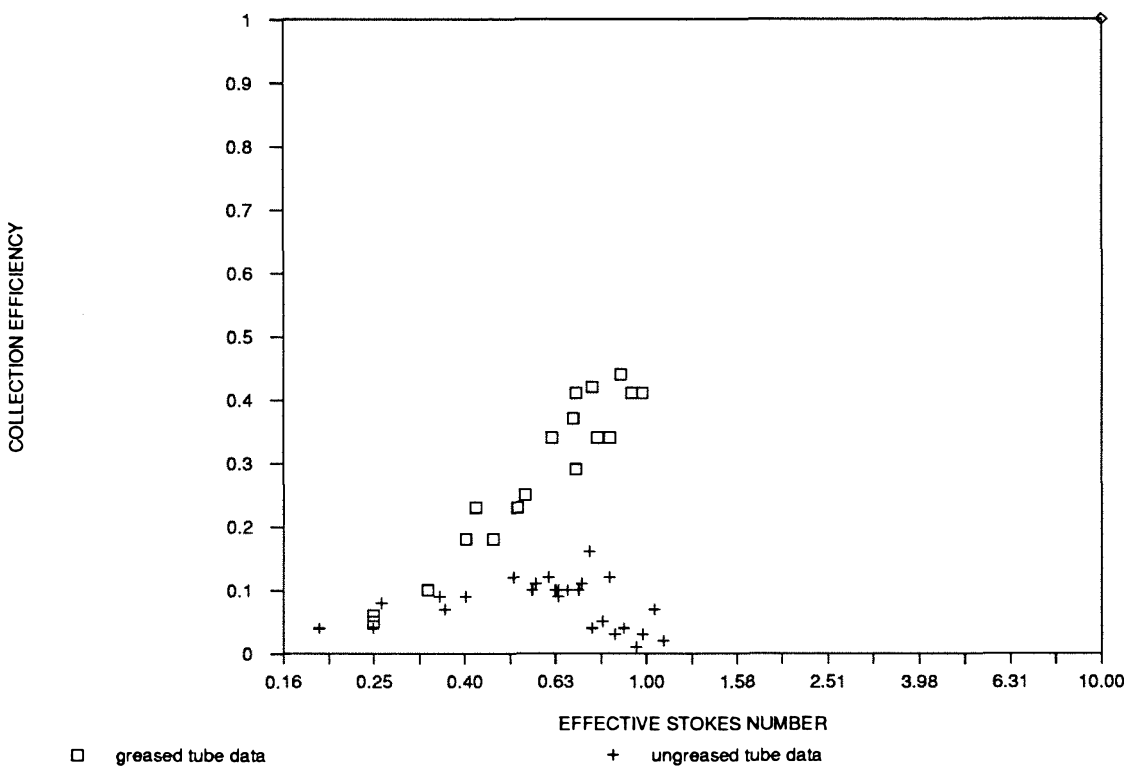

Figure 4.1. Experimental results: collection of approximately 5 micrometer diameter solid ammonium fluorescein particles on 0.635 centimeter diameter stainless steel heat exchanger tube in cross flow.

TABLE 4.1. EXPERIMENTAL DATA FOR COLLISIONS OF SOLID AMMONIUM FLUORESCEIN PARTICLES WITH UNGREASED STAINLESS STEEL TUBES IN CROSS-FLOW

St_{eff}	COLLECTION EFFICIENCY	PARTICLE DIAMETER (10^{-4} cm)	UPSTREAM FLUID VELOCITY (ft/min)	UPSTREAM FLUID VELOCITY (cm/sec)
0.19	0.04	4.77	1489	756
0.25	0.04	4.73	1980	1006
0.26	0.08	4.77	2118	1076
0.35	0.09	4.77	2909	1478
0.36	0.07	5.00	2706	1375
0.40	0.09	5.08	3004	1526
0.51	0.12	4.77	4514	2293
0.56	0.10	5.00	4560	2316
0.57	0.11	4.77	5214	2649
0.61	0.12	5.00	5104	2593
0.63	0.10	4.73	5927	3011
0.64	0.10	4.76	6299	3200
0.64	0.09	4.76	6299	3200
0.67	0.10	4.77	6254	3177
0.71	0.10	5.08	5831	2962
0.72	0.11	5.00	6204	3152
0.75	0.16	5.00	6520	3312
0.76	0.04	4.77	7378	3748
0.80	0.05	5.00	7118	3616
0.83	0.12	5.08	7183	3649
0.85	0.03	4.77	8520	4328
0.89	0.04	4.73	9100	4623
1.09	0.02	5.29	9224	4686

TABLE 4.2. EXPERIMENTAL DATA FOR COLLISIONS OF SOLID AMMONIUM FLUORESCEIN PARTICLES WITH GREASED STAINLESS STEEL TUBES IN CROSS-FLOW

St_{eff}	COLLECTION EFFICIENCY	PARTICLE DIAMETER (10^{-4} cm)	UPSTREAM FLUID VELOCITY (ft/min)	UPSTREAM FLUID VELOCITY (cm/sec)
0.25	0.05	4.35	2371	1204
0.25	0.06	4.73	1980	1006
0.33	0.10	4.35	3361	1707
0.40	0.18	5.08	3004	1526
0.42	0.23	4.73	3683	1871
0.46	0.18	4.35	4935	2507
0.52	0.23	4.35	5733	2912
0.54	0.25	4.35	5975	3035
0.62	0.34	4.73	5831	2962
0.69	0.37	5.00	5879	2987
0.70	0.41	4.35	8180	4155
0.70	0.29	5.08	5733	2912
0.76	0.42	4.35	9037	4591
0.78	0.34	5.47	5633	2862
0.83	0.34	5.08	7183	3649
0.88	0.44	4.73	9037	4591
0.93	0.41	5.00	8553	4345
0.98	0.41	5.08	8750	4445

that particle bounce is negligible. As St_{eff} increases, however, more particles strike the tube, but fewer particles stick. This can be seen in Figure 4.1 as the divergence of the ungreased tube data from the greased tube results. This divergence increases with St_{eff} until, for the largest effective Stokes numbers studied here, virtually no particles are captured. It is clear that at the lower effective Stokes numbers examined the collection efficiency is limited by the number of particles that strike the tube, while at higher effective Stokes numbers, the collection efficiency is limited by particle bounce. Again, refer to Chapter 3 for more details on experimental procedure.

4.2 ANALYSIS

4.2.1 TRAJECTORY GENERATION

A computer program that is capable of calculating particle trajectories in an inviscid flow field around a cylinder has been developed, using a procedure similar to that of Brun et al. (1). Particles far upstream of the tube are assumed to have the freestream velocity of the fluid. As the particles approach the tube, the inertia of the particles causes them to move relative to the fluid, and their trajectories are calculated, using Equation (2.23). The flow field is assumed to be independent of the presence of the particles, a reasonable assumption for a light aerosol loading. With this program, particle trajectories can be calculated, using initial particle positions from the stagnation streamline outward, until the starting position of the marginal particle that just misses collision with the tube is determined. See Figure 4.2. This procedure determines the fraction of the particles in the upstream cross-sectional area of the tube that will strike the tube. This defines the collection efficiency for the perfect sticking case. In addition, for particles that strike the cylinder, it is possible to estimate the magnitude of the impact velocity as well as its

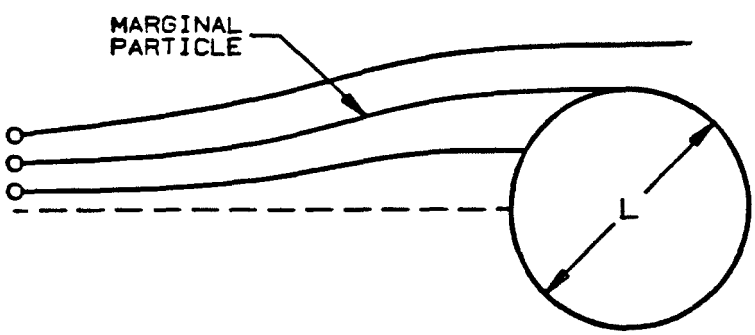

Figure 4.2. Typical trajectories for solid particles approaching a cylinder in cross-flow. Paths shown include a particle which is unable to follow streamlines around the tube and strikes the tube, a particle which passes the tube and the marginal particle which just strikes the tube at its outermost edge.

normal and tangential components. A small enough time step was used during trajectory integration that the predicted collection efficiency was no longer sensitive to changes in the step size.

Following the suggestions of Rosner et al. (2), the theoretically predicted particle collection efficiency for a tube in cross-flow has been plotted in Figure 4.3 for the case of perfect sticking, using the effective Stokes number as a parameter. Figure 4.3 shows the approximately 190 points generated for a range of particle sizes and upstream velocities. A smooth curve drawn through the theoretically predicted points is also shown.

4.2.2 GREASED TUBES

The smoothed theoretically predicted curve from Figure 4.3 has been transferred to Figure 4.4. Greased tube data are superimposed, showing that the computer program effectively predicts the experimental results.

4.2.3 UNGREASED TUBES

4.2.3.1 CRITICAL VELOCITY CURVES

The prediction of greased tube collection efficiencies can be extended to an analysis of the collection efficiency of clean tubes as well. Cheng and Yeh (3) have documented particle bounce for the case of a flat plate in a cascade impactor. As discussed in Chapter 2, Dahneke (4-6) has postulated the existence of a critical particle velocity normal to the collection surface, V_{ni}^{*}, above which particle bounce will occur. He has also noted

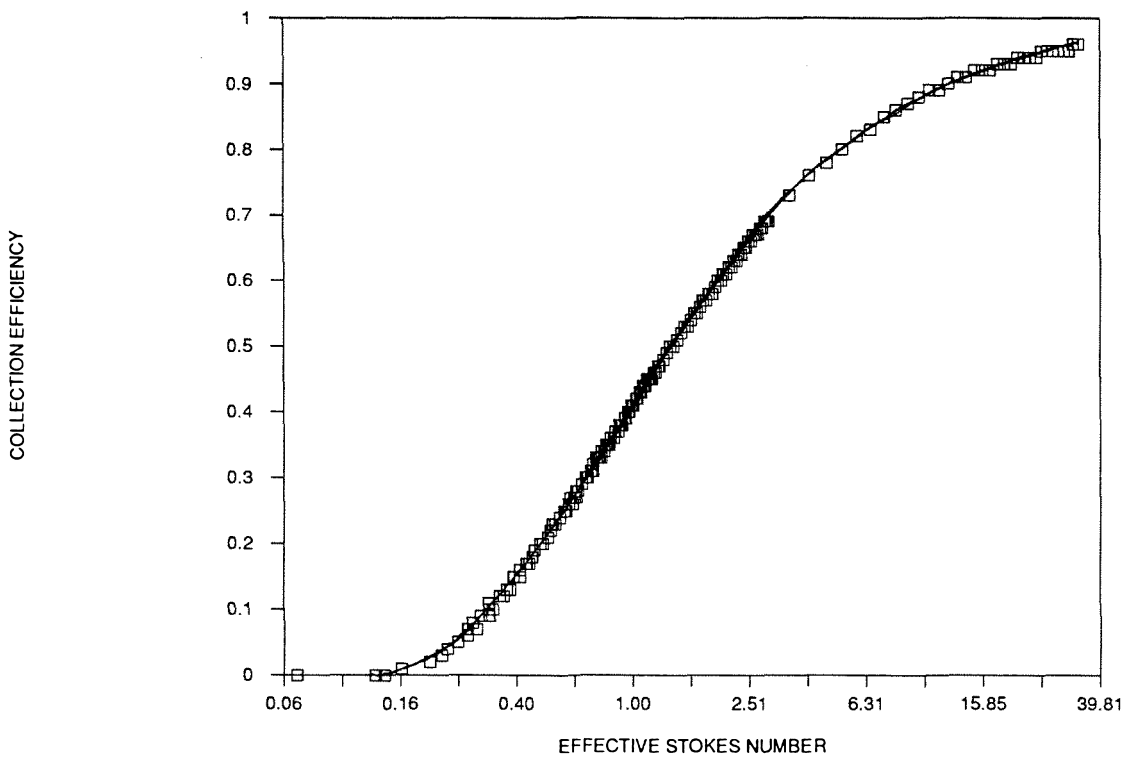

Figure 4.3. Collection efficiency for particle deposition onto a tube in cross-flow for the case of perfect sticking as predicted by theoretical calculation of particle trajectories.

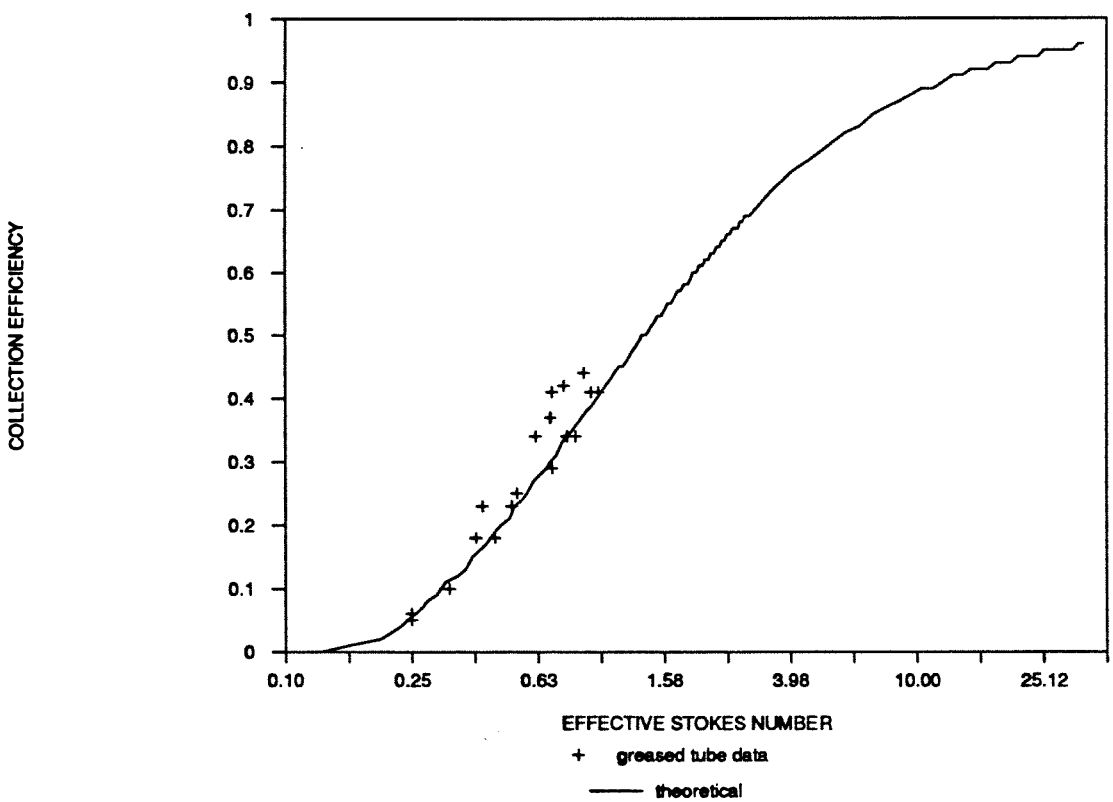

Figure 4.4. Comparison of theoretical collection efficiency curve based on particle trajectory calculations (Figure 4.3) to experimental data from Figure 4.1 for the case of solid particle collisions with greased tubes in cross-flow.

briefly (7) that he expects the critical velocity to be on the order of 1 meter/second for the system of gold wire and polystyrene latex spheres studied by Bhutra and Payatakes (8). See Section 2.5.2.3 for an explanation of the critical velocity.

The computer program used in the present work calculates impact velocities for particles that strike the tube. By assuming a critical incident particle velocity normal to the tube surface V_{ni}^{*}, above which the particles will bounce with enough energy to escape collection by the tube, the particle collection efficiency as a function of effective Stokes number in the presence of particle bounce can be predicted. In this sense, the critical velocity has a slightly different meaning than in some prior studies. Here the critical velocity is not the velocity at which bounce first occurs, but rather the velocity above which capture does not occur. The critical velocity needed to escape capture by the tube may be higher than that needed to induce one bounce, since it is possible that a particle that just barely bounces will hit the tube more than once. If the particle does not retain sufficient kinetic energy after its first collision, it will be captured on the second collision with the tube. If several different values of V_{ni}^{*} are chosen, a family of particle collection efficiency curves will be generated for the different assumed critical velocities. Figures 4.5 and 4.6 show such families of curves. These curves all have the property that as effective Stokes number increases, they initially follow the increasing particle collection efficiency curve that was observed in the perfect sticking case. At higher values of $St_{eff,}$ the particles begin to strike the tube at velocities exceeding the critical velocity, and particle bounce occurs. As the effective Stokes number continues to increase, more and more particles have sufficient incident normal velocity to bounce with enough energy to escape capture by the tube, and the particle collection efficiency declines until virtually all particles that hit the tube fail to stick. In both Figures 4.5 and 4.6, the plotted points

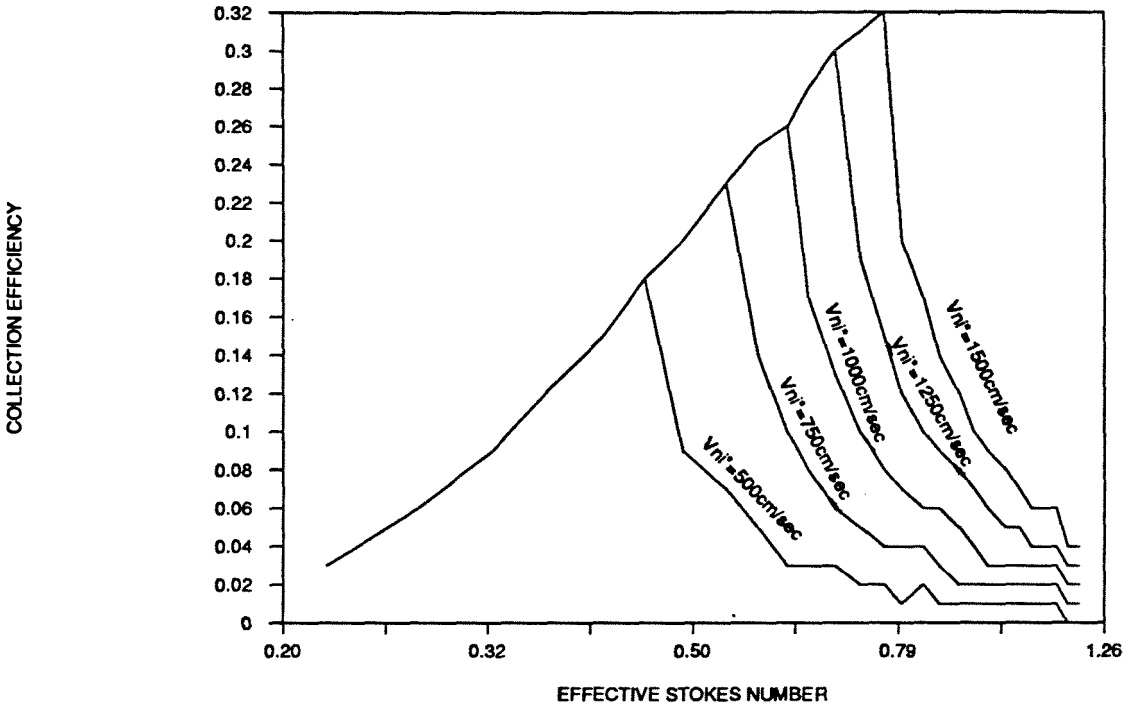

Figure 4.5. Predicted collection efficiency for constant diameter solid particle-ungreased tube collisions for the case where particle bounce is important. Five micrometer diameter particles were used in the simulations and the upstream velocity was varied to achieve the various effective Stokes numbers needed. The effects of various choices for the critical normal incident velocity V_{ni}^{*}, above which the particle will bounce with enough energy to escape capture by the tube, are shown.

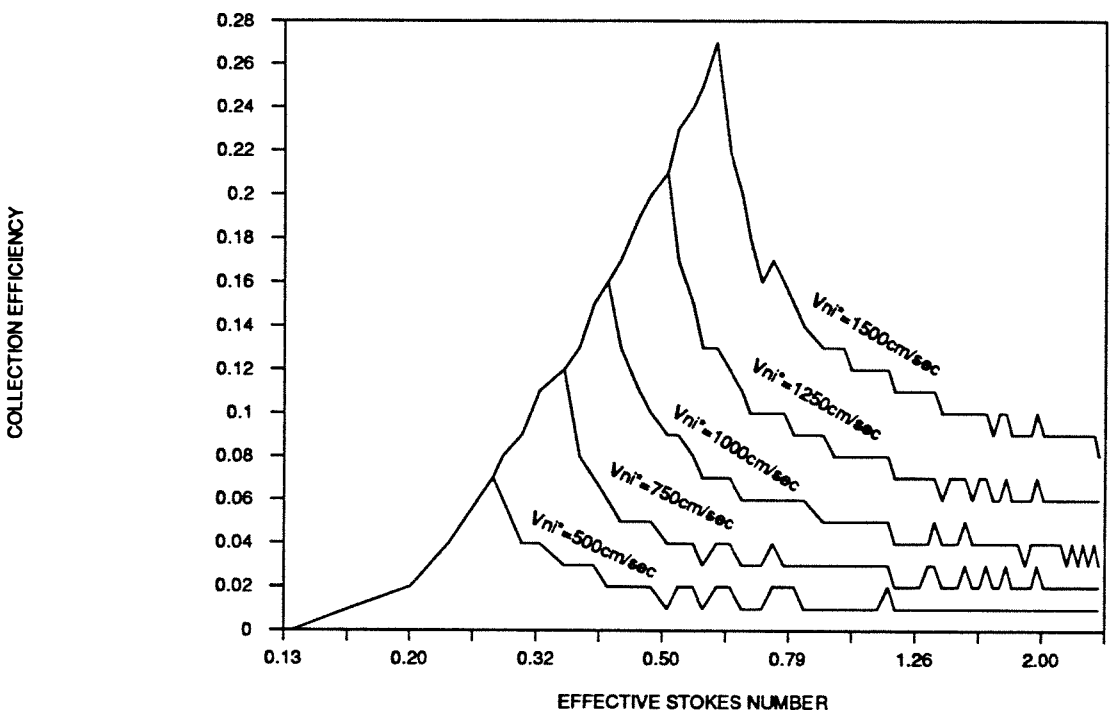

Figure 4.6. Predicted collection efficiency for solid particle-ungreased tube collisions with constant upstream velocity for the case where particle bounce is important. The upstream velocity was fixed at 4000 centimeters/second and particle diameters were varied to achieve the various effective Stokes numbers needed. The effects of various choices for the critical normal incident velocity V_{ni}^{*}, above which the particle will bounce with enough energy to escape capture by the tube, are shown.

are the results of the computer simulation. Since the simulation produces results for a limited number of particles spaced evenly across the upstream cross-sectional area of the tube, collection efficiencies can be determined only to 2 decimal places.

Although the perfect sticking collection efficiency is a function only of the effective Stokes number, Figures 4.5 and 4.6 show that a unique dependence on that one dimensionless group is not seen when particle bounce is included in the calculation. Figure 4.5 was generated for the range of St_{eff} by choosing a particle size and varying the upstream fluid velocity, while Figure 4.6 was generated by choosing an upstream fluid velocity and varying the particle size. If particle bounce were a function of the effective Stokes number alone, these two figures would be identical. The curves are not the same, and although two particles that have the same effective Stokes number will follow the same trajectory, if they have different sizes and upstream velocities (although having the same St_{eff}), they will collide with the tube with different incident velocities. Since the experiments described here held particle size approximately constant while varying the upstream fluid velocity, the calculation procedure used to generate Figure 4.5 has been used for the rest of this analysis.

4.2.3.2 COMPARISON OF EXPERIMENTAL DATA TO PREDICTED COLLECTION EFFICIENCY CURVES

Since collection efficiency predictions for the case of particle bounce depend on particle size, several graphs are needed to correlate the data for solid particle collisions with ungreased tubes. Because it is difficult to reproduce exactly a given particle size with the particle generation equipment, clean tube experimental results were sorted into three

groups of particles with diameters of approximately 4.75, 5.0, and 5.5 microns. Figures 4.7, 4.8, and 4.9 show the experimental data for solid particle collisions with ungreased tubes plotted on appropriate curves. In each case it can be seen that the assumption of a critical incident normal particle velocity needed to completely escape collection by the tube of 1000 centimeter/second as a criterion for particle bounce provides a good fit to the data in the regime where particle bounce is negligible (i.e., for small St_{eff}) and in the regime where particle bounce dominates (i.e., for high St_{eff}). Some additional clarification is still needed in the transition regime where bounce is beginning to occur but collection efficiency is still relatively high (i.e., for medium St_{eff}).

The departure of the experimental data from the perfect sticking curve appears to occur at or before $V_{ni}^{*} = 500$ cm/sec, suggesting that some particles are bouncing at least once at normal incident velocities at or below 500 cm/sec. The fact that it takes normal incident velocities in the range of 1000 cm/sec to completely clear all bouncing particles from the tube suggests that some particles may need enough initial kinetic energy to rebound from more than one collision with the tube in order to escape capture.

4.3 CONCLUSIONS

Experimentally determined collection efficiencies for the perfect sticking case (greased tubes) confirm the theoretical predictions of Brun et al. (1). See Figure 4.4.

Experiments show that solid particle collection on ungreased tubes is significantly less than would be the case if all particle-tube collisions resulted in capture. Collection efficiency for the ungreased tube case initially increases along the perfect sticking curve as effective Stokes number increases, then deviates from the perfect sticking curve and

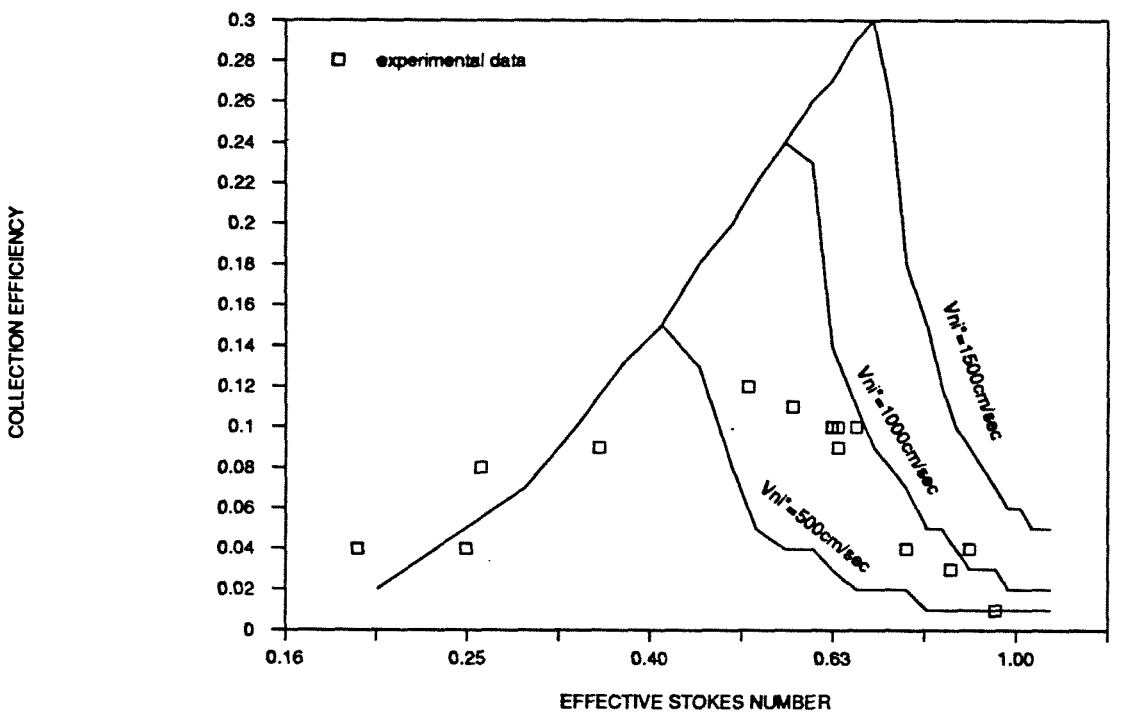

Figure 4.7. Comparison of theoretical collection efficiency curves for 4.75 micrometer diameter particles and ungreased tubes to experimental data. Theoretical curves are based on particle trajectory calculations and various assumed critical normal incident velocities, V_{ni}^{*}, above which particles will bounce with enough energy to escape collection by the tube. Experimental data are results from Figure 4.1 for the case of approximately 4.75 micrometer solid ammonium fluorescein particle collisions with ungreased stainless steel tubes in cross-flow.

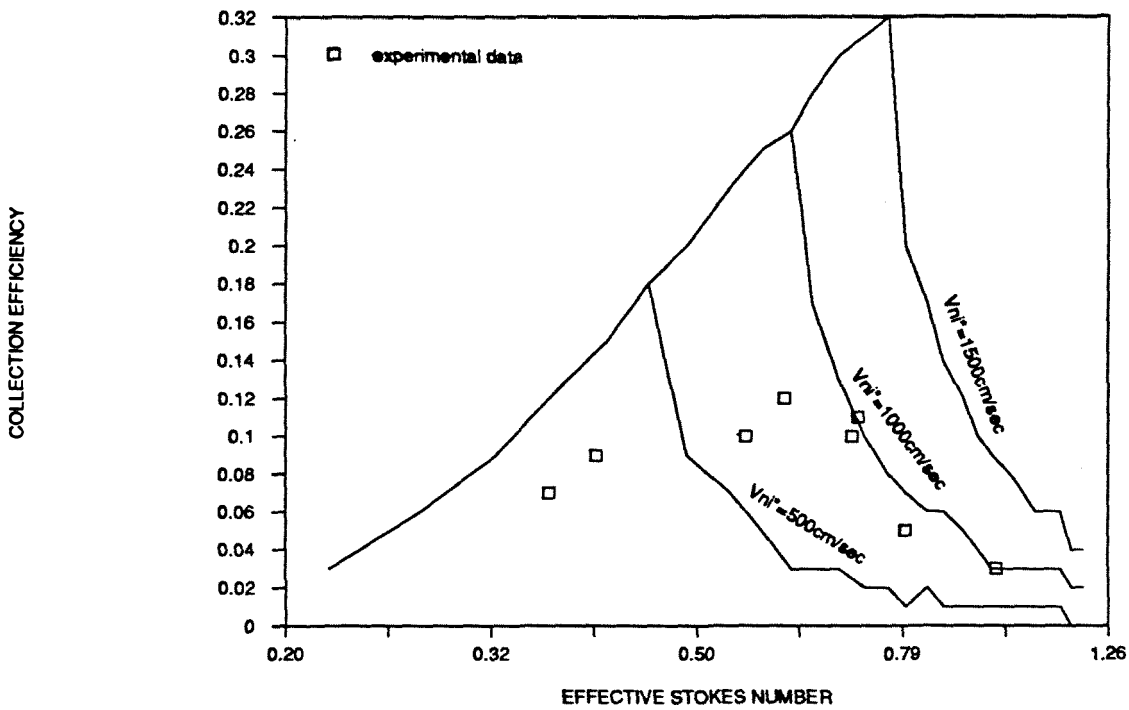

Figure 4.8. Comparison of theoretical collection efficiency curves for 5.0 micrometer diameter particles and ungreased tubes to experimental data. Theoretical curves are based on particle trajectory calculations and various assumed critical normal incident velocities, V_{ri}^{*}, above which particles will bounce with enough energy to escape collection by the tube. Experimental data are results from Figure 4.1 for the case of approximately 5.0 micrometer solid ammonium fluorescein particle collisions with ungreased stainless steel tubes in cross-flow.

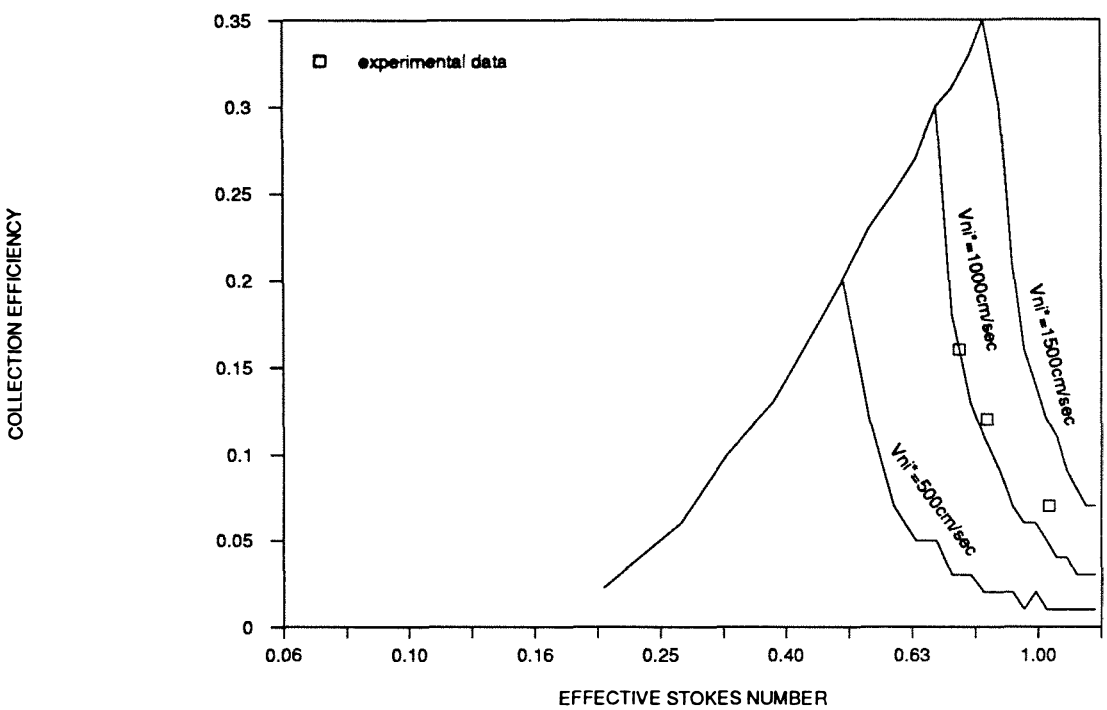

Figure 4.9. Comparison of theoretical collection efficiency curves for 5.5 micrometer diameter particles and ungreased tubes to experimental data. Theoretical curves are based on particle trajectory calculations and various assumed critical normal incident velocities, V_{ni}^{*}, above which particles will bounce with enough energy to escape collection by the tube. Experimental data are results from Figure 4.1 for the case of approximately 5.5 micrometer solid ammonium fluorescein particle collisions with ungreased stainless steel tubes in cross-flow.

begins to decrease as particle bounce starts to occur. As St_{eff} continues to increase, the particle collection efficiency approaches zero as particle bounce becomes dominant. Bounce increases with increased particle size and/or increased flow velocity, but is not a function only of the effective Stokes number. By deliberately selecting a high enough fluid velocity, one can retard the accumulation of particles on heat exchanger tubes in cross-flow.

Particle collection efficiencies can be modeled for the perfect sticking case by tracking particle trajectories through the flow field as the particles approach the tube. The onset of particle bounce can be explained for the case of solid particle-clean tube collisions based on a critical normal incident velocity needed to induce particle bounce. For ammonium fluorescein particles on stainless steel tubes in cross-flow, the first signs of particle bounce appear at or below 500 cm/sec, but a critical velocity of 1000 centimeter/second is needed to cause all particles to bounce with enough energy to completely escape capture by the tube.

Values in the range of 500 cm/sec or less for the initial onset of particle bounce for the ammonium fluorescein particle and stainless steel tube system can be compared to Dahneke's rough estimate (7) of 1 m/sec for the critical incident velocity for polystyrene latex spheres collected upon gold wire, based on the data of Bhutra and Payatakes (8).

In spite of the consensus that some bounce will be encountered at lower velocities, an effective initial incident velocity of 1000 cm/sec should be used for design purposes if the

objective is to completely clear particles from the tube. The added incident velocity increment may be needed to overcome the effect of multiple collisions between the particle and the tube surface.

4.4 BIBLIOGRAPHY

1. Brun, R.J., Lewis, W., Perkins, P.J., and Serafini, J.S., Impingement of cloud droplets on a cylinder and procedure for measuring liquid-water content and droplet sizes in supercold clouds by rotating multicylinder method, Report 1215, 141-183 (1955).

2. Rosner, D.E., Gokoglu, S. and Israel, R., Rational correlations of diffusional and inertial particulate deposition behavior in nonisothermal forced convection environments. Presented at the International Conference on Fouling of Heat Exchanger Surfaces, White Haven, PA (1982).

3. Cheng, Y-S., and Yeh, H-C., Particle bounce in cascade impactors, Environmental Science and Technology, 13, 1392-1396 (1979).

4. Dahneke, B., The capture of aerosol particles by surfaces, Journal of Colloid and Interface Science, 37, 342-353 (1971).

5. Dahneke, B., The influence of flattening on the adhesion of particles, Journal of Colloid and Interface Science, 40, 1-13 (1972).

6. Dahneke, B., Measurements of bouncing of small latex spheres, Journal of Colloid and Interface Science, 45, 584-590 (1973).

7. Dahneke, B., and Padilya, D., Comments on the paper "Experimental investigation of dendritic deposition of aerosol particles," Journal of Aerosol Science, 11, 567-569 (1980).

8. Bhutra, S., and Payatakes, A. C., Experimental investigation of dendritic deposition of aerosol particles, Journal of Aerosol Science, 10, 445 (1979).

5 TRANSIENT SINGLE TUBE EXPERIMENTS

The transient deposition of particles on single tubes is described in this chapter. Using the aerosol processes wind tunnel described in Section 3.1.2 and Figure 3.10, experiments were conducted to determine the rate of accumulation of particles as a function of the total deposit accumulated over time on both clean and greased tubes. Data were collected for high, medium and low effective Stokes numbers. The experiments at high St_{eff} were designed to examine the rate of accumulation of deposits when particle bounce from clean tubes is prevalent and controls particle deposition. See point 3 on Figure 5.1. Medium effective Stokes number experiments were designed to determine the transient behavior when short-term particle collection efficiency for ungreased tubes is at its maximum. This is at the peak of the collection efficiency curve for ungreased tubes, at point 2 in Figure 5.1. Finally, the small St_{eff} experiments examined transient particle collection under conditions when short-term collection (as seen in Chapter 4) is determined by the number of particles that hit the tube. At point 1 in Figure 5.1, most particles are able to follow the fluid streamlines around the tube and those particles that do strike the tube generally stick, giving similar short-term collection efficiencies for greased and ungreased tubes. These experiments determined whether that similarity prevails over time.

One factor that may be expected to alter the rate of particle deposition on surfaces as the deposits accumulate is the increased likelihood of incident particle-captured particle interactions in addition to incident particle-surface interactions. For greased tubes a decrease in the deposition rate might be expected with increasing prior deposits; particle bounce might occur for an incident particle-captured particle interaction while an incident

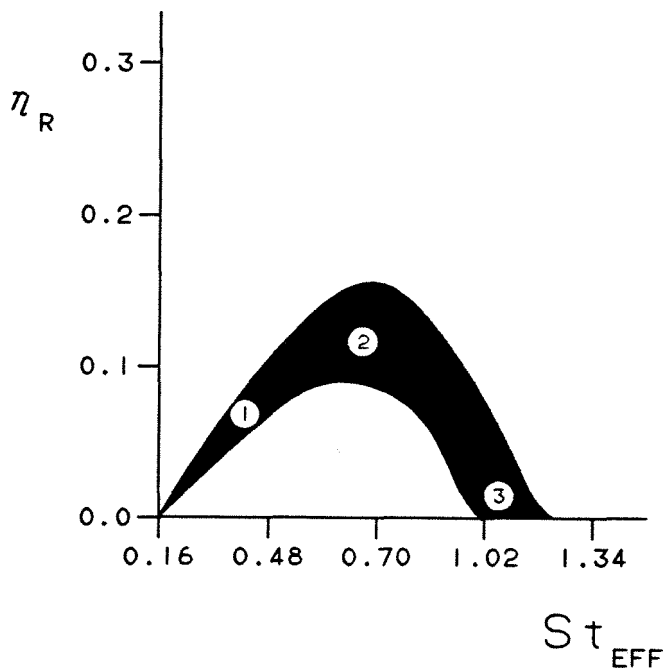

Figure 5.1. Experimental conditions for transient experiments. The shaded band represents the range of initial collection efficiencies from Chapter 4 for deposition of solid particles onto ungreased stainless steel tubes in cross-flow. Numbers 1, 2, and 3 represent the values of the effective Stokes numbers for which extended particle deposition experiments were performed.

particle-greased surface collision has been shown in Chapter 4 to result in capture. Figures 2.3 and 2.4 show different proposed transient fouling profiles; it was desired to determine if either was applicable to the various cases for which data were gathered.

For the case of deposition of particles onto initially clean surfaces, the rate of accumulation of particles might decrease or increase over time. If the accumulation of particles provided a surface (stickier or softer, perhaps) that could absorb more kinetic energy from subsequent incident particles, particle capture might be facilitated and the deposition rate would increase. Declining rates of deposition might result if particle-particle collisions on the surface result in detachment of previously captured particles or if aerodynamic forces dislodge loosely attached particles or groups of particles. As discussed in Chapter 2, a competition between particle attachment and detachment may lead to an asymptotic deposit thickness if the two mechanisms become equal in magnitude. Such a process may explain the asymptotic fouling resistances that are seen in the heat transfer data taken from many "in-service" heat exchangers.

5.1 EXPERIMENTS

5.1.1 GREASED TUBES

Experiments were conducted at a small effective Stokes number of 0.30, medium effective Stokes numbers of 0.64 and 0.65, and a high effective Stokes number of 1.04. The duration of the experiments varied from 5 minutes to 240 minutes. Data were collected for each experiment, using the procedure described in Section 3.2. For the longer experiments, it was necessary to dilute the fluorescein solutions extracted from the filters and tubes to bring the solution concentrations within the range of the Aminco-

Beckman Spectrophotofluorimeter. From the concentrations of the solutions, the particle size as determined by scanning electron microscopy, and Equations 3.3-3.8, it is possible to determine the number of particles deposited on the tube, the number of particles in the upstream cross-sectional area of the tube, and the overall collection efficiency for each experiment.

In addition, it is possible to determine approximately the fraction, F, of the projected front face area of the tube that is covered with particles:

$$F = \frac{N_t\left(\frac{\pi d_p^2}{4}\right)}{A_t}. \tag{5.1}$$

Here N_t is the number of particles on the tube, d_p is the diameter of the particle, and A_t is the projected cross-sectional area of the tube. Equation 5.1 represents the overall fraction of the entire front face that is covered. Clearly, if the value of F approaches unity, all incident particles will strike previously deposited particles instead of the surface of the tube. However, because the particles have finite diameters, the center of an incident particle need only approach within one particle diameter of the center of a previously deposited particle in order for a particle-particle collision to occur at the tube surface. As a result, particle-particle collisions at the collection surface will be probable at values of F below unity.

Tables 5.1, 5.2, and 5.3 present experimental conditions together with the results of the calculations described above for the low, medium and high St_{eff} cases, respectively. Figures 5.2, 5.3 and 5.4 present the number of particles collected on the tube as a function

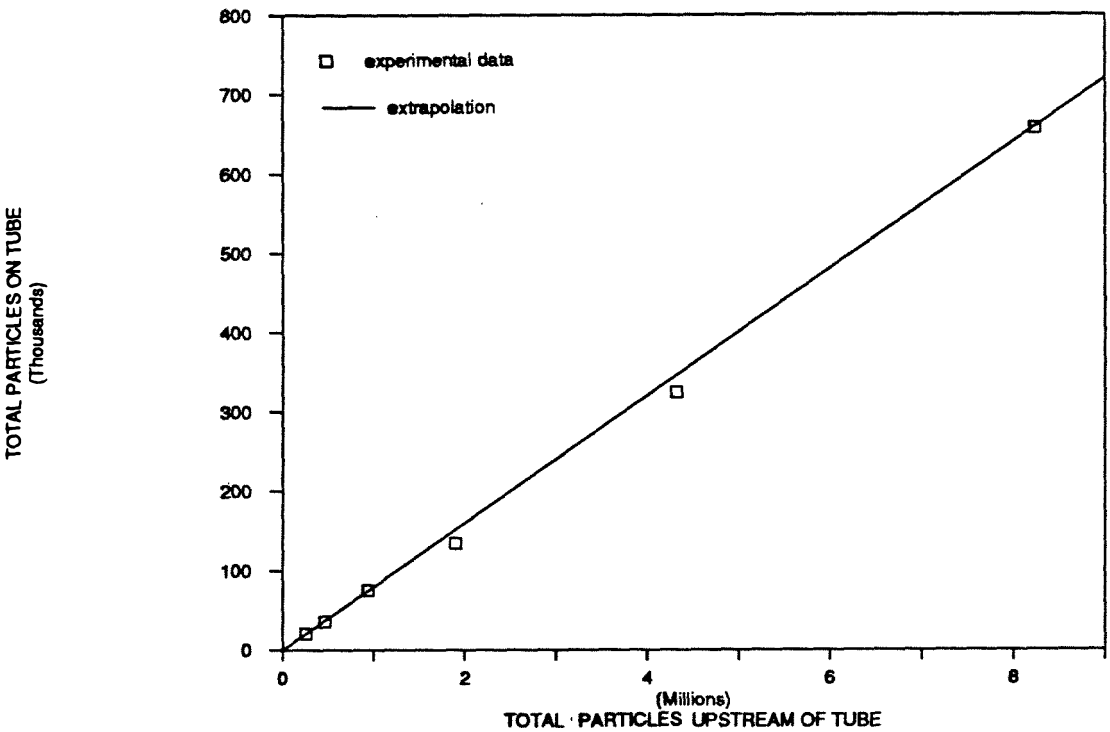

Figure 5.2. Transient particle collection of a greased stainless steel tube in cross-flow for a small effective Stokes number of 0.30. The line represents an extrapolation of the initial deposition rate and the small squares are experimental results.

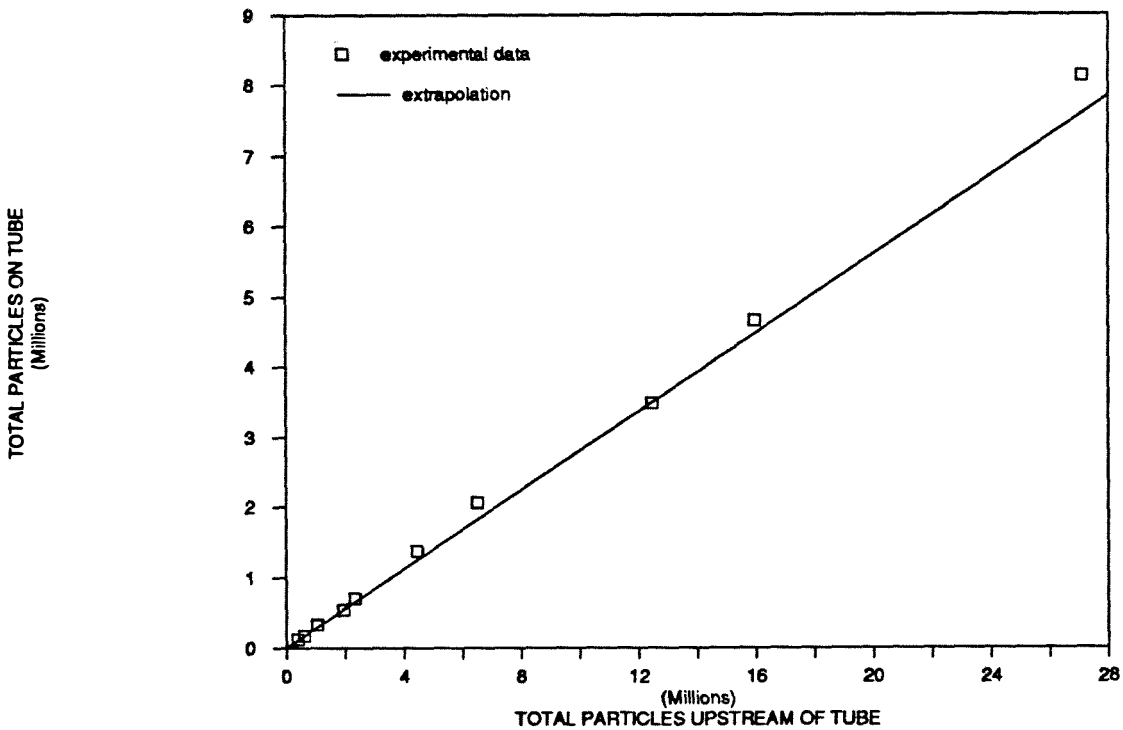

Figure 5.3. Transient particle collection of a greased stainless steel tube in cross-flow for a medium effective Stokes number of 0.64 or 0.65. The line represents an extrapolation of the initial deposition rate and the small squares are experimental results.

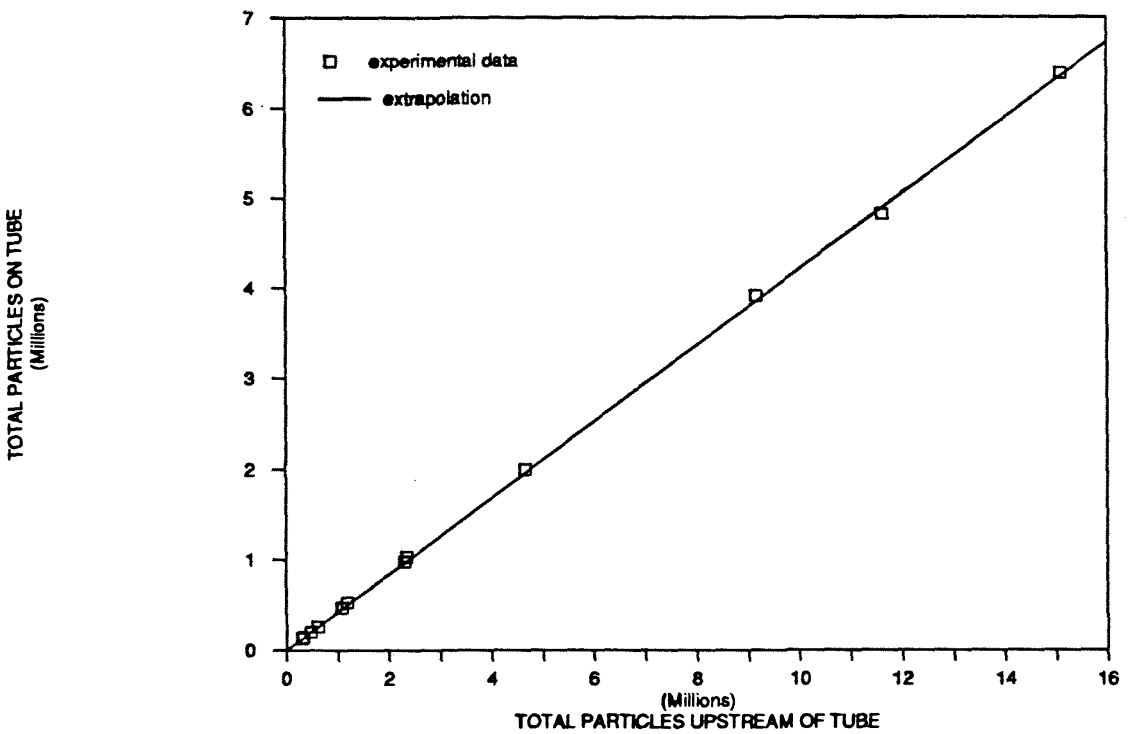

Figure 5.4. Transient particle collection of a greased stainless steel tube in cross-flow for a large effective Stokes number of 1.04. The line represents an extrapolation of the initial deposition rate and the small squares are experimental results.

TABLE 5.1. TRANSIENT SINGLE TUBE EXPERIMENTS: experimental results for small effective Stokes numbers and greased tubes

d_p=4.60x10^{-4} cm fluid velocity=2600 ft/min =1321 cm/sec St_{eff}=0.30

TIME (min)	TOTAL PARTICLES UPSTREAM OF TUBE	PARTICLES COLLECTED ON TUBE	COLLECTION EFFICIENCY	FRACTIONAL COVERAGE, F
5	2.52E+05	2.04E+04	0.081	0.001
10	4.60E+05	3.59E+04	0.078	0.002
20	9.38E+05	7.56E+04	0.081	0.004
40	1.90E+06	1.34E+05	0.071	0.007
80	4.32E+06	3.24E+05	0.075	0.018
160	8.24E+06	6.57E+05	0.080	0.036

TABLE 5.2. TRANSIENT SINGLE TUBE EXPERIMENTS: experimental results for medium effective Stokes numbers and greased tubes

TIME (min)	TOTAL PARTICLES UPSTREAM OF TUBE	PARTICLES COLLECTED ON TUBE	COLLECTION EFFICIENCY	FRACTIONAL COVERAGE, F
d_p=4.81x10^{-4}cm		fluid velocity=5782 ft/min =2937 cm/sec		St_{eff}=0.64
5	6.14E+05	1.75E+05	0.28	0.01
10	1.05E+06	3.26E+05	0.31	0.02
20	2.34E+06	7.01E+05	0.30	0.04
40	4.45E+06	1.37E+06	0.31	0.08
80	1.25E+07	3.48E+06	0.28	0.21
160	2.71E+07	8.12E+06	0.30	0.49
d_p=4.88x10^{-4}cm		fluid velocity=5782 ft/min =2937 cm/sec		St_{eff}=0.65
5	4.01E+05	1.25E+05	0.31	0.01
20	1.95E+06	5.37E+05	0.28	0.03
80	6.53E+06	2.07E+06	0.32	0.13
160	1.60E+07	4.67E+06	0.29	0.29

TABLE 5.3. TRANSIENT SINGLE TUBE EXPERIMENTS: experimental results for large effective Stokes numbers and greased tubes

d_p=5.14x10^{-4} cm fluid velocity=9224 ft/min =4686 cm/sec St_{eff}=1.04

TIME (min)	TOTAL PARTICLES UPSTREAM OF TUBE	PARTICLES COLLECTED ON TUBE	COLLECTION EFFICIENCY	FRACTIONAL COVERAGE, F
5	3.00E+05	1.33E+05	0.43	0.01
5	3.18E+05	1.43E+05	0.44	0.01
10	4.68E+05	1.99E+05	0.42	0.01
10	6.10E+05	2.60E+05	0.42	0.02
20	1.19E+06	5.26E+05	0.44	0.04
20	1.09E+06	4.70E+05	0.43	0.03
40	2.30E+06	9.84E+05	0.43	0.07
40	2.35E+06	1.04E+06	0.44	0.07
80	4.67E+06	2.00E+06	0.43	0.14
160	9.16E+06	3.91E+06	0.43	0.27
160	1.16E+07	4.82E+06	0.42	0.36
240	1.51E+07	6.38E+06	0.42	0.47

of the total number of particles that were ever present in the upstream cross-sectional area of the tube, again for the low, medium and high St_{eff} cases, respectively. Also given on Figures 5.2, 5.3, and 5.4 is a line showing the numbers of particles that would have been collected on the tubes if the initial deposition rate had been maintained indefinitely and no removal had occurred. For the greased tube experiments, that initial particle deposition rate, in fact, continued unaltered over the times studied and indicated that no removal of previously deposited particles occurred for the experimental conditions.

5.1.2 UNGREASED TUBES

Experiments were conducted at a small effective Stokes number of 0.30, medium effective Stokes numbers of 0.64, 0.65, and 0.66 and a high effective Stokes number of 1.09. The duration of the experiments varied from 5 minutes to 400 minutes. Data were collected for each experiment, using the procedure described in Section 3.2. For the longer experiments it was necessary to dilute the fluorescein solutions extracted from the wind tunnel after filter to bring the solution concentrations within the range of the Aminco-Beckman Spectrophotofluorimeter. From the concentrations of the solutions, the particle size as determined by the scanning electron microscopy, and Equations 3.3-3.8, it is possible to determine the number of particles deposited on the tube, the number of particles in the upstream cross-sectional area of the tube, and the overall particle collection efficiency for each experiment. In addition, it is possible to calculate the fraction of the front face of the tube that has been covered by particles, using Equation 5.1. Equation 5.1 represents the overall fraction of the entire front face that is covered. From the results of Section 4, however, we know that for solid particles striking ungreased tubes, particles are not collected over the entire surface of the tube but only in that region where incident velocities are low enough that particle capture occurs. By

performing trajectory calculations for the appropriate particle sizes and velocities, using the computer program described in Section 4.2.1, impact velocities and positions for a range of particles across the front face of the tube can be determined. From these results it is possible to determine the fraction of the front face, f, over which particle capture can occur. Then an adjusted fractional coverage, F_a may be calculated:

$$F_a = \frac{N_t\left(\frac{\pi d_p^2}{4}\right)}{fA_t} = \frac{F}{f}, \tag{5.2}$$

which represents the fraction of surface coverage by particles over that portion of the tube surface on which particles are actually deposited.

Tables 5.4, 5.5, and 5.6 present experimental conditions together with the results of the calculations described above for the low, medium and high St_{eff} cases, respectively. Figures 5.5, 5.6 and 5.7 present the number of particles collected on the tube as a function of the total number of particles that were ever present in the upstream cross-sectional area of the tube, again for the low, medium and high St_{eff} cases, respectively. Also given on Figures 5.5, 5.6, and 5.7 is a line showing predicted numbers of particles that would have been collected on the tubes if the initial deposition rate had been maintained indefinitely and no particle removal had occurred. Deviations from these predictions can be seen, indicating that removal is significant.

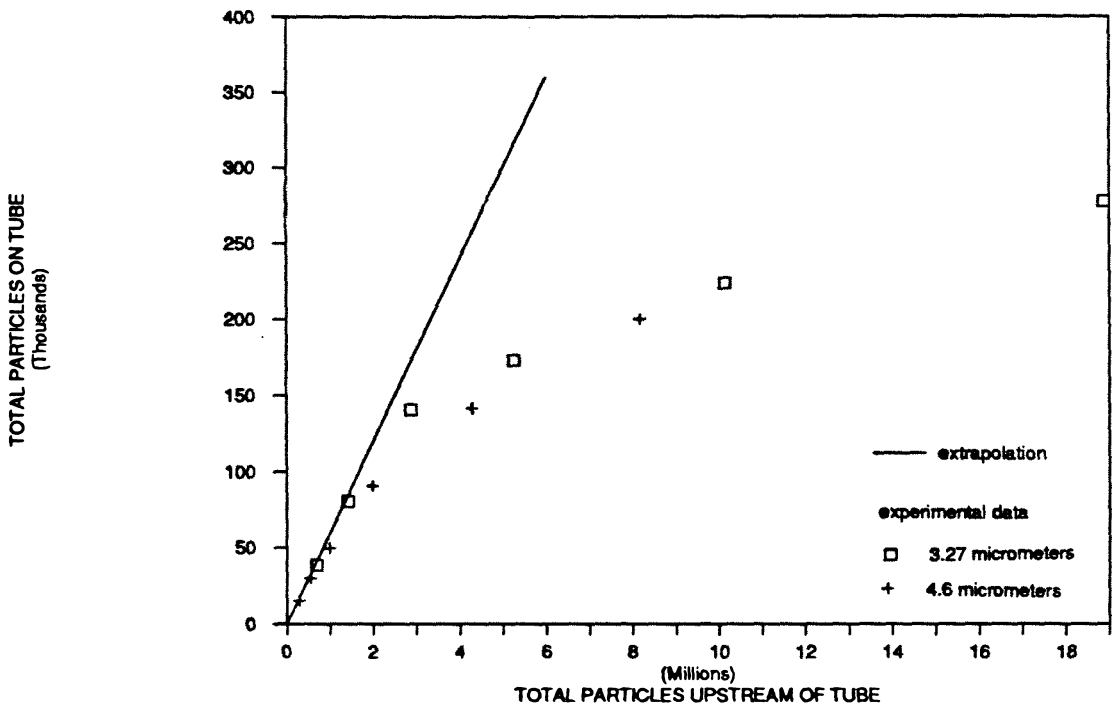

Figure 5.5. Transient particle collection of an ungreased stainless steel tube in cross-flow for a small effective Stokes number of 0.30. The line represents an extrapolation of the initial deposition rate and the small squares and crosses are two sets of experimental results.

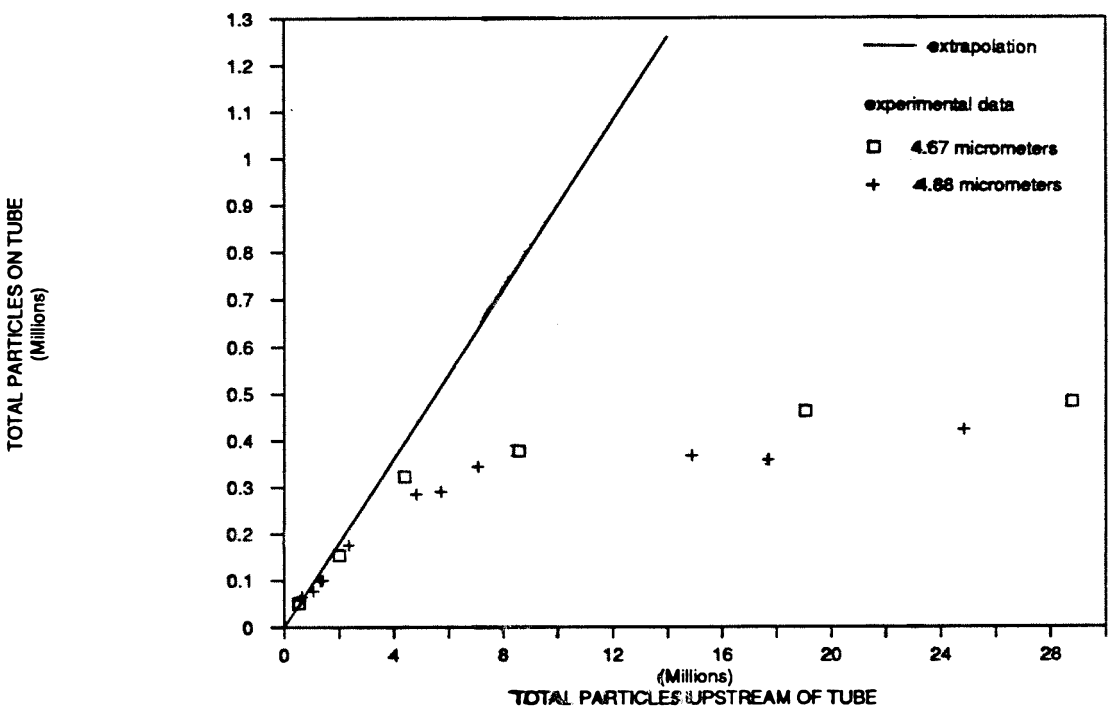

Figure 5.6. Transient particle collection of an ungreased stainless steel tube in cross-flow for a medium effective Stokes number. The line represents an extrapolation of the initial deposition rate. The small squares represent data taken for a St_{eff} of 0.64 and the crosses represent data taken for effective Stokes numbers between 0.64 and 0.66.

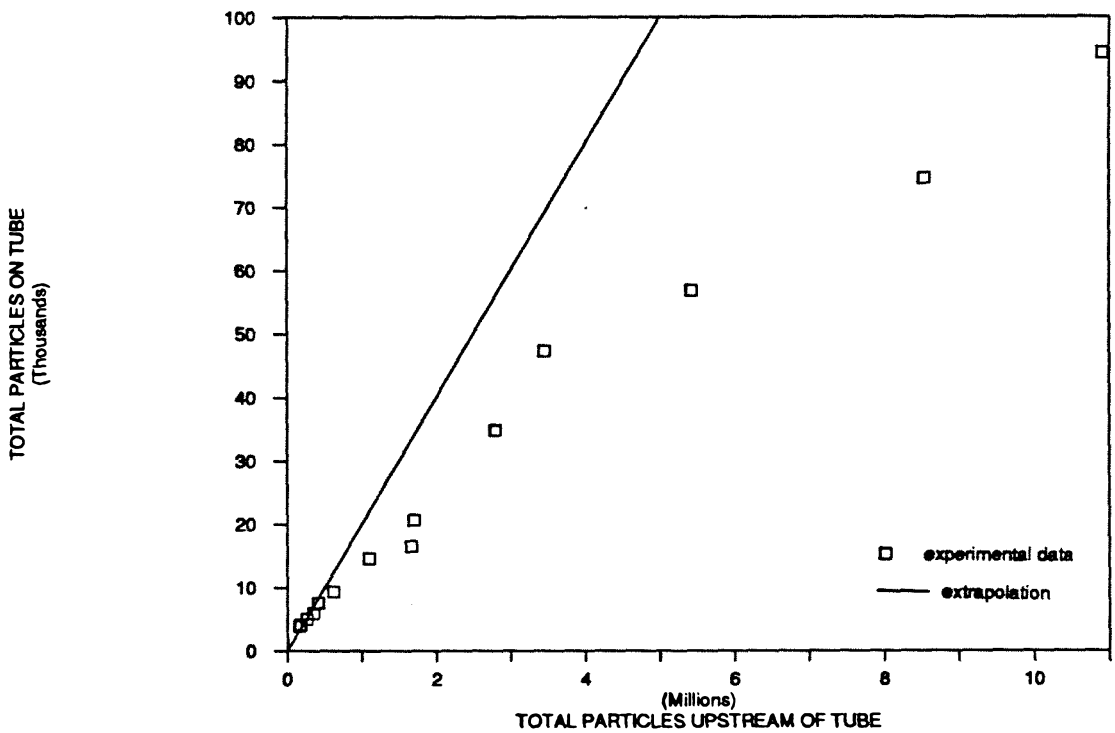

Figure 5.7. Transient particle collection of an ungreased stainless steel tube in cross-flow for a large effective Stokes number of 1.09. The line represents an extrapolation of the initial deposition rate and the small squares are experimental results.

TABLE 5.4. TRANSIENT SINGLE TUBE EXPERIMENTS: experimental results for small effective Stokes numbers and ungreased tubes

TIME (min)	TOTAL PARTICLES UPSTREAM OF TUBE	PARTICLES COLLECTED ON TUBE	COLLECTION EFFICIENCY	ADJUSTED FRACTIONAL COVERAGE, F_a
d_p=3.27x10^{-4} cm		fluid velocity=5632 ft/min =2861 cm/sec		St_{eff}=0.30
5	6.98E+05	3.88E+04	0.06	0.001
10	1.41E+06	8.08E+04	0.06	0.002
20	2.87E+06	1.41E+05	0.05	0.004
40	5.25E+06	1.73E+05	0.03	0.005
80	1.01E+07	2.24E+05	0.02	0.006
160	1.89E+07	2.78E+05	0.01	0.008
d_p=4.60x10^{-4} cm		fluid velocity=2600 ft/min =1321 cm/sec		St_{eff}=0.30
5	2.87E+05	1.53E+04	0.05	0.001
10	5.39E+05	3.02E+04	0.06	0.002
20	9.84E+05	5.00E+04	0.05	0.003
40	1.98E+06	9.09E+04	0.05	0.005
80	4.30E+06	1.42E+05	0.03	0.008
160	8.18E+06	2.00E+05	0.02	0.011

TABLE 5.5. TRANSIENT SINGLE TUBE EXPERIMENTS: experimental results for medium effective Stokes numbers and ungreased tubes

TIME (min)	TOTAL PARTICLES UPSTREAM OF TUBE	PARTICLES COLLECTED ON TUBE	COLLECTION EFFICIENCY	ADJUSTED FRACTIONAL COVERAGE, F_a
d_p=4.67x10^{-4} cm		fluid velocity=6299 ft/min =3200 cm/sec		St_{eff}=0.64
5	5.07E+05	5.05E+04	0.10	0.004
5	5.57E+05	5.20E+04	0.09	0.005
20	2.00E+06	1.54E+05	0.08	0.014
40	4.40E+06	3.22E+05	0.07	0.029
80	8.58E+06	3.77E+05	0.04	0.033
160	1.91E+07	4.61E+05	0.02	0.041
320	2.88E+07	4.81E+05	0.02	0.043
d_p=4.86x10^{-4} cm		fluid velocity=5782 ft/min =2937 cm/sec		St_{eff}=0.64
5	6.48E+05	6.51E+04	0.10	0.006
10	1.33E+06	9.93E+04	0.07	0.009
15	1.40E+06	1.00E+05	0.07	0.009
20	2.36E+06	1.76E+05	0.07	0.015
40	4.80E+06	2.85E+05	0.06	0.025
80	7.08E+06	3.44E+05	0.05	0.030
160	1.49E+07	3.67E+05	0.02	0.032
d_p=4.88x10^{-4} cm		fluid velocity=5782 ft/min =2937 cm/sec		St_{eff}=0.65
5	5.83E+05	5.76E+04	0.10	0.005
40	5.72E+06	2.90E+05	0.05	0.025
160	1.77E+07	3.58E+05	0.02	0.031
d_p=4.90x10^{-4} cm		fluid velocity=5782 ft/min =2937 cm/sec		St_{eff}=0.66
7	5.80E+05	5.78E+04	0.10	0.005
15	1.05E+06	7.80E+04	0.07	0.007
320	2.48E+07	4.22E+05	0.02	0.037

TABLE 5.6. TRANSIENT SINGLE TUBE EXPERIMENTS: experimental results for large effective Stokes numbers and ungreased tubes

d_p=5.29x10^{-4}cm fluid velocity=9224 ft/min =4686 cm/sec St_{eff}=1.09

TIME (min)	TOTAL PARTICLES UPSTREAM OF TUBE	PARTICLES COLLECTED ON TUBE	COLLECTION EFFICIENCY	ADJUSTED FRACTIONAL COVERAGE, F_a
5	1.63E+05	3.92E+03	0.011	0.001
5	1.81E+05	4.03E+03	0.010	0.001
10	2.60E+05	4.98E+03	0.011	0.001
10	3.41E+05	5.83E+03	0.011	0.002
20	4.13E+05	7.57E+03	0.013	0.002
20	6.21E+05	9.34E+03	0.012	0.003
40	1.09E+06	1.46E+04	0.011	0.004
40	1.66E+06	1.65E+04	0.009	0.004
80	1.70E+06	2.06E+04	0.011	0.006
80	2.80E+06	3.48E+04	0.012	0.009
120	3.46E+06	4.72E+04	0.013	0.013
160	5.43E+06	5.68E+04	0.010	0.015
320	8.54E+06	7.45E+04	0.009	0.020
400	1.09E+07	9.44E+04	0.008	0.025

5.2 ANALYSIS

5.2.1 GREASED TUBES

Data for all three greased tube transient experiments are shown on Figure 5.8. It can be seen that the greased tube results show a constant rate of particle deposition throughout the time periods tested. The larger the effective Stokes number (i.e., the larger the particles or the faster the fluid flow), the higher the rate of deposition, since for the higher Stokes numbers fewer particles are able to follow the fluid streamlines around the tube. Overall collection efficiencies for all three greased tube cases are in good agreement with those predicted by the computer program used in Section 4.

The fraction, F, of the projected front face surface area covered by particles was as high as 0.47 for the longer greased tube experiments. In spite of this coverage, no decrease in the rate of collection of particles was seen and no removal was occurring. Although it is reasonable to assume at the higher coverage fractions that some incident particles were hitting other already captured particles, the incident particles are still being captured, suggesting that surface coverage greater than a monolayer of captured particles will be required for particle bounce or removal to occur from the greased tubes. A possible explanation is that the grease layer is either thick enough or mobile enough that the first incident particles become covered with grease presenting a sticky surface on which subsequent particles also are captured.

5.2.2 UNGREASED TUBES

Figure 5.9 shows data for all transient ungreased tube cases on a single combined graph. The rate of particle deposition is highest for the medium Stokes number cases. The curve

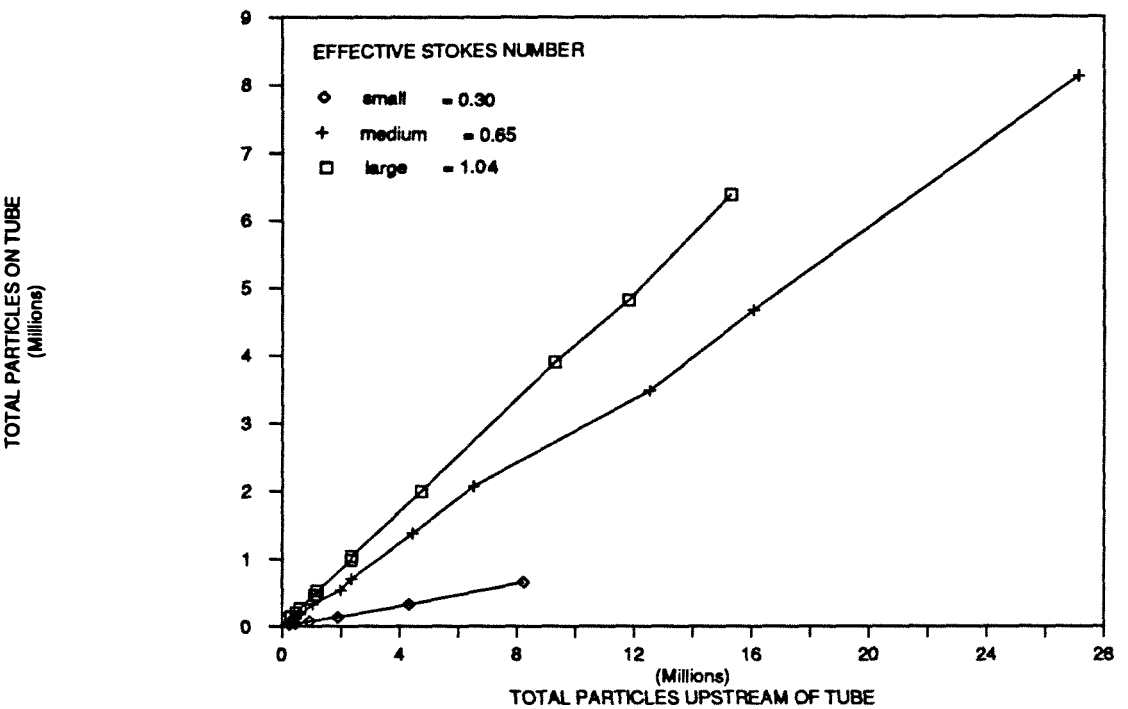

Figure 5.8. Transient particle collection of a greased stainless steel tube in cross-flow for small, medium, and large effective Stokes numbers. The small diamonds represent data taken for an effective Stokes number of 0.30, the crosses represent data taken for effective Stokes numbers of 0.64 and 0.65, and the squares represent data taken for an St_{eff} of 1.04.

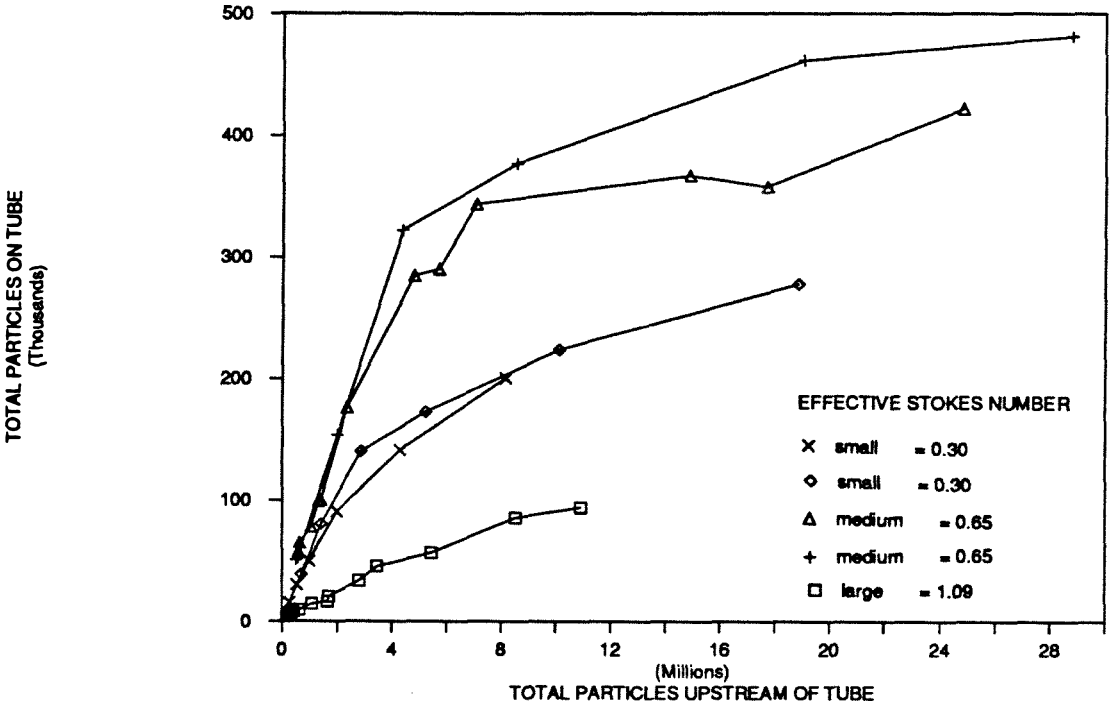

Figure 5.9. Transient particle collection of an ungreased stainless steel tube in cross-flow for small, medium, and large effective Stokes numbers. The small diamonds and x's represent two sets of data taken for an effective Stokes number of 0.30, the crosses represent data taken for an effective Stokes number of 0.64, the triangles represent data taken for effective Stokes numbers between 0.64 and 0.66, and the squares represent data taken for an St_{eff} of 1.09.

where St_{eff} is 0.64 was produced using particles with a diameter of 4.67×10^{-4} centimeters, while the 0.65 curve was produced using particles with diameters between 4.86×10^{-4} and 4.90×10^{-4} centimeters. Both curves show a leveling off toward a constant number of particles on the tube, although the eventual number is slightly different for the two sets of data. From these results it is clear that deposit removal is occurring at a rate approaching that for particle attachment. Since the adjusted fractional surface coverage, F_a, is still small (0.043 for the largest case), it is difficult to explain the approach toward an asymptotic number of particles entirely in terms of incoming particle interactions with previously captured particles leading to particle re-entrainment. Perhaps the explanation is that incoming particles are not simply captured, but that they may slide along the surface for some distance before coming to rest as postulated by Gillespie (1). This would increase the chances of deposit disturbance because of particle-particle interaction and possible subsequent particle re-entrainment from the surface.

With the experimental apparatus described in Chapter 3 and within the time frame available, it was not possible to continue the curves beyond the times and total number of particles used. (A different particle generation system, such as a spinning disk aerosol generator, which produces many more particles in any given time, would make it possible to continue the data to higher numbers of particles. A continuous feed system for the vibrating orifice aerosol generator would make it possible to run the experiments for longer times and again, larger numbers of particles.) Thus, it was not possible to determine what the effect of attempting to collect particles on the tube surface for longer times might be. It is possible that the apparent steady state for the medium St_{eff} cases,

which is similar to that proposed in Figure 2.3 but reached at low surface coverage, might eventually give way to build-up of more particles, in a manner similar to that presented in Figure 2.4.

Comparing the solid lines in Figures 5.2 and 5.4, it is seen that the initial deposition rate of particles in the small effective Stokes number case was nearly identical for greased and ungreased tubes. Figure 5.4 shows that the number of particles collected on the ungreased tube has fallen to half the number that would be present if the inertial deposition rate were maintained for the time that approximately 5×10^6 particles have passed through the upstream cross-sectional area of the tube. The small effective Stokes number curves in Figure 5.9 (St_{eff}=0.30) were produced using particles of diameter 3.67×10^{-4} and 4.60×10^{-4} centimeters. The longer curve, which was generated with the larger particles, shows a continually decreasing slope with increasing duration of the experiment, which parallels the behavior seen in the medium Stokes number cases above. In this case the highest adjusted fractional coverage, F_a, obtained was 0.011. Particle-particle collisions on the surface are even less likely to provide a full explanation for the declining rate of particle deposition over time than was the case for the medium effective Stokes number experiments involving ungreased tubes. For each of the two small St_{eff} curves the numbers of particles collected on the tubes relative to the number that passed through the system is smaller than for the medium Stokes number cases. This is a reflection of the fact that fewer particles are hitting the tube, since they are more easily able to follow the fluid streamlines.

For the large St_{eff} experiments, data were collected with particles of 5.29×10^{-4} centimeters at an effective Stokes number of 1.09. Collection efficiencies for the data in this set were

all very small (approximately 0.01). At such low efficiencies, it takes a long time to accumulate many particles on the tube. Since particle bounce dominates initial collection rates at high effective Stokes numbers, however, particles deposit only on a small fraction of the tube, and the adjusted fractional coverage, F_a, reached is as high as 0.025. This is on the same order as for the small and medium St_{eff} cases discussed above. As seen in Figure 5.7, the number of particles ultimately collected on the ungreased tubes in the high effective Stokes number cases is less than half the number that would have been collected if the low initial clean tube particle attachment had been maintained throughout the experiment.

The result of passing solid particles over a single heat exchanger tube at large St_{eff} is to establish an initially low rate of particle accumulation by inducing particle bounce. That low initial rate of particle accumulation is further reduced as the duration of the deposit accumulation process is extended. If the tendency toward accumulation of a constant number of particles on the tube continues in the large effective Stokes number case as in the medium St_{eff} case, then the tube will reach a quasi-steady-state with a very small fouling deposit of about 10^5 particles as opposed to a still growing deposit of more than $6x10^6$ particles in the comparable greased tube case.

5.3 CONCLUSIONS

The transient accumulation of particle deposits on a single heat exchanger tube in cross-flow has been examined. Cases studied involve the collision of solid ammonium fluorescein particles with both greased and ungreased stainless steel tubes that were initially free of particle deposits.

Experiments conducted using greased (sticky) tubes show that essentially all particles that strike the tube will stick even for overall surface coverages by deposits approaching half of the projected front surface area of the tube. (Data were gathered for effective Stokes numbers of 1.04 and less because of equipment limitations.) At that degree of front surface coverage, many incident particles can be expected to strike previously deposited particulate matter, yet essentially all particles still stick. This suggests that a sticky coating on the tube surface is capable of creating a sticky particle deposit to which additional incident particles will adhere.

By comparison, for the case of inertial deposition of solid particles onto ungreased stainless steel tubes, the number of particles deposited quickly approaches a steady state, where particle deposition is balanced by particle removal phenomena. In Chapter 4, it was seen that the initial rate of solid particle deposition onto clean heat exchanger tubes could be kept to very low levels by setting the effective Stokes number of the particles high enough to induce particle bounce. In this chapter, it was found that that low initial rate of particle deposition can be translated into a very low quasi-steady-state number of deposited particles, with adjusted coverage fractions, F_a, of that part of the projected front face of the tube on which particles are captured, held to less than 0.05. The total fraction of the tube surface covered by particles at steady state in this case is even lower. Since the fraction of the surface covered at steady state is so low, it is unlikely that the progressive reduction in the rate of deposit accumulation over time is due entirely to incident particles striking previously deposited particles. Thus, it is not certain whether the steady state is reached because of re-entrainment of already deposited particles, particle sliding along the surface which causes particle-particle collisions and subsequent re-entrainment, or some other cause as yet unknown.

5.4 BIBLIOGRAPHY

1. Gillespie, T., On the adhesion of drops and particles on impact at solid surfaces, I., Journal of Colloid Science, 10, 266-280 (1955).

6 TUBE BANK EXPERIMENTS

The deposition of aerosol particles on heat exchanger tube banks is described in this section. Model compact heat exchanger tube banks were placed in the test section of the aerosol processes wind tunnel described in Section 3.1.2 and Figure 3.10, and particle deposition on the tubes was measured. Data were collected for two configurations of tubes: in-line tube banks, and staggered tube banks. See Figure 3.4. Both greased tube and ungreased tube cases were studied.

6.1 IN-LINE TUBE BANKS

A five-by-five bank of stainless steel tubes was placed in the wind tunnel test section. Tubes were in-line; that is, the center of each tube was directly in-line with its counterpart in the preceding and succeeding rows. Tube outer diameter was 0.635 cm (0.25 inches), center-to-center spacing between adjacent tubes in each row was 0.953 cm (0.375 inches), and center-to-center spacing between rows was 0.794 cm (0.3125 inches). Tube diameter and spacing were based on an actual compact heat exchanger geometry described in Kays and London (1). See Figure 3.4. Two cases were tested, ungreased and greased tubes. The greased tube experiments examined the deposition when all particles thathit the tubes stuck and the ungreased tube experiments were designed to investigate the effects of particle bounce. In each case the upstream air flow velocity was 1320 cm/sec (2599 ft/min). With the large pressure drop caused by the close packing of the tubes in the test section, this was as large a velocity as could be produced by the experimental equipment. The air flowing through the test section contained solid ammonium fluorescein particles created and introduced as described in Chapter 3.

Particle size for both tests was 4.82×10^{-4} cm. Tube rows were designated by letters A (upstream) through E (downstream) from top to bottom, and individual tubes within each row were designated by numbers 1 through 5. The duration of each experiment was 10 minutes, chosen to allow enough particles to collect on the tubes, but to avoid any appreciable removal of previously deposited particles as was seen in Chapter 5. After particles had passed through the system for 10 minutes, the tubes and the after filter were removed and each was extracted, following the procedures in Section 3.2. From the fluorescein concentrations of the extracts, the particle size as determined by the scanning electron microscope, and Equations 3.3-3.8, it was possible to determine the number of particles collected on each tube. For the in-line tube bank case, overall collection efficiencies for each row have been defined somewhat differently than in the single tube case. The collection efficiency for the first row is determined by taking the number of particles in the upstream cross-sectional area of the tubes and comparing that number to the number actually deposited on the first row of tubes:

$$\eta_{RA} = \frac{\sum_{i=1}^{5} N_{Ai}}{(N_{tot}/1.5)}, \tag{6.1}$$

where η_R is the collection efficiency, N is the number of particles, the subscript tot indicates the total number of particles passing through the system, letter subscripts indicate row, and number subscripts indicate tube number as described above. Then since it is difficult to determine how many particles are actually in the upstream cross-sectional areas of subsequent tube rows, that number is assumed to be simply the number in the upstream cross-sectional area of the previous row less the number of particles actually collected on that row:

$$\eta_{RB} = \sum_{i=1}^{5} \frac{N_{Bi}}{\left(\frac{N_{tot}}{1.5} - \sum_{i=1}^{5} N_{Ai}\right)}$$

.

.

. (6.2)

.

$$\eta_{RE} = \sum_{i=1}^{5} \frac{N_{Ei}}{\left(\frac{N_{tot}}{1.5} - \sum_{i=1}^{5} (N_{Ai} + N_{Bi} + N_{Ci} + N_{Di})\right)}.$$

An overall collection efficiency for the tube bank as a unit has also been defined. For this overall efficiency, and to ease comparison with later data for staggered tube banks, the tube bank is assumed to have an overall upstream cross-sectional area equivalent to its outer dimensions. That is, the upstream cross-sectional area is assumed to extend across the tube bank from the outermost edge of tube 1 to the outmost edge of tube 5 and from wall to wall in the other dimension. This leads to

$$\eta_{Rbank} = \sum_{i=1}^{5} \frac{(N_{Ai} + N_{Bi} + N_{Ci} + N_{Di} + N_{Ei})}{(N_{tot}/1.0714)} \tag{6.3}$$

6.1.1 GREASED TUBES

Data for the greased in-line tube bank case are presented in Figures 6.1 and 6.2 and Table 6.1. It can be seen that the first row of tubes, row A, collected almost all (69%) of the total number of particles removed by the tube bank. After the first row, particle

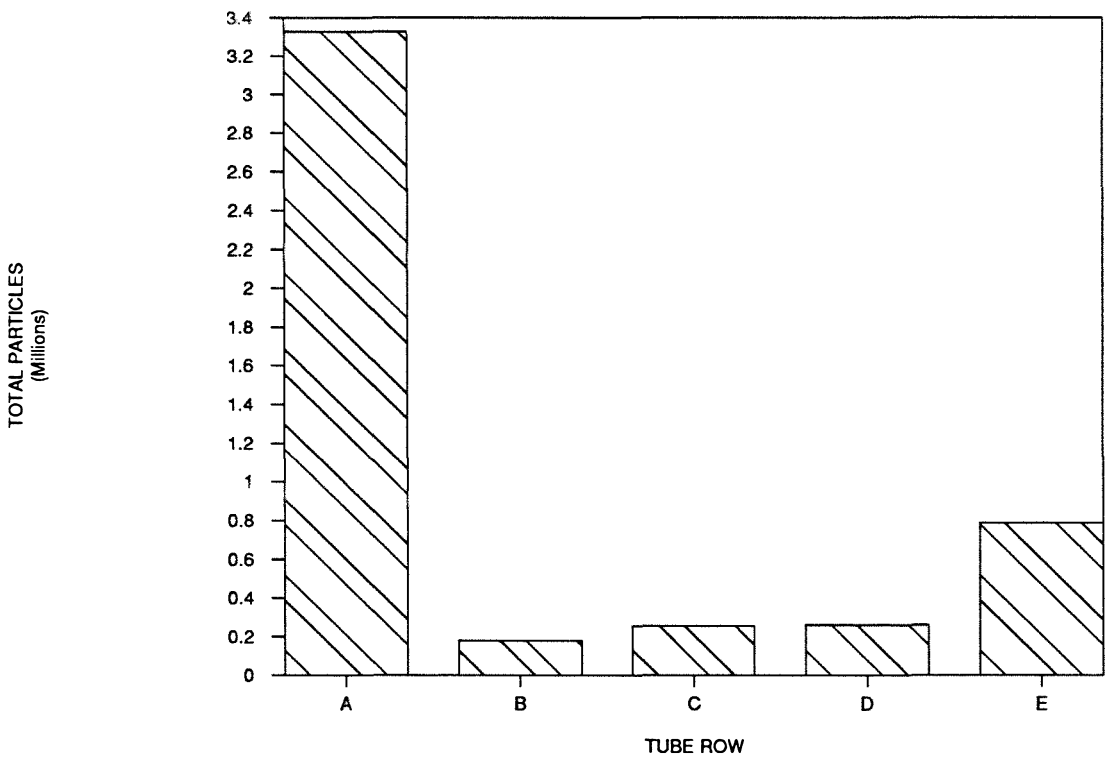

Figure 6.1. Total number of particles on each row for the case of solid ammonium fluorescein particles in cross-flow over a greased in-line tube bank. Tube rows are identified by letters A through E in the upstream to downstream direction.

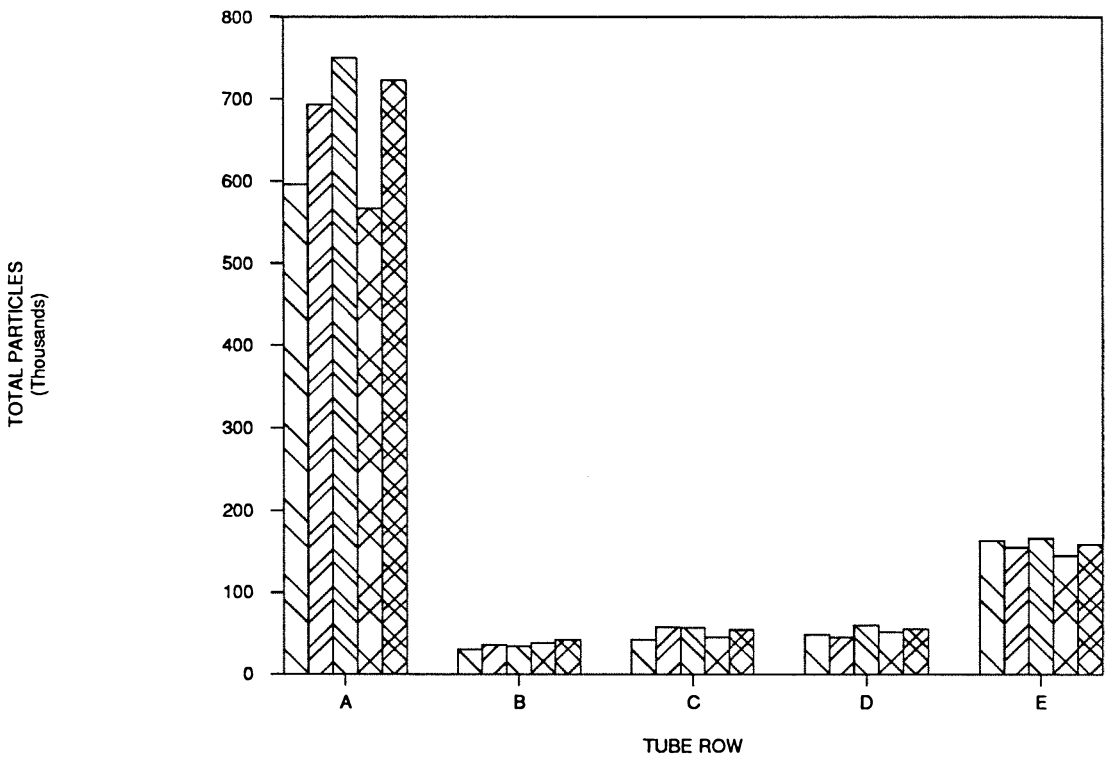

Figure 6.2. Total number of particles on each tube for the case of solid ammonium fluorescein particles in cross-flow over a greased in-line tube bank. Tube rows are identified by letters A through E in the upstream to downstream direction.

Table 6.1 Data for greased in-line tube bank

upstream flow velocity:	1320 cm/sec (2599 ft/min)
particle diameter:	4.82×10^{-4} cm
St_{eff}:	0.32
total particles through system:	3.68×10^{7}
total particles collected:	4.81×10^{6}
fraction particles collected:	0.13
overall collection efficiency:	0.14

INDIVIDUAL TUBE PARTICLE COUNTS (THOUSANDS)

row	tube 1	tube 2	tube 3	tube 4	tube 5	TOTAL PARTICLES ON EACH ROW	FRACTION OF COLLECTED PARTICLES ON EACH ROW
A	596	693	750	567	723	3330000	0.69
B	30.7	35.8	34.1	38.5	41.8	181000	0.04
C	42.5	57.6	57.0	45.0	54.2	256000	0.05
D	48.2	45.2	60.1	51.5	55.7	261000	0.05
E	164	155	166	145	159	788000	0.16

ROW COLLECTION EFFICIENCIES:
A: 0.134
B: 0.009
C: 0.012
D: 0.013
E: 0.038

collection dropped substantially by a factor of about 18 on the next row of tubes, row B, and then increased slightly over the last three rows (C-E). The number of particles collected by the last row, row E, was about one-fourth that collected by the first row, row A. Figure 6.1 shows the total number of particles collected by each row of tubes, and Figure 6.2 shows the total number of particles collected by each tube. Overall collection efficiencies for each row as calculated, using Equations 6.1 and 6.2 range from 0.009 to 0.13. The tube bank removed 13% of the particles that passed through the system for an overall collection efficiency, calculated using Equation 6.3, of 0.14. The data are presented in Table 6.1.

6.1.2 UNGREASED TUBES

Data for the ungreased in-line tube bank case are presented in Figures 6.3 and 6.4 and Table 6.2. It can be seen that the first row of tubes, row A, collected most (37%) of the total number of particles removed by the tube bank. After the first row, particle collection dropped by a factor of about 3 on the next row of tubes, row B, and then increased slightly over the last three rows (C-E). The number of particles collected by the last row, row E, was about half that collected by the first row, row A. Figure 6.3 shows the total number of particles collected by each row of tubes, and Figure 6.4 shows the total number of particles collected by each tube. Again, using Equations 6.1 and 6.2, the row collection efficiencies have been determined to range from 0.008 to 0.021. The tube bank removed 3.7% of the particles that passed through the system for an overall collection efficiency of 0.040. See Equation 6.3. The data are presented in Table 6.2.

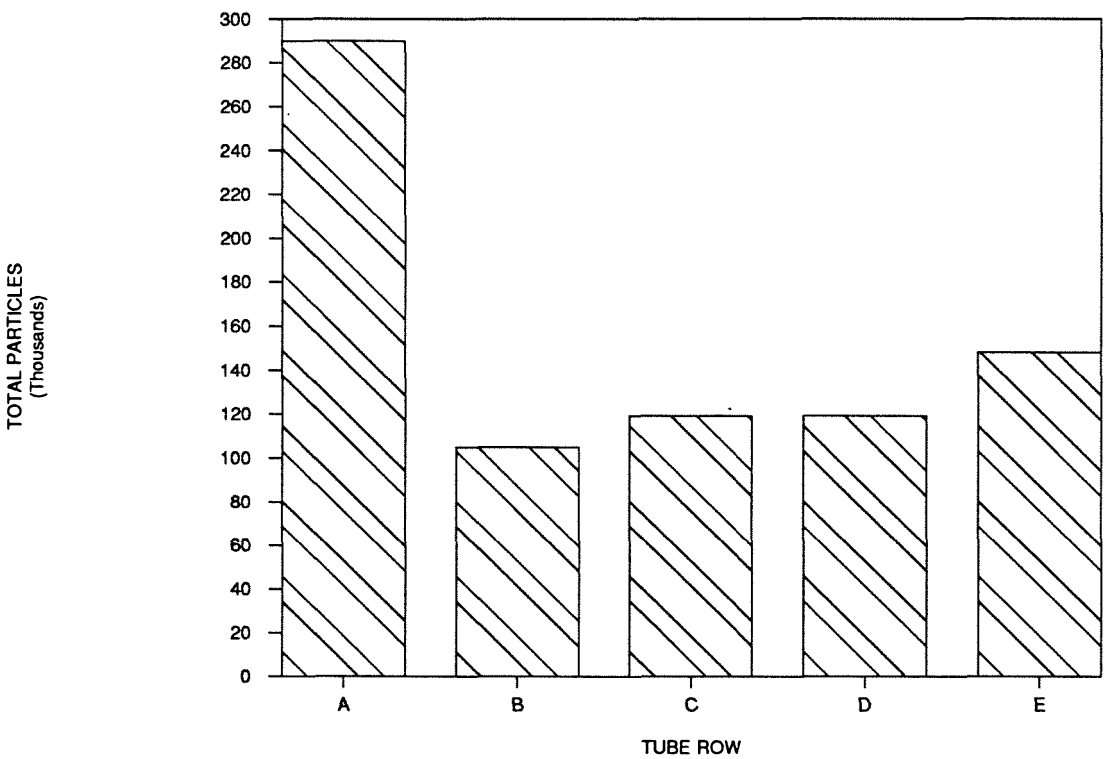

Figure 6.3. Total number of particles on each row for the case of solid ammonium fluorescein particles in cross-flow over an ungreased in-line tube bank. Tube rows are identified by letters A through E in the upstream to downstream direction.

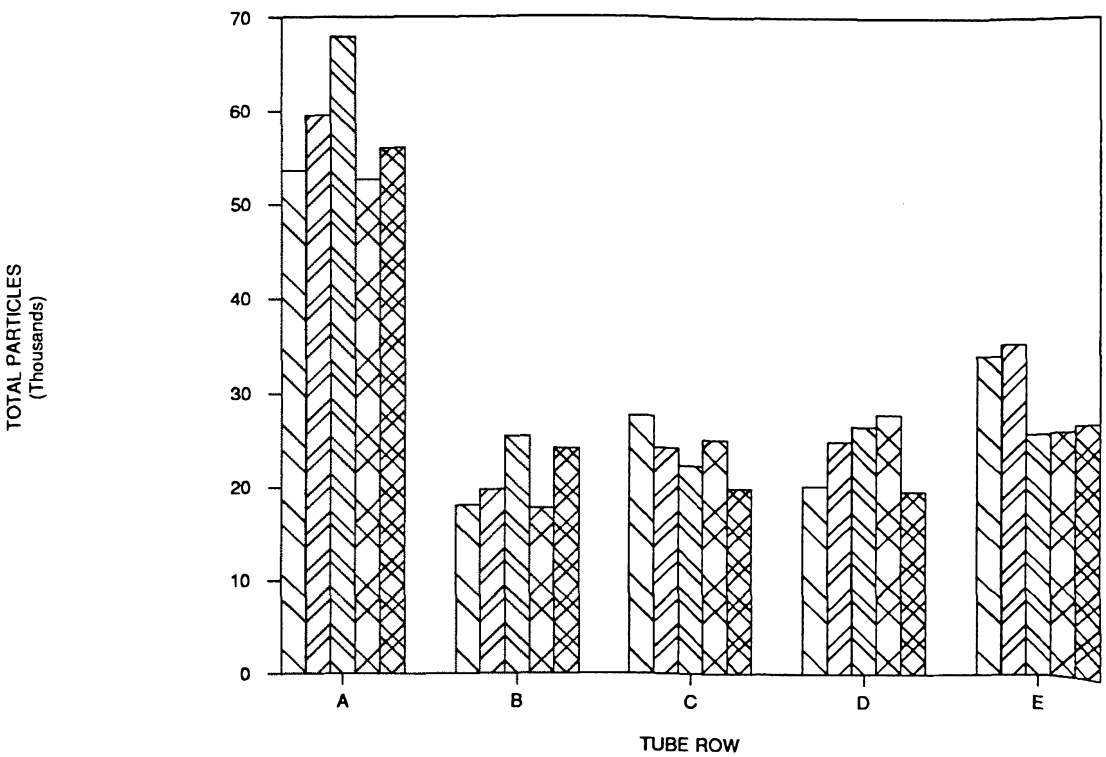

Figure 6.4. Total number of particles on each tube for the case of solid ammonium fluorescein particles in cross-flow over an ungreased in-line tube bank. Tube rows are identified by letters A through E in the upstream to downstream direction.

Table 6.2 Data for ungreased in-line tube bank

upstream flow velocity:	1320 cm/sec (2599 ft/min)
particle diameter:	4.82×10^{-4} cm
St_{eff}:	0.32
total particles through system:	2.10×10^{7}
total particles collected:	7.81×10^{5}
fraction particles collected:	0.037
overall collection efficiency:	0.040

INDIVIDUAL TUBE PARTICLE COUNTS (THOUSANDS)							
row	tube 1	tube 2	tube 3	tube 4	tube 5	TOTAL PARTICLES ON EACH ROW	FRACTION OF COLLECTED PARTICLES ON EACH ROW
A	53.6	59.5	67.9	52.7	56.1	290000	0.37
B	18.0	19.7	25.4	17.7	24.1	105000	0.13
C	27.6	24.2	22.3	25.1	20.0	119000	0.15
D	20.2	24.9	26.6	27.9	19.7	119000	0.15
E	34.1	35.4	25.9	26.0	26.6	148000	0.19

ROW COLLECTION EFFICIENCIES:
A: 0.0208
B: 0.0077
C: 0.0088
D: 0.0089
E: 0.0111

6.2 STAGGERED TUBE BANKS

A five-row bank of stainless steel tubes was placed in the wind tunnel test section. Tubes were staggered; that is, the center of each tube was directly downstream from the space between two tubes in the row before it. Tube outer diameter was 0.635 cm (0.25 inches), center-to-center spacing between adjacent tubes in each row was 0.953 cm (0.375 inches), and center-to-center spacing between rows was 0.794 cm (0.3125 inches). Tube diameter and spacing were based on an actual compact heat exchanger geometry described in Kays and London (1). See Figure 3.4. Two cases were tested, ungreased and greased tubes. As for the in-line tube banks above, the greased tube experiments examined the deposition when all particles that hit the tubes stuck and the ungreased tube experiments were designed to investigate the effects of particle bounce. In each case the upstream air flow velocity was 1320 cm/sec (2599 ft./in). With the large pressure drop caused by the close packing of the tubes in the test section, this was as large a velocity as could be produced by the experimental equipment. The air flowing through the test section contained solid ammonium fluorescein particles created and introduced as described in Chapter 3. Particle size for both tests was 4.82×10^{-4} cm. Tube rows were designated by letters A (upstream) through E (downstream) from top to bottom, and individual tubes within each row were designated by numbers 1 through 5. Since the tubes were staggered, rows B and D had only four tubes, while rows A, C, and E had five tubes. A run time of 10 minutes was chosen to allow enough particles to collect on the tubes, but to avoid any appreciable removal of previously deposited particles as was seen in Chapter 5. After particles had passed through the system for 10 minutes, the tubes and after filter were removed and each was extracted following the procedures in Section 3.2.

From the concentrations of the extracted solutions, the particle size as determined by the scanning electron microscope, and Equations 3.3-3.8, it was possible to determine the number of particles on each tube and an overall collection efficiency for the tube bank.

For the staggered tube bank case, overall collection efficiencies for each row have been defined somewhat differently than for either the single tube or the in-line tube bank cases. As for the in-line case, the collection efficiency for the first row is determined by taking the number of particles in the upstream cross-sectional area of the tubes and comparing that number to the number actually deposited on the first row of tubes:

$$\eta_{RA} = \sum_{i=1}^{5} \frac{N_{Ai}}{(N_{tot}/1.5)}. \tag{6.4}$$

Again it is difficult to determine how many particles are actually in the upstream cross-sectional areas of subsequent tube banks. For the staggered tube banks, however, the tubes in each subsequent row are downstream from the spaces in the previous row, and the number of particles in the upstream cross-sectional area of a row is assumed to be simply the number of particles passing through the spaces of the previous row. For the second row, this number is assumed to be simply the number of particles in the upstream cross-sectional area of the spaces of the first row plus the number of particles in the upstream cross-sectional area of the tubes of the first row which were forced around those tubes. For the third and later rows, the number of particles in the upstream cross-sectional area of the row is assumed to be the number of particles passing through the spaces of the previous row. This number will simply be the total number of particles approaching the previous row less the number of particles collected on that row, leading to

$$\eta_{RB} = \sum_{i=1}^{4} \frac{N_{Bi}}{\left(\frac{N_{tot}}{1.0714} - \sum_{i=1}^{5} N_{Ai} \right)}$$

.

. (6.5)

.

$$\eta_{RE} = \sum_{i=1}^{5} \frac{N_{Ei}}{\frac{N_{tot}}{1.0714} - \sum_{i=1}^{5} (N_{Ai} + N_{Ci}) - \sum_{i=1}^{4} (N_{Bi} + N_{Di})}.$$

An overall collection efficiency for the tube bank as a unit has also been defined. For this overall efficiency, and to ease comparison with earlier data for in-line tube banks, the tube bank is assumed to have an overall upstream cross-sectional area equivalent to its outer dimensions. That is, the upstream cross-sectional area is assumed to extend across the tube bank from the outermost edge of tube 1 to the outermost edge of tube 5 and from wall to wall in the other dimension. As for the in-line tube banks, this leads to Equation 6.3.

6.2.1 GREASED TUBES

Data for the greased staggered tube bank case are presented in Figures 6.5 and 6.6 and Table 6.3. It can be seen that the first two rows of tubes, rows A and B, collected most (49%) of the total number of particles removed by the tube bank. Row B (28%) collected

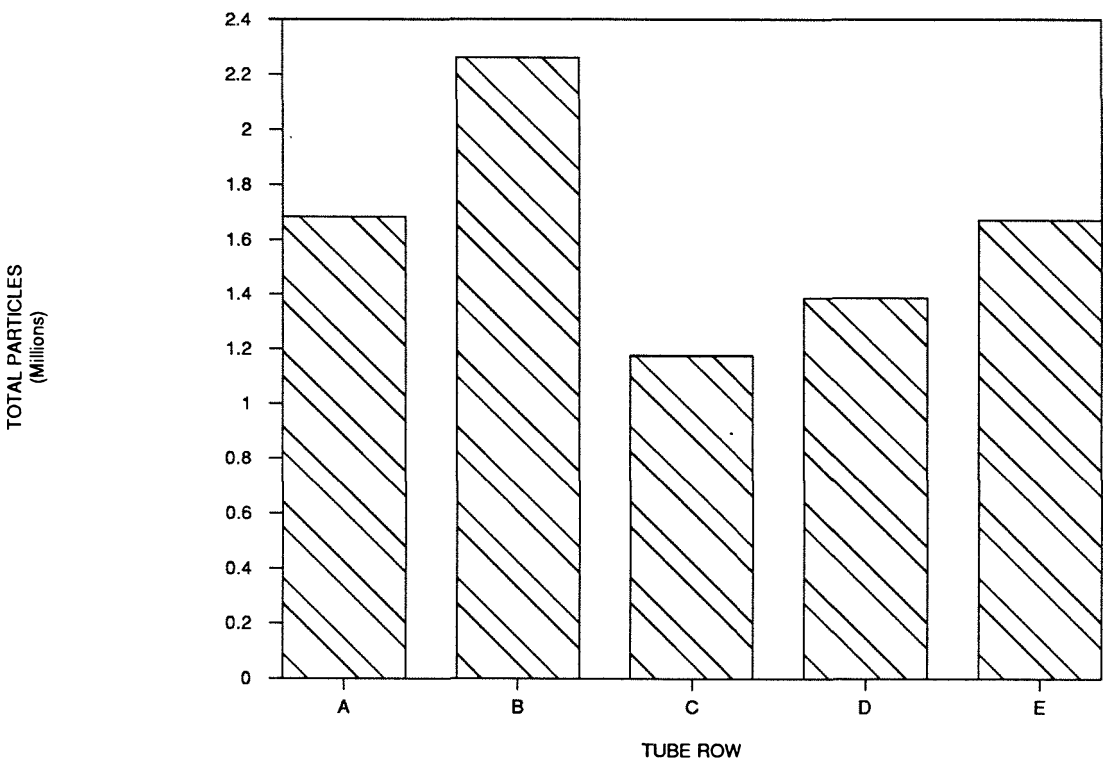

Figure 6.5. Total number of particles on each row for the case of solid ammonium fluorescein particles in cross-flow over a greased staggered tube bank. Tube rows are identified by letters A through E in the upstream to downstream direction.

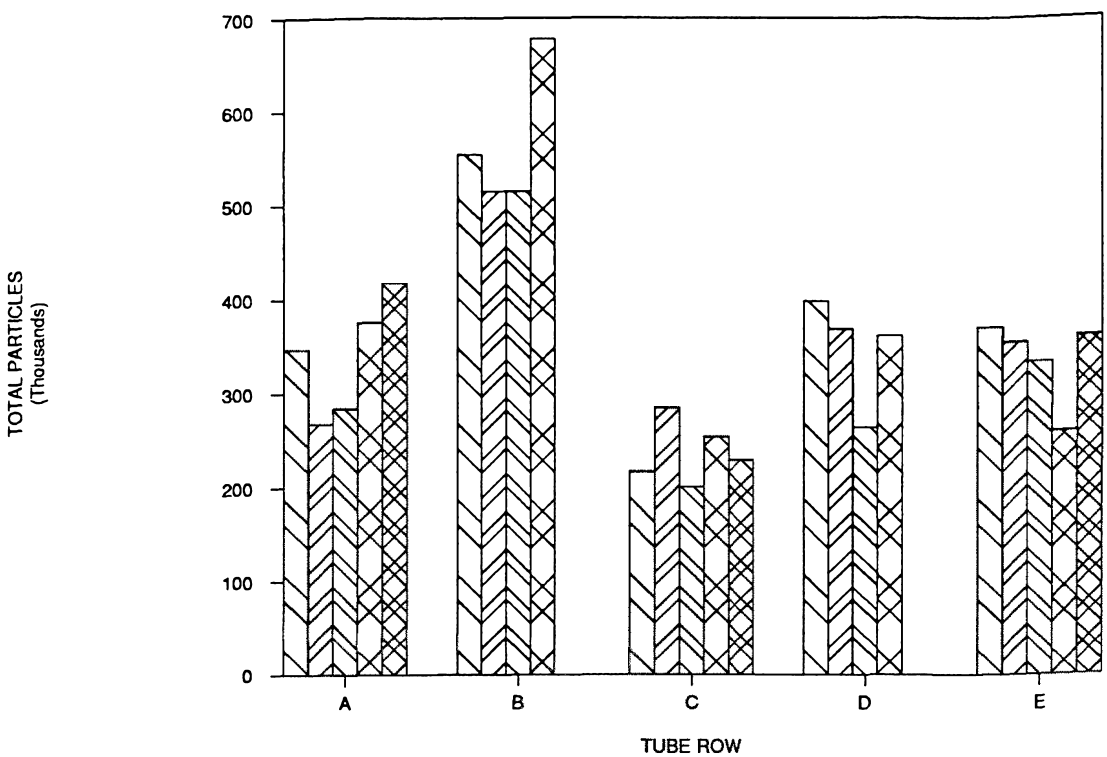

Figure 6.6. Total number of particles on each tube for the case of solid ammonium fluorescein particles in cross-flow over a greased staggered tube bank. Tube rows are identified by letters A through E in the upstream to downstream direction.

Table 6.3 Data for greased staggered tube bank

upstream flow velocity:	1320 cm/sec (2599 ft/min)
particle diameter:	4.82×10^{-4} cm
St_{eff}:	0.32
total particles through system:	2.25×10^{7}
total particles collected:	8.18×10^{6}
fraction particles collected:	0.36
overall collection efficiency:	0.39

INDIVIDUAL TUBE PARTICLE COUNTS (THOUSANDS)

row	tube 1	tube 2	tube 3	tube 4	tube 5	TOTAL PARTICLES ON EACH ROW	FRACTION OF COLLECTED PARTICLES ON EACH ROW
A	345	267	283	374	415	1680000	0.21
B	554	515	515	678		2260000	0.28
C	215	283	199	252	227	1180000	0.14
D	397	368	263	360		1390000	0.17
E	369	353	332	258	359	1670000	0.20

ROW COLLECTION EFFICIENCIES:
A: 0.115
B: 0.117
C: 0.069
D: 0.087
E: 0.115

slightly more particles than row A (21%). After the first two rows, particle collection dropped by a factor of about 2 to the next row of tubes, row C, and then increased slightly on the last two rows, rows D and E. The number of particles collected by the last row, row E, was about two-thirds that collected by the second row, row B. Figure 6.5 shows the total number of particles collected by each row of tubes, and Figure 6.6 shows the total number of particles collected by each tube. Overall collection efficiencies for each row, calculated using Equations 6.4-6.6, range from 0.07 to 0.12. The tube bank removed 36% of the particles that passed through the system for an overall collection efficiency, calculated with Equation 6.3, of 0.39. The data are presented in Table 6.3.

6.2.2 UNGREASED TUBES

Data for the ungreased staggered tube bank case are presented in Figures 6.7 and 6.8 and Table 6.4. It can be seen that the first two rows of tubes, rows A and B, collected most (59%) of the total number of particles removed by the tube bank. Row B (32%) collected slightly more particles than row A (27%). After the first two rows, particle collection dropped by a factor of about 3 to the next two rows of tubes, rows C and D, and then increased slightly on the last row, row E. The number of particles collected by the last row, row E, was about half that collected by the second row, row B. Figure 6.7 shows the total number of particles collected by each row of tubes, and Figure 6.8 shows the total number of particles collected by each tube. Using Equations 6.4-6.6, overall collection efficiencies for each row were found to range from 0.006 to 0.020. The tube bank removed 4.9% of the particles that passed through the system for an overall collection efficiency of 0.053. See Equation 6.3. The data are presented in Table 6.4.

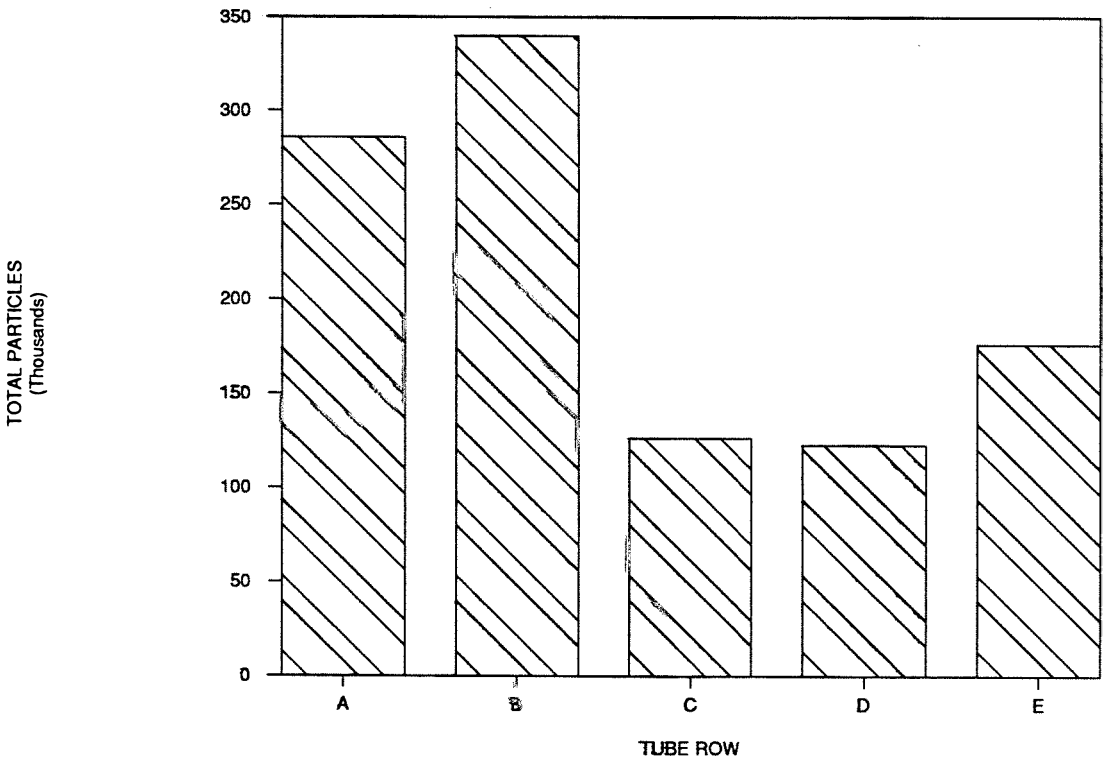

Figure 6.7. Total number of particles on each row for the case of solid ammonium fluorescein particles in cross-flow over an ungreased staggered tube bank. Tube rows are identified by letters A through E in the upstream to downstream direction.

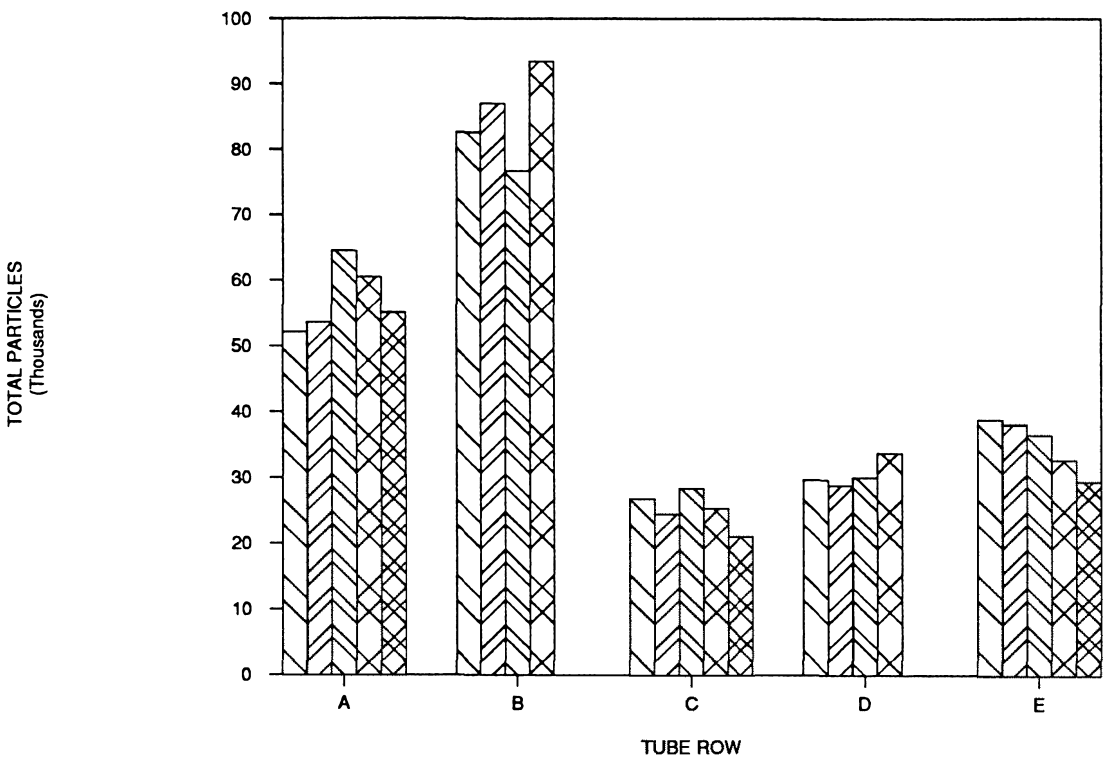

Figure 6.8. Total number of particles on each tube for the case of solid ammonium fluorescein particles in cross-flow over an ungreased staggered tube bank. Tube rows are identified by letters A through E in the upstream to downstream direction.

Table 6.4 Data for ungreased staggered tube bank

upstream flow velocity:	1320 cm/sec (2599 ft/min)
particle diameter:	4.82×10^{-4} cm
St_{eff}:	0.32
total particles through system:	2.12×10^{7}
total particles collected:	1.05×10^{6}
fraction particles collected:	0.049
overall collection efficiency:	0.053

INDIVIDUAL TUBE PARTICLE COUNTS (THOUSANDS)

row	tube 1	tube 2	tube 3	tube 4	tube 5	TOTAL PARTICLES ON EACH ROW	FRACTION OF COLLECTED PARTICLES ON EACH ROW
A	52.2	53.6	64.5	60.5	55.1	286000	0.27
B	82.6	87.1	76.7	93.5		340000	0.32
C	26.8	24.5	28.3	25.3	21.1	126000	0.12
D	29.8	28.8	30.1	33.8		123000	0.12
E	38.9	38.2	36.5	32.8	29.5	176000	0.17

ROW COLLECTION EFFICIENCIES:
A: 0.0202
B: 0.0174
C: 0.0066
D: 0.0064
E: 0.0093

6.3 ANALYSIS

A comparison of the overall row and overall bank collection efficiencies for the four cases is presented in Figure 6.9.

6.3.1 IN-LINE TUBE BANKS

Figure 6.10 shows a comparison between the ungreased and greased tube collection efficiencies for each row in the in-line tube bank. First, it is clear that the clean tubes collect far fewer particles than the greased tubes. Overall collection efficiency for the clean tubes is only 0.040, while the overall collection efficiency for the greased tubes is 0.14. For both cases it is obvious that flow channeling is occurring. Most of the particles in both cases are deposited on the first row of tubes when the flow is forced to diverge around the tubes. The number of particles deposited on subsequent rows is small, since particles in the flow are able to bypass the tubes in the later rows. Figure 6.10 shows that the problem of particle transport to the tube surface is the most important factor governing the deposition on the second and subsequent rows of the in-line tube bank, rather than the problems associated with particle bounce. In fact, for these rows (B through E), collection efficiencies are virtually the same for the greased and ungreased cases. For the greased case, a slight increase in the number of particles collected is seen for the last row when compared to the middle rows; a possible explanation is that some particles are entrained into the wakes of the final row of tubes and thus have additional opportunities to deposit on the downstream surfaces of the tubes. On a smaller scale, this phenomenon may also be seen for the ungreased tube case. (This is better seen in Figure 6.1 than in Figure 6.10.) Although the deposits on rows B-E of the tube bank are small,

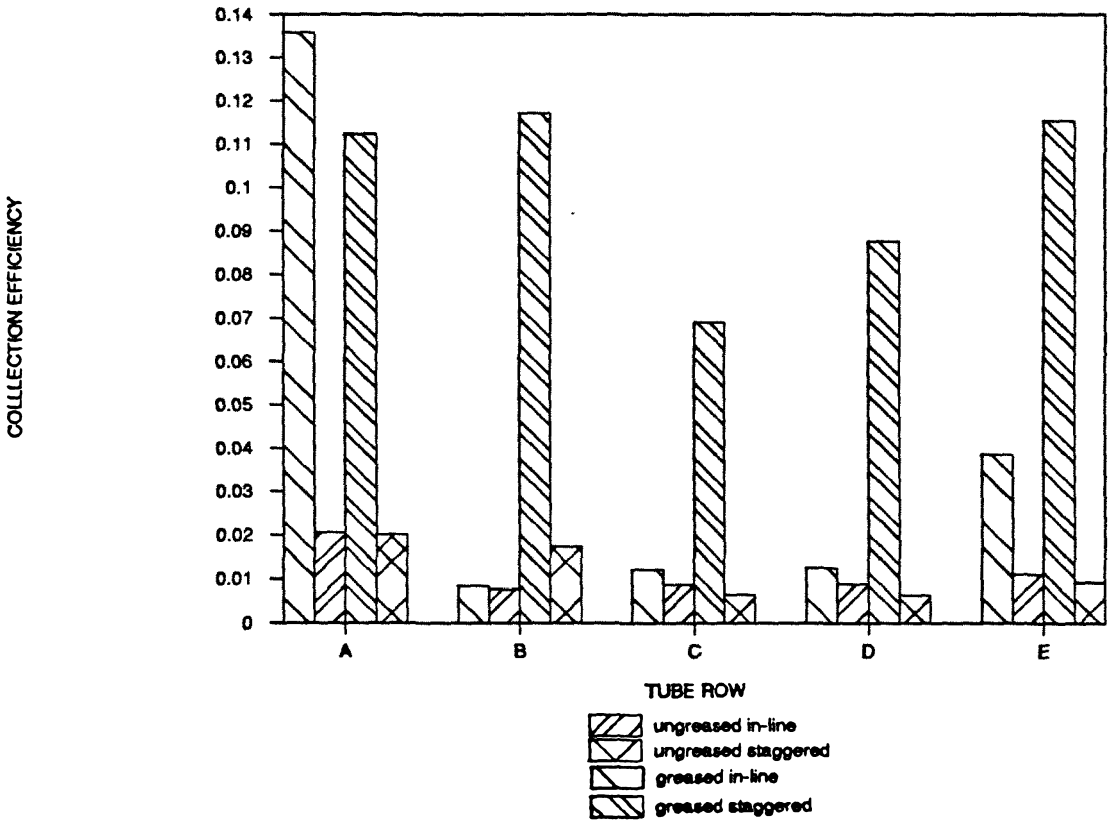

Figure 6.9. Particle collection efficiency for tubes in each row for the four cases of solid ammonium fluorescein particles in cross-flow over greased and ungreased staggered tube banks and greased and ungreased in-line tube banks. Tube rows are identified by letters A through E in the upstream to downstream direction.

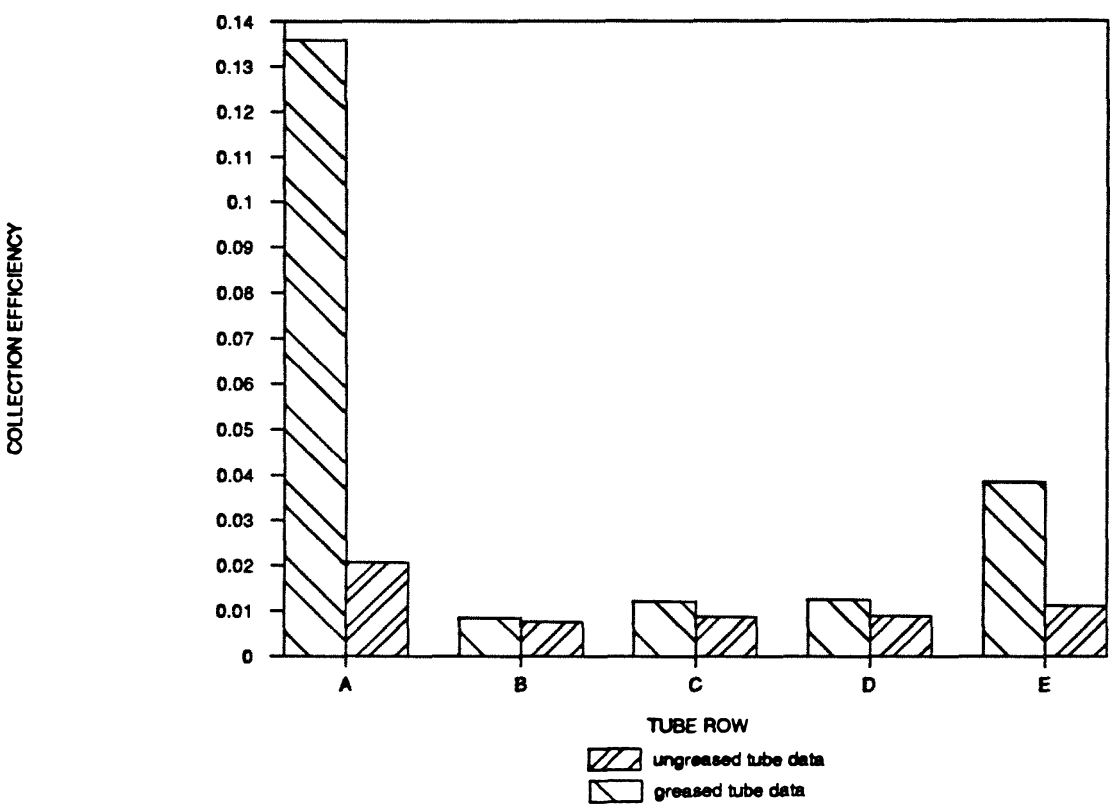

Figure 6.10. Particle collection efficiency for tubes in each row for the two cases of solid ammonium fluorescein particles in cross-flow over greased and ungreased in-line tube banks. Tube rows are identified by letters A through E in the upstream to downstream direction.

the use of in-line tube banks in order to reduce fouling should be considered carefully, since the flow channeling phenomenon that reduces fouling will also retard the heat transfer to the later rows of tubes.

6.3.2 STAGGERED TUBE BANKS

Figure 6.11 shows a comparison between the ungreased and greased tube collection efficiencies for each row in the staggered tube bank. Again, it is clear that the clean tubes collect far fewer particles than the greased tubes. Overall collection efficiency for the clean tubes is only 0.053, while the overall collection efficiency for the greased tubes is 0.39. For the staggered tubes, however, the particle deposition pattern is much different than for the in-line tubes. For the greased staggered tubes, the first row collects many particles; however, the second row collects even more. This is probably a result of a combination of two phenomena. First, the acceleration of the flow as it passes through the spaces in the first row contributes to an increase in the inertia of the particles carried along in the flow and thus to higher effective Stokes numbers and more particle-surface collisions. Second, there is a forced concentration of particles in the flows in the spaces between the first row of tubes, as some of the particles that are in the upstream cross-sectional area of the first tubes are diverted into the flows through the spaces between the tubes to join the particles that were initially upstream from those spaces. Since in the staggered tube arrangement, each row of tubes has its tube centers directly downstream from the spaces in the previous row of tubes, the second row of tubes will see a more concentrated particle stream than the first row. After the first two rows of tubes, the collection efficiency still remains high, since the staggered pattern continues to encourage inertial deposition. As in the in-line cases described above, a slight increase is

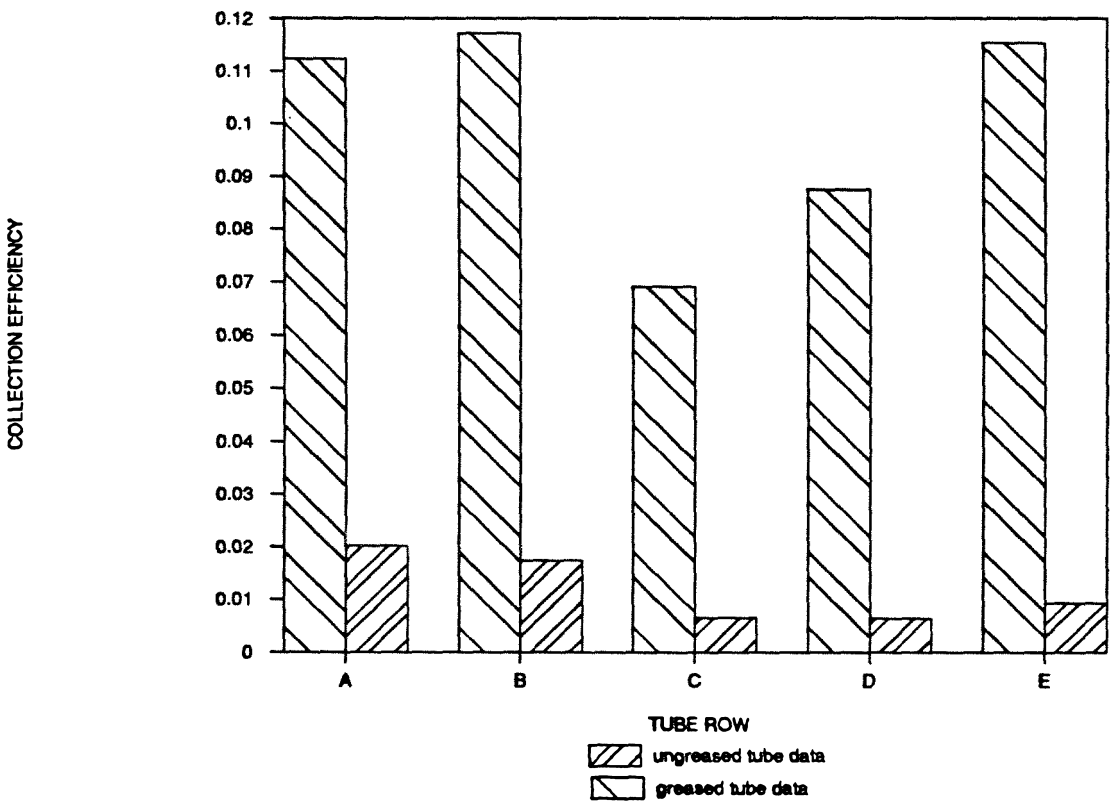

Figure 6.11. Particle collection efficiency for tubes in each row for the two cases of solid ammonium fluorescein particles in cross-flow over greased and ungreased staggered tube banks. Tube rows are identified by letters A through E in the upstream to downstream direction.

seen in the particle collection of the last row of tubes. The behavior of the staggered ungreased tube bank is qualitatively similar to that of the staggered greased tube bank; however, all ungreased row collection efficiencies are much smaller than corresponding greased row collection efficiencies. This leads to the conclusion that unlike the in-line tube bank, particle collection on clean tubes is limited by particle bounce, not by particle transport to the tube surfaces. The staggered tube arrangement results in much more efficient heat transfer; however, an increased pressure drop and the deposition of more particles are also results of the staggered tube arrangement.

6.3.3 COMPARISON TO SINGLE TUBE EXPERIMENTS

The average collection efficiency for a tube in any row in a tube bank can be easily determined. In fact, it is the same as the overall collection efficiency of the row. This follows from the definition of the collection efficiency as the ratio of the number of particles collected on a collector to the number of particles in the upstream cross-sectional area of the collector. Since the upstream cross-sectional area of a row of five tubes is simply five times the upstream cross-sectional area of a single tube, and since the number of particles collected on the row of five tubes is simply five times the average number of particles collected by a single tube in the row, the average collection efficiency of a single tube in the row is the same as the collection efficiency of the row.

For all four cases tested, the upstream air flow velocity was 1320 cm/sec (2599 ft/min), and the particle diameter was 4.82×10^{-4} cm. These parameters give a superficial estimate of the effective Stokes number for a tube in row A of the tube bank, St_{eff}, of 0.32. For a single tube in cross-flow, the results of Chapter 4 predict a collection efficiency, η_R, of

0.09 for both greased and ungreased tubes. See Figure 4.1. The predicted collection efficiencies for the two single tube cases are the same because the St_{eff} of 0.32 is small enough that particle bounce is not occurring.

By inspecting the collection efficiencies for tubes in the first rows of each of the four tube banks examined, however, it can be seen that the single tube results are not directly applicable to the tube bank data. (Tubes in the first rows are chosen for this comparison because the flow field and particle distribution are not yet as disturbed approaching the first row as later in the tube bank.) The collection efficiencies of tubes in the first rows of both types (staggered and in-line) of ungreased tube banks were found to be 0.02. The collection efficiencies for tubes in the first rows of the greased tube banks were determined to be much higher, 0.13 for the in-line case and 0.12 for the staggered case. The large difference in collection efficiencies of the tubes in the first rows of the greased and ungreased tube banks indicates that particle bounce is, in fact, occurring. In addition, the observed collection efficiencies of the tubes in the first rows of the greased tube banks are higher than the predicted greased single tube case collection efficiency. Both these observations lead to the conclusion that the incoming particles have much more inertia than the low St_{eff} of 0.32 would indicate. This is a reasonable conclusion since the restriction of the flow area available in the test section is much greater with the tube bank in place than with a single tube in place. Thus, the flow will accelerate more as it approaches the tube bank and the particles approaching the tube bank will have more inertia than similar sized particles approaching a single tube in the test section.

6.4 CONCLUSIONS

As was expected, the experimentally determined overall collection efficiencies of the ungreased tube banks were much smaller than those of the greased tube banks, regardless of geometry. However, for corresponding geometries (i.e., in-line or staggered), the qualitative deposition pattern was similar for both the clean and the greased tube experiments. For the in-line tube banks, it was found that for the downstream tube rows (B-E), the collection of particles was limited by particle transport to the tubes rather than by particle bounce.

The overall collection efficiencies for the clean and the greased staggered tube banks were higher than the corresponding in-line values. Although the staggered tube bank gives improved heat transfer, an increased pressure drop results from this geometry. From the data gathered here it can also be seen that deposition of more particles results.

The staggered tube banks show a more even distribution of particles on the rows. In-line tube banks are subject to flow channeling and thus have a significant portion of the particle impaction occurring only on the first row of tubes. This leads to lower overall collection efficiencies. The flow channeling also adversely affects the heat transfer.

For in-line tube banks, the results suggest that an upstream, dummy, easily removable and cleanable row of "tubes" to collect most of the particles might be an effective antifouling approach. Unfortunately, this dummy row of tubes would also inhibit the heat transfer in the remainder of the tube bank. For staggered tubes, the relatively even particle distribution over the rows of tubes precludes the use of dummy tubes.

Antifouling recommendations would have to include the need to maintain dry, clean surfaces and particles as long as possible to enhance particle bounce and the use of velocities as high as consistent with the heat transfer or energy consumption constraints on the system, also to enhance particle bounce.

6.5 BIBLIOGRAPHY

1. Kays, W.M., and London, A.L., Compact Heat Exchangers, McGraw-Hill, New York, 1964.

7 SUMMARY AND CONCLUSIONS

7.1 OVERVIEW

Although the magnitude of the fouling problem in heat transfer equipment is well recognized, few investigations have been conducted into the mechanisms that lead to such fouling. The previous work that has been done has been concentrated mainly on empirical descriptions of cooling water fouling, not on the mechanisms of gas-side particulate fouling of heat exchangers. The work reported in this thesis has been designed to examine gas-side fouling mechanisms that involve the inertial impaction of small particles onto tubular heat exchanger surfaces.

The experimental apparatus consisted of a wind tunnel with a test section capable of holding full-scale tubular compact heat exchanger sections, and particle generation equipment capable of producing monodisperse ammonium fluorescein aerosols in the 4 to 6 micron diameter range. Particles were introduced upstream from the test section, allowed to mix uniformly with the air stream, and then passed through the test section in cross-flow with respect to the tubes. An after filter downstream from the test section collected particles that passed through the test section. By extracting the tubes and after filters, and using spectrophotofluorimetric measurements of the resulting solutions, it was possible to determine the number of particles deposited on the tubes and on the after filters. Using this information, it was possible to draw conclusions about the mechanisms of aerosol particle collection on the tubes.

Three sets of experiments were performed. First, single heat exchanger tubes exposed to a cross-flow of particulate laden air were studied to gather data on the interactions of the

particles with a single tube. Experimental results compared favorably with the results of a numerical simulation of the transport mechanisms.

Second, the transient deposition of particles onto single heat exchanger tubes in cross-flow was studied. It was found that a steady-state condition (i.e., a constant number of particles on the tube) could be reached in some cases. Finally, the deposition patterns for the aerosol particles as they passed through a tube bank were studied. The quantities of aerosol deposited on various tubes depended on the position within the tube bank as well as on the overall geometry of the bank.

7.2 SUMMARY OF RESULTS

7.2.1 SINGLE TUBE EXPERIMENTS

The single tube experiments showed that it is possible to predict the collection efficiencies of tubes exposed to particle-laden air in cross-flow when all the particle-tube collisions result in particle capture (i.e., in the greased tube cases), using a computer simulation model based on the method of Brun et al. (1). Both theory and experiment show that for the case of "perfect sticking," particle collection efficiency increases with increasing effective Stokes number, St_{eff}, as more and more particles impact against the tube and are captured.

Particle collection efficiencies for the impaction of solid particles onto ungreased tubes are much lower than for impaction onto greased tubes, except at very low effective Stokes numbers. A model for particle capture on clean tubes, based on the hypothesis that a critical incident particle velocity normal to the tube exists, above which particles

will bounce with enough energy to completely escape capture by the tube, predicts the collection efficiencies of the ungreased tubes for both the low St_{eff} cases where bounce is not occurring and for the high effective Stokes number cases, where most particles that strike the tube bounce. It has been shown that although particle bounce increases with increased particle size and/or increased particle velocity, particle bounce is not a function only of the effective Stokes number. The data suggest that some particles are bouncing at least once at normal incident velocities at or below 500 cm/sec. A critical incident particle velocity normal to the tube surface of 1000 cm/sec has been estimated as necessary to cause all particles that hit the tube to escape capture, including those particles that may strike the tube more than once, for the 4 to 5.5 micron diameter ammonium fluorescein particle-stainless steel tube interaction.

Since particle bounce is a phenomenon that will occur at large incident velocities, it is possible to retard the accumulation of solid particles on tubes in cross-flow by selecting high enough fluid velocities. Using the developments reported in this thesis, heat exchangers could be designed deliberately to operate at velocities high enough to retard the accumulation of fouling deposits.

7.2.2 TRANSIENT EXPERIMENTS

The deposition over time of solid particles on a single tube in cross-flow was studied both for the greased and the ungreased tube cases. For the greased tube cases, essentially all particles that strike the tube stick and will continue to stick even at surface coverages near half of the projected front face area of the tube. Although for such a high coverage fraction, many incident particles are expected to strike other particles already on the

surface, the incident particles continue to stick. This suggests that the greased coating on the tubes causes the first particles that strike the surface to become coated with sticky material to which additional particles become attached.

The case of particle attachment to ungreased tubes in cross-flow shows markedly different results than the greased tube case. For the range of effective Stokes number covered (0.29 to 1.04), the number of particles deposited on the tube quickly reaches a steady-state, where particle deposition and particle removal are occurring at equal rates. The steady-state is reached at surprisingly small front surface coverage fractions (0.05 and less).

As in the case of the short-term, single tube experiments discussed in Chapter 4 and in Section 7.2.1 above, selection of a high enough fluid velocity to promote particle bounce leads to high incident particle velocities and to a retardation of particle accumulation. In the transient case, this means that a steady-state particle deposit coverage with fewer total particles on the tube is achieved when the clean tube-solid particle system is operated at high fluid velocities. Again, this observation reinforces the premise that some heat exchangers could be designed to retard the accumulation of fouling deposits by deliberately designing them to operate at high velocities. This design advice is appropriate only for systems with clean tubes and solid particles and with no adhesive material present in the system.

7.2.3 TUBE BANK EXPERIMENTS

Again, both greased and ungreased tube banks were studied. Two geometries of tube banks were examined, an in-line and a staggered tube arrangement. As expected, the

ungreased tube banks showed much lower overall collection efficiencies than the greased tube banks. However, the qualitative nature of the deposition pattern of particles within the tube bank depended on the geometry of the tube bank and was similar, regardless of the tube surface condition.

For the in-line tube banks it was found that a majority of the particles collected by the tube bank were deposited on the first row of tubes in both the greased and the ungreased tube experiments. Further deposition on subsequent rows of tubes was found to be limited by particle transport to the tubes, as flow channeling limited the exposure of the subsequent rows to the particle-laden stream. This channeling would also inhibit heat transfer.

The staggered tube banks showed a more even deposition pattern of particles throughout the bank, although the first two rows of tubes did collect a large percentage of the particles collected by the entire tube bank. Although a staggered tube arrangement enhances heat transfer from the fluid to the tubes, it has been shown that particle collection (fouling) is also enhanced.

7.3 CONCLUSIONS

1. An aerosol processes wind tunnel has been constructed which facilitates quantitative studies of particle interactions with heat exchanger surfaces. The test section of the wind tunnel is suitable for testing full-scale models of compact heat exchanger surfaces.

2. Brun et al.'s (1) theoretical model for predicting particle collection by a single tube in cross-flow has been verified experimentally, using sticky tubes to imitate the case where all particle-tube collisions result in particle capture. Rosner et al.'s (2) development of the effective Stokes number concept has also been verified experimentally for the "perfect sticking" case.

3. Particle bounce has been quantified for the case of clean, stainless steel tubes and incident ammonium fluorescein particles. Using Dahneke's (3-5) suggestion of a critical incident velocity for the onset of particle bounce, a model has been developed, which predicts particle collection efficiencies for high effective Stokes numbers where particle bounce is prevalent. The model also predicts particle bounce in the low St_{eff} region, where particle collection is limited by particle transport to the surface.

4. Particle deposits have been shown to reach a steady-state quickly and at low front surface area coverage fractions for the case of clean tubes in a cross-flow of solid particles that deposit by inertial impaction. Such a steady-state was not reached for solid particle deposition onto greased tubes in the times studied in the experiments. Since appreciable (0.49) coverage of the front surface was attained during these greased tube transient experiments and particle accumulation still continued, it is clear that particle collection is very sensitive to the presence of any adhesive material that can enhance the capture of particles.

5. Overall solid particle collection efficiencies of ungreased tube banks have been shown to be lower than overall solid particle collection efficiencies of greased tube banks. These results were expected and are consistent with the results of the single

tube experiments. A staggered tube bank arrangement, often used to enhance heat transfer, collected significantly more particles than an in-line tube bank geometry, using the same number of tube rows with tubes of the same size.

6. Conditions have been identified in which the aerosol deposits that lead to gas-side heat exchanger fouling can be kept to very low levels by deliberately selecting high fluid velocities that induce solid particles to bounce upon impact with the heat exchanger surfaces. Transient fouling experiments have identified conditions under which high fluid velocities can be used to achieve very low, steady-state particle accumulations on tubes in a cross-flow of solid particles. Using these findings, heat exchangers can be designed that will resist gas-side fouling.

7.4 BIBLIOGRAPHY

1. Brun, R.J., Lewis, W., Perkins, P.J., and Serafini, J.S., Impingement of cloud droplets on a cylinder and procedure for measuring liquid-water content and droplet sizes in supercold clouds by rotating multicylinder method, Report 1215, 141-183 (1955).

2. Rosner, D.E., Gokoglu, S. and Israel, R., Rational engineering correlations of diffusional and inertial particulate deposition behavior in nonisothermal forced convection environments. Presented at the International Conference on Fouling of Heat Exchanger Surfaces, White Haven, PA (1982).

3. Dahneke, B., The capture of aerosol particles by surfaces, Journal of Colloid and Interface Science, 37, 342-353 (1971).

4. Dahneke, B., The influence of flattening on the adhesion of particles, Journal of Colloid and Interface Science, 40, 1-13 (1972).

5. Dahneke, B., Measurements of bouncing of small latex spheres, Journal of Colloid and Interface Science, 45, 584-590 (1973).